KINETIC STUDIES OF THE REACTIONS OF ALKYL AND SILYL HYDRIDES

DISSERTATION

Presented to the Graduate Council of the

University of North Texas in Partial

Fulfillment of the Requirements

For the Degree of

DOCTOR OF PHILOSOPHY

By

Jessie Yuan, B.S., M.S.

Denton, Texas

August, 1996

KINETIC STUDIES OF THE REACTIONS OF ALKYL AND SILYL HYDRIDES

DISSERTATION

Presented to the Graduate Council of the

University of North Texas in Partial

Fulfillment of the Requirements

For the Degree of

DOCTOR OF PHILOSOPHY

By

Jessie Yuan, B.S., M.S.

Denton, Texas

August, 1996

PM

Yuan, Jessie, Kinetic Studies of the Reactions of Alkyl and Silyl Hydrides. Doctor of Philosophy (Chemistry), August, 1996, 125 pp., 25 tables, 20 illustrations, references, 134 titles.

The Kinetics of the reactions involving alkyl and silyl hydrides were studied by the flash photolysis / resonance fluorescence technique.

The reactions of alkyl radicals (R = C_2H_5, i-C_3H_7, t-C_4H_9) with HBr have been studied at room temperature and the rate constants obtained (units are in $cm^3\ s^{-1}$) are: $k_{3.3}$ = (7.01 ± 0.15) x 10^{-12} , $k_{3.2}$ = (1.25 ± 0.06) x 10^{-11} , $k_{3.1}$ = (2.67 ± 0.13) x 10^{-11}. These results, combined with previously determined reverse rate constants and other kinetic information, yield bond dissociation enthalpies (units in kJ mol^{-1}) at 298 K : primary C-H in C_2H_5-H (423.6 ± 2), secondary C-H in i-C_3H_7-H (409.9 ± 2), tertiary C-H in t-C_4H_9-H (405.1 ± 2). These rate constants and bond energies are in good agreement with previous results. Temperature-dependent rate constants for n-C_3H_7 + HBr, $Si(CH_3)_3$ + HBr, and Br + Si_2H_6 were obtained in the following temperature ranges and the Arrhenius expression for each reaction (A / ($cm^3\ s^{-1}$), E_a / (kJ mol^{-1})) are: $k_{3.4}$ = (6.19 ± 1.12) x 10^{-13} exp (7.14 ± 0.58 / RT), 296 -520 K; $k_{3.6}$ = (8.1 ± 2.0) x 10^{-12} exp (5.12 ± 0.72 / RT), 289 - 515 K; $k_{3.8}$ = (1.35 ± 0.12) x 10^{-10} exp (-3.05 ± 0.3 / RT), 295 - 556 K. The bond energies (kJ mol^{-1}) derived for primary C-H in n-C_3H_7-H, tertiary Si-H in $Si(CH_3)_3$-H, and primary Si-H in Si_2H_5-H are: 425.3 ± 3, 397.8 ± 2, and 371.9 ± 5, respectively. These bond strength determinations confirm that the methyl group decreases the C-H bond strength in alkanes,

while it increases the Si-H bond energy in silane. Also, the Si-H bond energy in silane is decreased by silyl-substituent.

Rate constants for the Cl + HI reaction have been measured from 297 - 390 K and the Arrhenius expression is $k_{4.1} = (1.18 \pm 0.31) \times 10^{-10} \exp(-(0.45 \pm 0.77)\ \text{kJ mol}^{-1} / RT)$ $\text{cm}^3\ \text{s}^{-1}$. The almost zero barrier of the reaction in this determination is coincident with the results from other techniques.

A kinetic study of the reaction H + SiH_4 has been conducted over the temperature range 290 - 660 K. The temperature-dependent rate constants are summarized by $k_{5.1} = (1.78 \pm 0.11) \times 10^{-10} \exp(-(16.0 \pm 0.2)\ \text{kJ mol}^{-1} / RT)\ \text{cm}^3\ \text{s}^{-1}$. Kinetic modeling using TST theory with a Wigner tunneling correction gives $k_{5.1} = 2.44 \times 10^{-16} (T / K)^{1.903} \exp(-1102\ K / T)\ \text{cm}^3\ \text{s}^{-1}$ (290 - 2000 K).

The rate constants for reactions of hydroxyl with silane, and mono, di-, tri, and tetramethylsilane have been determined at room temperature, and the values (units in $\text{cm}^3\ \text{s}^{-1}$) are : $k_{6.3} = (1.22 \pm 0.12) \times 10^{-11}$, $k_{6.4} = (3.43 \pm 0.34) \times 10^{-11}$, $k_{6.5} = (4.48 \pm 0.45) \times 10^{-11}$, $k_{6.6} = (2.67 \pm 0.27) \times 10^{-11}$, $k_{6.7} = (1.09 \pm 0.11) \times 10^{-12}$. These rate constants indicate that reaction proceeds by H abstraction mainly from the Si-H bonds and that the bond reactivity per Si-H bond towards OH increases with the increasing number of methyl groups.

ACKNOWLEDGMENTS

First, I would like to thank my major professor, Dr. Paul Marshall, for his instructions which guide me to finish the research. Dr. Marshall taught me everything from the basic method to the advanced theory with great patience and high enthusiasm. Then, I gratefully appreciate Dr. Abdell Goumri and all my research colleagues who gave me a lot of encouragement and assistance in this research project.

Finally, I thank Texas Instruments, Inc., the Robert A. Welch Foundation (Grand B-1174), and UNT Organized Research Fund for their financial support.

TABLE OF CONTENTS

LIST OF TABLES

LIST OF ILLUSTRATIONS

CHAPTER I

INTRODUCTION

A. Basic Properties of Silicon and Carbon

In view of basic knowledge of chemistry, silicon and carbon are very similar in a lot of aspects because both of them are located in the same group (group IV) of the periodic table. Besides the analogies, there are also some dramatic differences between these two elements due to the different periods in which they are found. Two major properties, size and electronegativity, distinguish silicon from carbon. Silicon atoms are about 50% larger and less electronegative than carbons, which means silicon forms more polar σ and less stable π bonds with other elements.[1] Also, in contrast to carbon, the possible participation of empty 3d orbitals increases the likelihood of forming 5 and 6-coordinated complexes for silicon atom.[2] So another difference between silicon and carbon is that silicon prefers fewer stable multiple bonds but has stable derivatives with more than four bonds.[1] Since the electronegativity of hydrogen (2.2) is greater than that of silicon (1.74 - 2.0) and less than that of carbon (2.5),[2] the polarities of the Si-H and C-H bonds are inverted.

Thermodynamic data for silicon compounds are limited, but the general conclusions from recent data are that Si-C/C-C bonds as well as Si-H/C-H bonds are close in energy in some cases whereas bonds to elements from Group V, VI, VII (the more electronegative nonmetals) are stronger to silicon than to carbon (see Table 1). The methyl

effect which weakens the C-H bonds in alkanes is not present in silanes, instead, a silyl-weaking effect has been clarified.[3] However, recent research based on the photoacoustic technique showed an increasing trend in the Si-H bond dissociation energy by the methyl-effect.[4]

Table 1: Measured C-X/ Si-X as well as Si-C/C-C and Si-H/C-H Bond Energies in Some Molecules[3]

Bond	D_0 (kJ mol^{-1})	Bond	D_0 (kJ mol^{-1})
Me_3Si-I	322	Me_3C-I	213
Me_3Si-OH	535	Me_3C-OH	380
$C_6H_5SiH_2$-H	369	$C_6H_5CH_2$-H	367
Me_3Si-H	377	Me_3C-H	385
H_3Si-CH_3	369	H_3C-CH_3	368
$MeSiH_2$-CH_3	369	$MeCH_2$-CH_3	355
Me_2SiH-CH_3	368	Me_2CH-CH_3	351

B. Major Methods to Determine R-H Bond Dissociation Enthalpies

Bond dissociation enthalpies (BDEs), which are defined as the enthalpy changes associated with the bond formation and breakage between atoms in a molecule, are important concepts in a variety of areas of chemistry. Bond dissociation measurements provide not only the fundamental information on the strength of bonds in important key molecules but also a framework of free-radical heats of formation. The kinetic data which

can be used to deduce accurate bond energies as well as other thermochemical constants determination for small organic and silyl molecules are also essential for atmospheric and combustion modeling.

Radical Kinetics /Equilibria. Many experimental techniques have been used to measure the BDEs for a large number of molecules, and one major approach that is commonly used to determine the R-H (R=alkyl, silyl) bond energies in the gas-phase is by the study of radical kinetics. Especially, studies of the kinetics of chemical equilibria involving the reaction of halogen atoms (X=Cl, Br, I), with a substance RH have been, and continue to be, a wealthy source for the determination of R-H bond strengths.[5,6,7]

$$X + RH \underset{k_{-1}}{\overset{k_1}{\rightleftharpoons}} R + HX \qquad (1.1)$$

By generating [X] under controlled conditions by flash or laser photolysis, one can determine the rate constants k_1 as a function of temperature by time-resolved techniques using either resonance fluorescence or photoionization mass spectroscopy to detect transient species. ΔH for reaction (1.1) is evaluated as the difference between the activation energy for k_1 with an assumed activation energy for the reverse reaction, k_{-1}. This "second law" method (for details see chapter 3) yields ΔH, which is the bond strength difference between H-X and R-H. The former quantity is already known, so the R-H BDE is determined. This technique, where X is the I-atom, has been reviewed by Golden and Benson,[8] and extended to many Si compounds by Walsh[2] and to F-containing compounds

by Rogers.[9]

Instead of measuring k_1 and k_{-1} independently, Benson and co-workers[10,11] have used the very low pressure reactor (VLPR) technique which is a variation of very low pressure pyrolysis[12] (VLPP) to measure the equilibrium constants for the following reactions directly:

$$CH_4 + Cl \rightleftharpoons HCl + CH_3 \quad (1.2)$$

$$c\text{-}C_3H_6 + Cl \rightleftharpoons HCl + c\text{-}C_3H_5 \quad (1.3)$$

If the equilibrium constant is measured at a single temperature, the R-H bond energy can be determined by the "third-law" method (for details see chapter 3). This method determines ΔH from the calculated ΔG from the equilibrium constant and a separately derived ΔS, then the bond energy of R-H is obtained as before. In a simple VLPR experiment, molecules of gas reactants are allowed to flow into a Knudsen cell reactor (typically pressure 0.1 - 10 mtorr), and the reaction mixture is analyzed by molecular-beam mass spectrometric detection which is designed to eliminate complicated secondary reactions of radicals on the walls of the mass spectrometry chamber. The same technique was applied by Choe and Choo[13] to determine the rate and equilibrium constants of Br with trimethylsilane and to estimate the Si-H bond strength in $(CH_3)_3SiH$.

Association / Dissociation Equilibria. Study of the association / dissociation equilibria, e.g.

$$R\text{-}R' \rightleftharpoons R + R' \quad (1.4)$$

$$R \rightleftharpoons \text{olefin} + H \text{ or } CH_3 \quad (1.5)$$

have provided another way to derive the bond strength for a series of molecules. A quantitative measure of the stability of the molecule is to measure the high-pressure rate parameters for thermal dissociation in combination with the corresponding numbers for the reverse process. From such an analysis, ΔG will be determined from the equilibrium constant and ΔS can be derived from thermochemical calculations with the information from either theoretical studies or separate experiments, such as matrix isolation infrared spectra studies.[14,15,16] The heat of reaction can be obtained by the relation $\Delta H = \Delta G + T\Delta S$. Since the heat of formation of the molecules and H or CH_3 are known, the ΔH_f of radicals can be calculated. One of the useful byproducts from determination of the BDE(R-H) is the radical heat of formation $\Delta H_f(R)$ which is related to the bond energy via the following relationship:

$$BDE\ (R\text{-}H) = \Delta H_f(R) + \Delta H_f(H) - \Delta H_f(R\text{-}H) \qquad (1.6)$$

One way to measure the dissociation constant of eq. (1.4) is by the single-pulse shock tube technique (SPST). This SPST technique which was developed in 1954 by Click et al.[17] has a surface-interaction-free method to study dissociation processes typically at above 1000 K. The mixture is heated up quickly by a shock wave to a very high temperature, followed by quick cooling. The reaction time (~ 1 ms) is short, thus surface effects as well as interfering side reactions are minimized. Tsang[18,19] modified this technique by use of SPST in the "comparative rate mode", by which the Arrhenius parameters of molecules were determined by comparing the fraction of decomposition with a "temperature standard" whose parameters were well known.

In addition to using the VLPP technique, another way to measure the rate constant

of association process, such as eq. (1.4), is the studies of the radical buffer system. The radical buffer method offers a procedure for measuring the ratio of rate constants for radical-radical recombinations based on the equilibrium:

$$R + SI \overset{K_{RS}}{\rightleftharpoons} RI + S \tag{1.7}$$

where R and S are alkyl groups. In the presence of the recombination processes

$$2R \xrightarrow{k_r} R_2 \qquad \text{and} \qquad 2S \xrightarrow{k_s} S_2 \tag{1.8}$$

the recombination rate constant k_r, k_s can be determined by the combination of equations (1.7) and (1.8)

$$k_s/k_r = ([S_2]/[R_2])([RI]/[SI])^2/ K_{RS}^2 \tag{1.9}$$

where K_{RS} has to be estimated from assumed thermochemical data, and the concentration of products can be analyzed by GLC from the experiments. By this technique, the rate constants for combination of a variety of pair radicals can be determined related to the known recombination rate of a certain species. Using this method, Hiatt and Benson measured the recombination rate constants for ethyl,[20,21] isopropyl[22] and t-butyl[23] radicals with a well-established rate constant for methyl recombination. To avoid K_{RS} and its dependence on assumed radical thermochemistry, Tsang modified the above formulas by relating to the detailed balancing

$$k_r/k_{-r} = K_f(R_2)/K_f^2(R) \quad \text{and} \quad k_s/k_{-s} = K_f(S_2)/K_f^2(S) \tag{1.10}$$

where the minus sign indicates the dissociation process, and $K_f(X)$ is the equilibrium constant for the formation of species X from its elements. Combination of (1.9) and (1.10) results the new expression

$$\left[\frac{K_f^2(RI)K_f(S_2)}{K_f^2(SI)K_f^2(R_2)}\right]^{\frac{1}{2}} \times \left(\frac{k_{-s}}{k_{-r}}\right)^{\frac{1}{2}} = \left(\frac{[S_2]}{[R_2]}\right)^{\frac{1}{2}} \times \left(\frac{[RI]}{[SI]}\right) \tag{1.11}$$

where the first term of the lefthand-side is the equilibrium constant for the reaction

$$2SI + R_2 \rightleftharpoons 2RI + S_2 \tag{1.12}$$

and the ratio of the dissociation constant can be determined. This modified procedure represents a better way to use the radical buffer method relating to the radical dissociation rate constant because of the more accurate estimates of the equilibrium constant available for (1.12) than K_{RS} (1.7).

The resulting heats of formation of ethyl, isopropyl, tert-butyl radicals from the experimental data on simple alkane and radical decomposition from shock-tube and radical buffer studies, together with the radical combination rates from VLPP and modulation spectroscopy as well as the entropies of alkyl radicals, have been reviewed by Tsang.[24,25] These values are about 10-20 kJ mol^{-1} higher than the numbers recommended by McMillen and Golden[26] from metathesis reactions like reaction (1.1).

Photoionization Mass Spectrometry. One alternative technique which utilizes a different method to measure the bond strength is photoionization mass spectrometry (PIMS), sometimes called the appearance/ionization potential (AP/IP) method. Consider the following ionization reaction

$$RH + h\nu_{AP} \rightarrow R^+ + H + e^- \tag{1.13}$$

One can measure the appearance energy of the dissociative process: E_{AP} (R^+, RH), and this threshold can be related to the ionization energy of the radical and the bond dissociation energy.

$$E_{AP} (R^+, RH) = BDE (R\text{-}H) + IP (R) \quad (1.14)$$

If E_{AP} and IP of the radicals are known, then the combination of these two will yield BDE (R-H), or the heat of formation of the cations can be obtained via:

$$\Delta H_f^\circ (R^+) = E_{AP} (R^+, RH) + \Delta H_f^\circ (RH) - \Delta H_f^\circ (H) \quad (1.15)$$

Ionization potentials of many radicals have been measured using both photoelectron spectroscopy[27] and electron impact appearance potentials,[28,29] but these are not easy to obtain due to the difficulty in generating transient species. One application of the AP/IP method has been to determine BDE ($H\text{-}C_2H_5$). The contribution of a weak photoion-pair production process ($C_2H_6 \rightarrow C_2H_5^+ + H^-$) interferes with observation of the E_{AP} of $C_2H_5^+$ from C_2H_6. However, an alternative approach based on photolysis of ethyl iodide overcomes this deficiency. Rosenstock et al.[30] have summarized earlier studies of ethyl halides, and included their own photoion-photoelectron study to obtain the threshold of appearance potential 10.52 ± 0.01 eV for C_2H_5I. Combination of the standard heat of formation of ethyl iodide and I atom leads to $\Delta H_{f\,0}^\circ (C_2H_5^+)$ =914.6 ± 2.1 kJ/mol. Ruscic and co-workers[31] prepared ethyl radicals by the F + C_2H_6 reaction, and studied them by photoionization mass spectrometry to yield an adiabatic IP of 8.117 ± 0.008 eV. Considering the thermochemical equation,

$$\Delta H_{f\,0}^\circ (C_2H_5) = \Delta H_{f\,0}^\circ (C_2H_5^\cdot) - IP (C_2H_5) \quad (1.16)$$

the combination of the above two results with the known heat of formations for H and C_2H_6 gives BDE ($H\text{-}C_2H_5$) = 416.9 ± 2.1 kcal/mol.[32] The transient species Si_2H_5, Si_2H_3, and Si_2H_2 were also prepared by reactions of Si_2H_6 + F atoms,[33] and an adiabatic ionization potential of 7.60 ± 0.05 eV was obtained for Si_2H_5. By combining the ionization potential with appearance potential obtained here from Si_2H_6, the standard heat of formation of Si_2H_5 at 0 K was inferred to be 247.5 kJ/mol.

C. Background to the Research

Despite the importance of BDEs, and the large amounts of work which had been done on radical systems for over several decades, considerable discrepancies in the heats of formation which provided uncertainties in the bond strength of small alkyl radicals still persist. For example, results from iodination and bromination studies have consistently yielded heats of formation for alkyl radicals which are 8-15 kJ mol^{-1} lower than those obtained from studies of association/dissociation equilibria.[24,25] A big breakthrough in the kinetic measurements of halogenation was made in 1988 by Gutman and co-workers. They developed a way to measure the backward rate constant k_{-1} (eq. (1.1)) using a tubular reactor coupled to a photoionization mass spectrometer. Prior to that year, many direct measurements for k_1 had been well established, while none of the data for k_{-1} was obtained directly from experiments due to the difficulty of detecting the polyatomic free radicals. The older thermodynamic data involving reaction (1.1) were derived from the measured activation energy for the forward reaction with an *assumed* small positive activation energy (8 ± 4 kJ/mol for R + HBr and 4 ± 4 kJ/mol for R + HI)[5,17] for the

reverse reaction. However, the direct measurement of k_{-1} showed negative activation energies, some as low as -8 kJ/mol. This investigation yielded new thermodynamic data, like the R-H bond strength, higher than those obtained from the previous studies. The higher heat of formation of radicals as well as the R-H bond dissociation energy were in good agreement with those obtained from studies from other equilibria.

For the silyl radicals, there is considerable variation in estimates of the bond strength Si-H in trimethylsilane. Studies of iodination by Walsh[34] yielded a value which is close to that for SiH_4, while McKean et al.[35] and Bernheim et al.[36] suggested that methylation weakens the Si-H bond. In contrast to their results, Ding and Marshall[37] proposed a bond strengthening behavior, based on the rate constants for Br + trimethylsilane with an estimated activation energy for the backward reaction. In order to gain more knowledge about the kinetic behavior of R + HBr reactions, in part to determine more accurately the bond dissociation energy of R-H for which there already exists well-known kinetic information for the reverse reactions, the following reactions have been investigated in this research:

$$C_2H_5 + HBr \rightarrow Br + C_2H_6 \quad (1.17)$$

$$i\text{-}C_3H_7 + HBr \rightarrow Br + C_3H_8 \quad (1.18)$$

$$n\text{-}C_3H_7 + HBr \rightarrow Br + C_3H_8 \quad (1.19)$$

$$t\text{-}C_4H_9 + HBr \rightarrow Br + C_4H_9 \quad (1.20)$$

$$Si(CH_3)_3 + HBr \rightarrow Br + HSi(CH_3)_3 \quad (1.21)$$

Also, to explore the silyl-substitution effect in the silane molecule and relate the activity to fundamental molecular properties, such as bond strength, kinetic experiments with disilane

were (1.22) performed in this research too.

$$Br + Si_2H_6 \rightarrow \text{products} \qquad (1.22)$$

The study of the kinetics and thermochemistry of alkyl and silyl radicals are summarized and discussed in chapter 3.

The reaction

$$Cl + HI \rightarrow HCl + I \qquad (1.23)$$

is one elementary step in chain reactions of halogen-hydrogen halide systems: the overall reaction is $HI + Cl_2 \rightarrow HCl + ICl$. This kind of process has been explored widely because of its particular importance in the practical understanding of chemical laser processes and the theoretical interpretation of elementary three-center exchange reactions. Additionally, this type of reaction is often used as an example to explain the characteristics of exothermic reactions.[38,39] In the 1970s, the detailed information from theoretical calculations on the potential energy surface of the three-body system was insufficient due to computational limitations. The kinetics of the halogen hydrogen-halide reactions have been studied experimentally by several techniques, such as crossed molecular beams[40] and infrared chemiluminescence.[41,42,43,44] Chapter 4 describes the kinetic study of atomic chlorine with hydroiodide.

The abstraction of hydrogen from silane,

$$H + SiH_4 \rightarrow SiH_3 + H_2, \qquad (1.24)$$

has been studied by many groups because of the involvement of the reactive silyl radical which is fundamentally important in the evaluation and formulation of mechanistic models of the silicon chemical vapor deposition (CVD) process.[45,46,47] The measured or estimated

rate constants of this reaction at room temperature show a large scatter, differing by a factor of more than 40, and only one of the studies reported a temperature-dependent rate constant.[48] As part of interest in the continuing study of Si-containing molecule, the kinetic measurements and modeling of the reaction of hydrogen atom with silane have been conducted and discussed in chapter 5.

Chapter 6 is concerned with the reaction of hydroxyl with silane compounds. The investigation of the process was challenging because several modifications on the detection system are necessary in order to enhance the sensibility of the hydroxyl UV fluorescence. Some data reported here represent the first study of this reaction.

CHAPTER 2

EXPERIMENTAL METHOD

A. Flash Photolysis / Resonance Fluorescence (FP-RF) Technique

FP-RF, one of the early techniques that overcame many limitations of classical techniques, has become a good way in studying elementary reactions in a stationary gas. In flash photolysis, a reactant is irradiated with an intense flash of UV or visible light that has sufficient intensity to initiate a chemical reaction, and the duration of the flash is short in time scale compared to the reaction studied. The reactive radicals generated in the flash are excited by the absorption of continuous wave radiation which is in resonance with a higher electronic state. If the lifetime for the emission of the unstable species is short compared to the other processes, such as quenching or dissociation, the resonance radiation is emitted with the same energy. This is the process of "resonance fluorescence". The scattered radiation can be detected by photon counting electronics and monitored as a function of time, which yields the concentration of radicals as a function of time because the intensity of fluorescence is proportional to the radical concentration.

The FP-RF apparatus has been described in detail previously.[49,50] A description of the general methodology is given briefly. For the alkyl + HBr reactions, alkyl radicals ($R=C_2H_5$, i-C_3H_7, n-C_3H_7, t-C_4H_9) were generated by pulsed photolysis of the alkyl iodide in a large excess of HBr diluted in Ar bath gas, by radiation from a EG&G Electro-Optics flash lamp system. This radiation passed through either MgF_2 ($\lambda > 120$ nm) or Suprasil

quartz ($\lambda > 165$ nm) windows. The flash energy was varied from 2.5 to 5 J by changing the capacitor voltage between 700 - 1000 V. The concentration of a reaction product, atomic Br, was monitored during the course of reaction by time-resolved resonance fluorescence at a wavelength of 149 - 163 nm (Br $(5s)^2P \rightarrow$ Br $(4p)^2P_{1/2,3/2}$).[51] Similar techniques were employed by Wine[52] and Pilling.[53] Resonance radiation was generated by a microwave-powered discharge lamp through which a mixture 0.5% of CH_2Br_2 in Ar gas was passed, and calcium fluoride optics were used to block any Lyman α radiation. The fluorescence signals, averaged over 100-1000 pulses, were detected by a solar-blind photomultiplier tube (Thorn EMI, 9423B) orthogonal to both the resonance and flash photolysis lamps, and processed through a multichannel scaler (EG&G Ortec ACE) with photon counting electronics. The timing of the experiments was controlled by a digital delay / pulse generator (Stanford Research Systems, DG35) which provided trigger pulses to the flash lamp and a computer-controlled multichannel scaler. The kinetic measurements for all the radicals were done at room temperature only except for n-propyl which was investigated as a function of temperature. For those higher temperature experiments, the temperature was measured at the beginning and the end of each run with a movable thermocouple (Omega, type K, chrome (+) vs alumel (-)) which was corrected for radiation errors of up to about 2%.[50]

For the trimethylsilyl + HBr experiments, the basic set up and procedures were similar to that employed for alkyl + HBr. Two precursors, trimethylsilyl iodide and hexamethyl disilane, were used to produce trimethylsilyl radicals. For some experiments a few mtorr of H_2 was added to the mixtures to quench any Br, if it existed in the excited

state, from $^2P_{1/2}$ to $^2P_{3/2}$. Actually, the rate constants observed did not show any effect for this addition because this reaction is not sufficiently exothermic to produce excited Br.

Kinetic measurements for Br + Si_2H_6 were made also by the same technique. Bromine atoms were generated by flash photolysis of CH_2Br_2, and were monitored by atomic resonance fluorescence as they reacted with excess Si_2H_6 under pseudo-first order conditions. The time scale for monitoring Br signals is of the order of 1-10 ms. For some measurements with low concentrations of Si_2H_6, a steady flow mixture was passed through the reactor for at least 20 minutes until the observed rate constant was reproducible. This might be attributed to adsorption of Si_2H_6 on the walls of the reactor.

B. Kinetic Experimental Procedure

Two reactors, steel and Pyrex, were used in kinetic studies. The steel reactor was constructed from stainless steel tubing with i.d. 2.2 cm and the glass one from Pyrex tubing with i.d. 2.7 cm. The steel reactor is assembled with a window-cooling system and can be employed for the high temperature measurements. Before starting measurements, the reactor was evacuated for at least several hours to remove any impurities stuck on the surface. For the steel reactor, routine cleaning with acetone was also performed especially when operating at higher temperatures. The gas-handling system was also pumped to near vacuum, by a combination of mechanical and diffusion pumps, until the pressure was as low as 10^{-4} torr. The readout was set to control the flow rate of the mixtures, and the pressure of the reaction was adjusted by a stopcock which was located near the end of the gas-handling system and connected to one port of the reactor. Experiments were carried

out under "slow flow " conditions in which a steady slow flow of mixtures (radical precursor and HBr) diluted in a large excess of Ar bath gas were passed to the reactor, and various experimental parameters were changed to see they influenced the measured rate constants. The flash energy, F, was altered by a factor of two, and the initial concentration of precursor was varied typically by a factor of 5. A doubling of F led to a higher concentration of alkyl or silyl radicals which would increase any secondary reactions of radicals with photolysis or reaction products. Changes in the initial concentrations of detected species also provide a check for any interference from radiation trapping.[54] The gas residence time, $\tau_{res,}$ the average time needed for gas to flow from the entrance port of the reactor to the reaction zone, was also changed by at least a factor of two. This checked whether any thermal decomposition of HBr occured in the experiments. The radiation from the flash lamp was focused through either magnesium fluoride or Suprasil quartz optics at room temperature, but only magnesium fluoride photolysis was employed at higher temperature because it gave higher radical concentrations. At room temperature both reactors were used. For the higher temperature measurements, only the steel reactor was employed. Rate constants from these two types of reactors were compared to check for any surface effects. For each set of experiments, the pseudo-first-order rate constants for at least five concentrations of reactants were measured. For Br + Si_2H_6 measurements, one of the concentrations includes $[Si_2H_6]=0$. For the R + HBr experiments, of course [HBr] > 0 is required to generate Br as a product.

C. HBr UV Absorption Experiments

In order to verify that HBr was not lost by adsorption on either the surface of the reactor or the gas-handling system, the effective HBr UV absorption cross section was measured under different conditions.The absorption experiments were performed at room temperature with either static or slowly flowing gas which mimicked the conditions in the kinetic measurements. A mixture of HBr/Ar (~ 0.45%) was passed through both the steel (modified to obtain a path length 61.6 cm) reactor and a long Pyrex tube (path length 80 cm), and the absorptions of the UV Hg spectral line at 186.5 nm was isolated by an Oriel 77250 monochromator with a resolution of 0.5 nm and detected by PMT at a voltage of 1200 volts. The concentration of HBr was varied by changing the pressure of the system. The transmitted intensity light I_{tr} for each HBr concentration as well as the background I_0 was read and analyzed by the Digital Oscilloscope Peripheral (DOP) program from Rapid Systems Inc. An important concept for this absorption test is the relationship between the concentration of HBr, I_{tr} and I_0, the Beer-Lambert law

$$I_{tr} = I_0 \exp(-\epsilon c l) \qquad (2.1)$$

where ϵ is the absorption coefficient, l is the path length and c is the concentration of HBr.

D. Laser-Photolysis / Resonance Fluorescence (LP-RF) Technique

The laser-photolysis / resonance fluorescence technique has been employed for the HI + Cl reaction. Cl_2 was photolyzed to produce Cl radicals by excimer laser (Questek 2010) radiation at 308 nm through a Suprasil quartz window, and the pulse energy E was calibrated with a Molectron J25 pyroelectric joulemeter. The Cl atoms reacted with HI to

form HCl and I and the course of reaction, either the decay of Cl or the growth of I, was monitored by time-resolved resonance fluorescence focused through a CaF_2 lens. The signals were captured by a solar-blind photomultiplier tube orthogonal to both the resonance lamp and excimer laser, and processed through a multichannel scaler with photon counting. Microwave-powered (90 W) discharge lamps generated resonance radiation: for Cl (λ = 134 - 140 nm),[51] a dilution of 0.3% of CCl_4 in Ar flowed continuously through the lamp, while a 0.5% CH_3I/Ar mixture was used for I (λ= 178 - 206 nm).[51]

The kinetic measurements for Cl + HI were made over the temperature range 297 - 390 K. Several parameters were varied to check their influence on the rate constants. The residence time, τ, was varied by a factor two and the concentration of Cl_2 was changed by a factor of four. $[Cl_2]$ and the photolysis energy E were varied to give different $[Cl]_0$. $[Cl]_0$ was placed on an absolute basis through the actinic photon flux, calculated from E, the laser beam cross section of 7.1 cm^2 and the absorption cross-section of Cl_2 of 1.85 x 10^{-19} cm^2,[55] combined with a quantum yield of 2 for atomic chlorine.[51] Two different reactors, Pyrex and stainless steel, were used to check for any surface effects. A 50% transmission filter was put in front of the entrance of the laser light for the reactor to see if there was any photolysis energy dependence.

E. Materials

Ar (99.998%, Big Three) was used directly from the cylinder. HBr (99.8 % nominal, Matheson) was separated from a substantial fraction of non-condensable gas,

such as H_2 and purified several times by low temperature distillations from 193 K to 77 K to remove any condensable impurities, such as Br_2. The pure HBr and dilutions in Ar were all stored in darkened Pyrex bulbs, and all gas-handling vacuum lines was also darkened to reduce the opportunities for photolysis of HBr while gases were transferred. To prevent from the interference of H_2 that potentially might be generated during storage, periodic condensations and distillations of HBr were performed. Iodoethane (99%, Lancaster), 1-iodopropane (99%, Aldrich), 2-iodopropane (99%, Aldrich),1-iodo-2-methyl propane (95%, Aldrich), trimethylsilyl iodide (Hüls America), were all degassed by repeated "freeze-pump-thaw" cycles at 77 K and stored in the dark, to avoid photochemical decomposition and I_2 removed as CuI_2, over several pieces of Cu foil. Hexamethyldisilane (Aldrich, 98%) and disilane (Matheson, 97% min.) were also purified in the same way as the other precursors. Gas mixtures were prepared from several percent of the pure vapor diluted in Ar and stored in either 2 or 5 l darkened bulbs. In order to have a uniform mixture, each mixture was prepared at least 2 hours before running the experiment to assure good mixing and diffusion.

HI and Cl_2 were synthesized in our laboratory. HI was made by the reaction of concentrated phosphoric acid with potassium iodide at 343 - 363 K.[56] The resulting HI was trapped by methanol slush (about 175 K), and purified several times by low temperature distillation from 240 K to remove any I_2 impurities until the final condensed HI was white. HI was stored in a darkened bulb to prevent any decomposition by room light. Cl_2 was produced by mixing concentrated HCl and $KMnO_4$ at room temperature,[57] and was purified in the same way as HI.

F. Data Analysis

For the R + HBr experiments, in which R represents an alkyl or silyl radical, the Br growth under pseudo-first-order conditions was analyzed according to the following scheme:

$$R + HBr \rightarrow RH + Br \quad (2.2)$$

$$R \rightarrow \text{other pseudo-first-order loss without generation of Br} \quad (2.3)$$

$$Br \rightarrow \text{pseudo-first-order loss by diffusion and other slow reactions} \quad (2.4)$$

The Br is expected[52,53] to vary as

$$[Br]=A \exp(-k_4 t) - B \exp(-k_{ps1} t) \quad (2.5)$$

where $k_{ps1} = k_2[HBr] + k_3$. The four parameters in eq. (2.5) were obtained in two steps from non-linear least-square fits to the fluorescence growth and decay. First, k_4 was obtained by fitting the Br signal plus constant background from scattered light to an exponential decay over a long time scale, such as that shown in Figure 1a. Then, k_{ps1}, A, and B were obtained from a weighted least-squares fit of eq. (2.5) to the fast growth of Br, see Figure 1b. The second-order rate constants k_2 were derived form the slope of the plots of pseudo-first-order growth vs. [HBr], as illustrated in Figure 2. Here, k_3 represents the slow diffusion of alkyl or silyl radicals to the reactor walls and a slow reaction with precursor while k_4 accounts for Br loss by diffusion and any other removal slow processes.

The decay of Br in the Br + Si_2H_6 experiments was analyzed by a simple exponential function because the concentration of Br is expected to vary as

$$-d[Br]/dt = k_6[Br][Si_2H_6] + k_{diff}[Br] = k_{ps1}[Br] \quad (2.6)$$

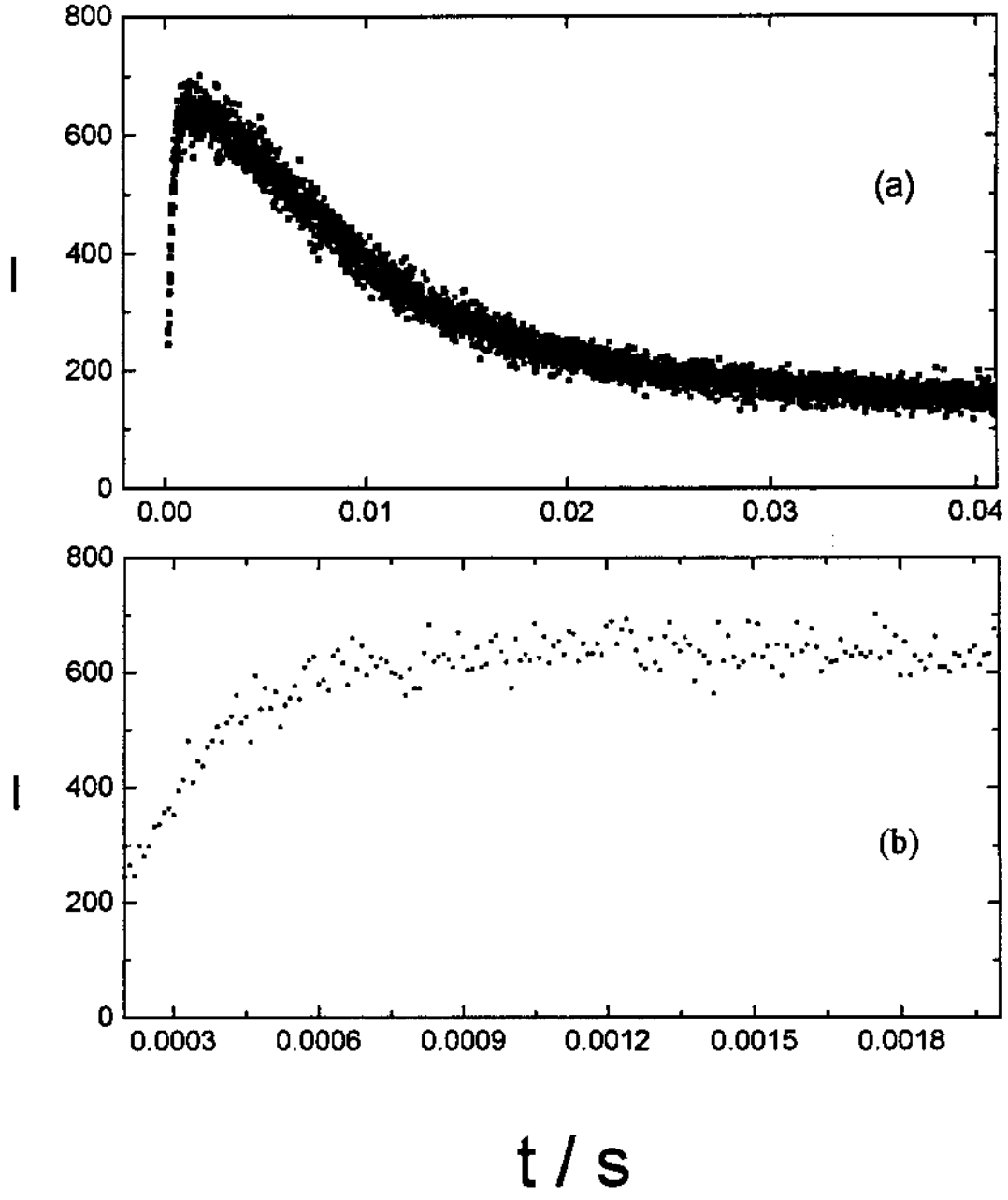

Figure 1. Plot of fluorescence intensity I (including background scattered light) of Br vs. time t obtained at (a) long time and (b) short time scale resolutions in R + HBr reaction, corresponding to the conditions of Figure 2.

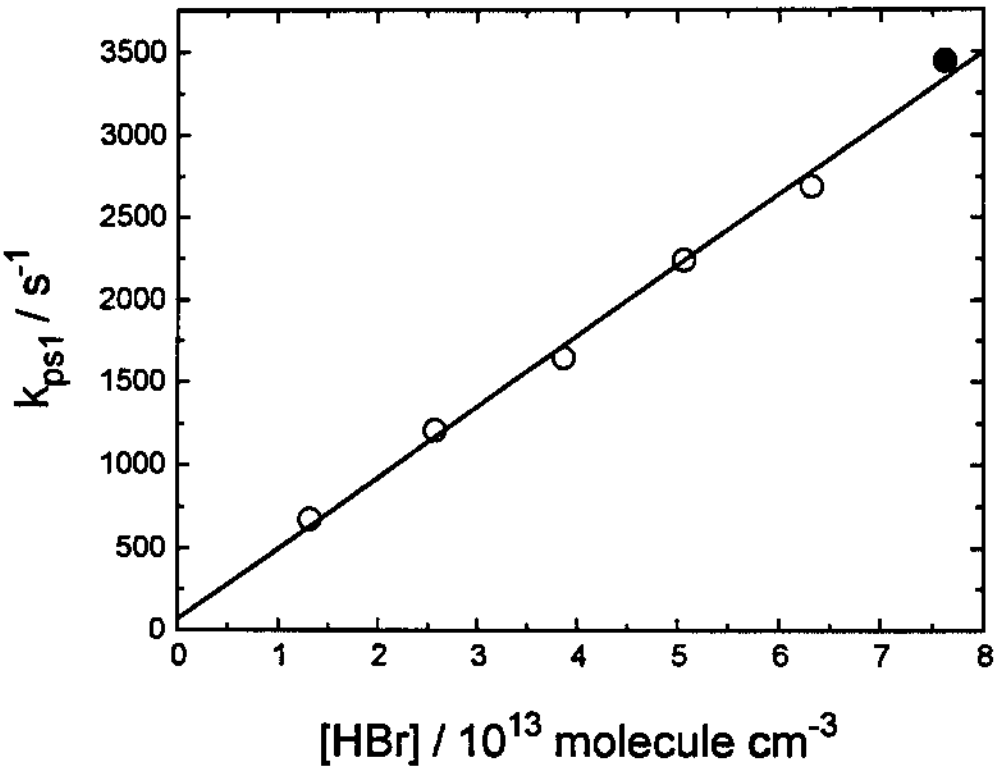

Figure 2. Plot of pseudo-first-order rate constant for formation of Br vs. [HBr] in n-propyl + HBr reaction at 463 K and 30.0 mbar. The filled circle corresponds to the data of Figure 1.

where k_{diff} represents the slow diffusion of Br from the reaction zone to the walls and any other loss pathways other than reaction with Si_2H_6. Integration of (2.6) results in

$$[Br] = [Br]_0 \exp(-k_{ps1}t) \quad (2.7)$$

where $[Br]_0$ is the concentration of Br at time 0. In the analysis algorithm, a steady background from the scattered light must be taken into account, so (2.7) can be modified as follows to account for the observed fluorescence signal I:

$$I = C \exp(-k_{ps1}t) + D \quad (2.8)$$

where C and D are constants and D represents the background. An example of a Br decay is shown in Figure 3. The second-order rate constant k_6 was derived from the slope a linear plot of k_{ps1} vs. $[Si_2H_6]$.

For Cl + HI experiment, HI and Cl_2 were premixed with the flow of Ar before entering the reactor, under "slow flow" conditions. Since the concentration of HI is much higher than the concentration of Cl, we can assume the reaction of Cl + HI is a pseudo-first-order reaction. The analysis of the signals (Cl or I) was carried out with different algorithms, both of them based on the following kinetic scheme:

$$Cl_2 \rightarrow 2Cl \quad (2.9)$$

$$Cl + HI \rightarrow HCl + I \quad (2.10)$$

$$Cl \rightarrow \text{pseudo-first-order loss by diffusion} \quad (2.11)$$

$$I \rightarrow \text{pseudo-first-order loss by diffusion} \quad (2.12)$$

The decay of Cl is analyzed by a simple exponential function because the [Cl] is expected to vary as

$$[Cl]=A \exp(-k_{ps1}t) \quad (2.13)$$

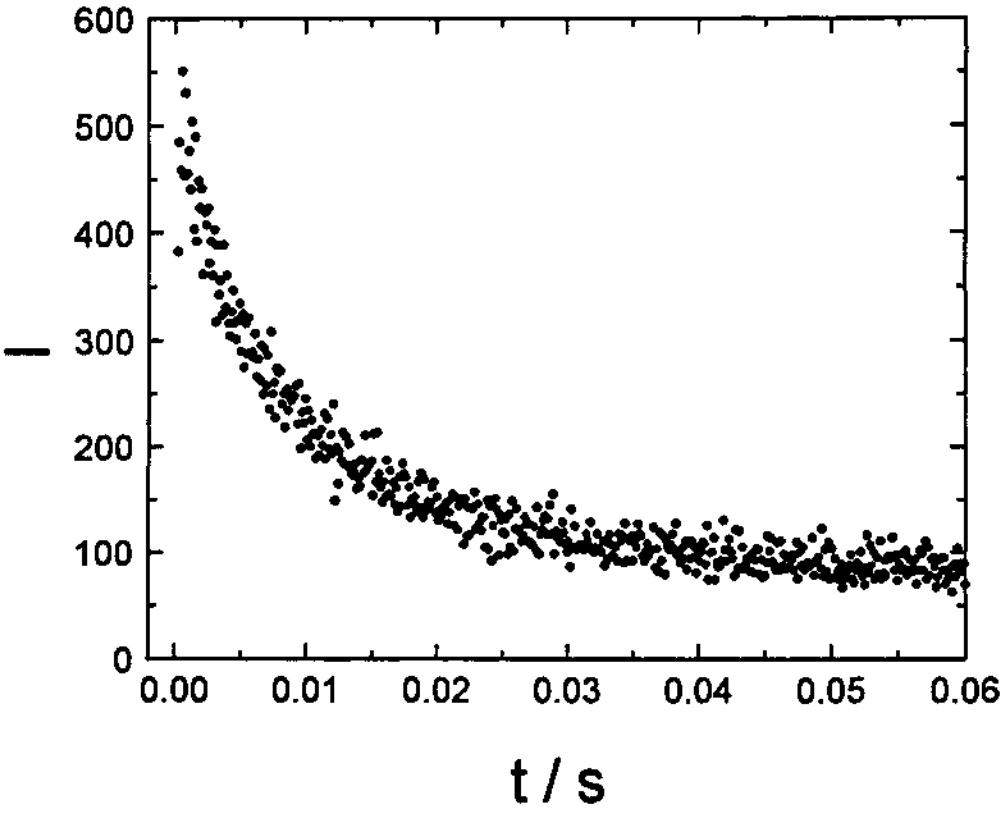

Figure 3. Plot of fluorescence intensity I (including background) of Br vs. time for Si_2H_6 + Br reaction at 73.3 mbar and 341 K

where $k_{ps1}=k_{10}[HI] + k_{11}$. The second-order rate constant k_{10} is derived from the slope of the plots of pseudo-first-order k_{ps1} vs [HI], and k_{11} represents the slow diffusion of Cl from the reaction zone to the walls. Figure 4a shows a typical Cl decay.

A double exponential function is used to express the growth of I:

$$[I]= B \exp(-k_{12}t) - C \exp(-k_{ps1}t) \qquad (2.14)$$

By integration of the rate law for the above reactions ((2.10)-(2.12)), $B = ([I]_0 (k_{12} - k_{ps1}) + k_{10}'[Cl]_0)/ (k_{12}-k_{ps1})$ and $C = k_{10}'[Cl]_0/(k_{12}-k_{ps1},)$ where $[Cl]_0$ is the Cl atom concentration at time 0 and $k_{10}' = k_{10}[HI]$. The four parameters in equation (2.14) were derived in two steps. First the diffusion constant of I, k_{12}, is obtained from fitting the I signals along with the background from scattered light by the simple exponential equation on a long time scale (such as 20 - 200 ms). Then k_{12} is employed in equation (2.14), a double exponential function, to find k_{ps1} by a weighted least-square fit over a short time scale (such as 0-15 ms). Figure 4b shows the growth of I followed by slow diffusional decay over this short time scale. k_{10} was obtained as the slope of a plot of k_{ps1} vs [HI]. An example is shown in Figure 5, where similar k_{10} values are seen for k_{ps1} derived from monitoring [Cl] or [I].

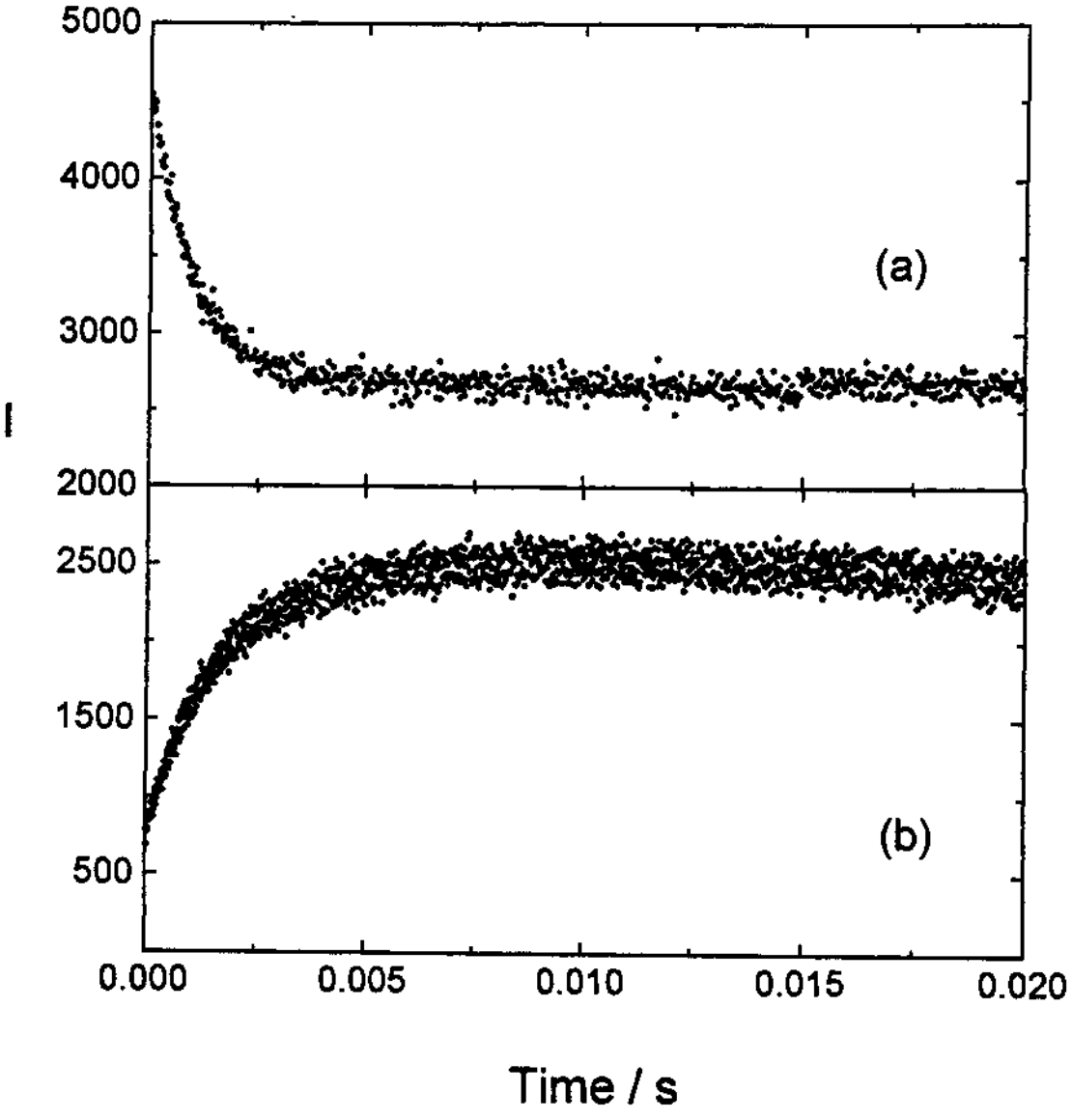

Figrue 4. Plot of fluorescence intensity (I) of (a) Cl decay and (b) I decay vs. Time at the same conditions.

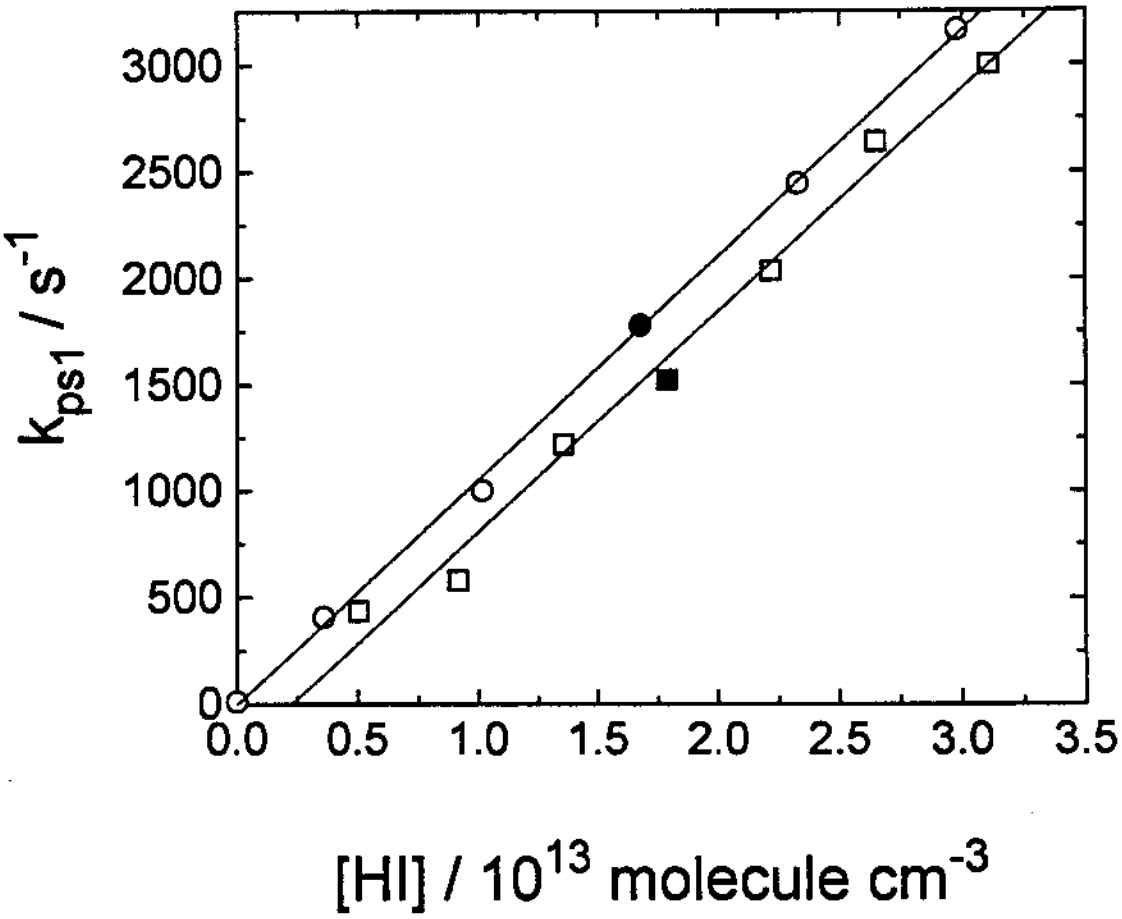

Figure 5. Plot of pseudo-first-order rate constants (k_{ps1}) for formation of I (□) and loss of Cl (○) vs. [HI] at 354 K. Solid symbols marked correspond to the data of Figure 4.

CHAPTER 3

KINETICS AND THERMOCHEMISTRY OF ALKYL AND SILYL RADICALS

A. HBr Absorption Cross Section (ϵ) Determination

HBr cross sections were measured under a variety of conditions. According to the Beer-Lambert law, ϵ (base e) at 186.5 nm was determined by the slope of $\ln(I_0/I)$ vs. [HBr] (eq.(2.1)) plots over the approximate [HBr] range of 0 - 10^{16} cm^{-3}. Figures 6 and 7 show Beer-Lambert plots for measurements in the Pyrex and steel reactors. In the Pyrex reactor $\epsilon = 1.85 \times 10^{-18}$ and 1.92×10^{-18} cm^2 $molecule^{-1}$ for "static HBr" and a value of 1.95×10^{-18} cm^2 $molecule^{-1}$ was obtained for a slow flow of diluted HBr. Here, "static HBr" means a certain amount of HBr was put into the reactor before starting any measurements which were performed with no gas flow. These values lie between the measurements of 1.77×10^{-18} cm^2 $molecule^{-1}$ by Romand[58] and 2.2×10^{-18} and 2.29×10^{-18} cm^2 $molecule^{-1}$ by Goodeve[59] and Nee[60], respectively. Static HBr in the steel reactor gave an ϵ value of 5.4×10^{-19} cm^2 $molecule^{-1}$, about 1/4 or less of the result from the Pyrex reactor, while for a slow flow of diluted HBr, values of 1.84×10^{-18} and 2.11×10^{-18} cm^2 $molecule^{-1}$ were obtained after a steady flow of mixtures was passed for 20 min. This indicated that there is no significant loss of HBr in either the steel or Pyrex reactor under slow flow conditions. The surface of the steel reactor needed to be saturated with HBr for at least 20 minutes before the actual kinetic data were taken.

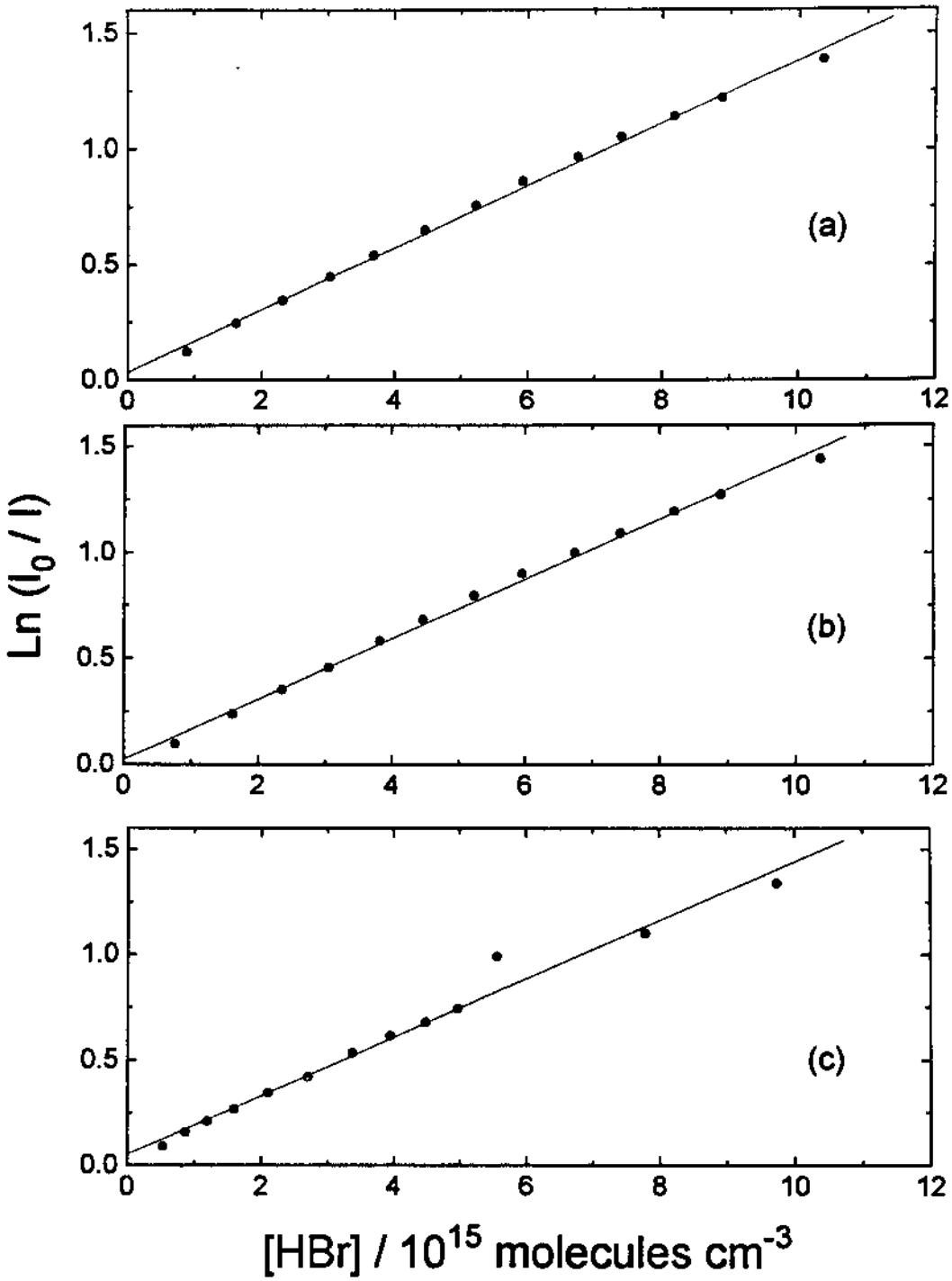

Figure 6. Measurement of the light absorption by HBr at 186.5 nm of wavelength $\ln(I_0 / I)$ vs. [HBr] in the Pyrex tube. (a) static HBr (b) static HBr (c) slow flow of HBr with Ar (30/50 sccm)

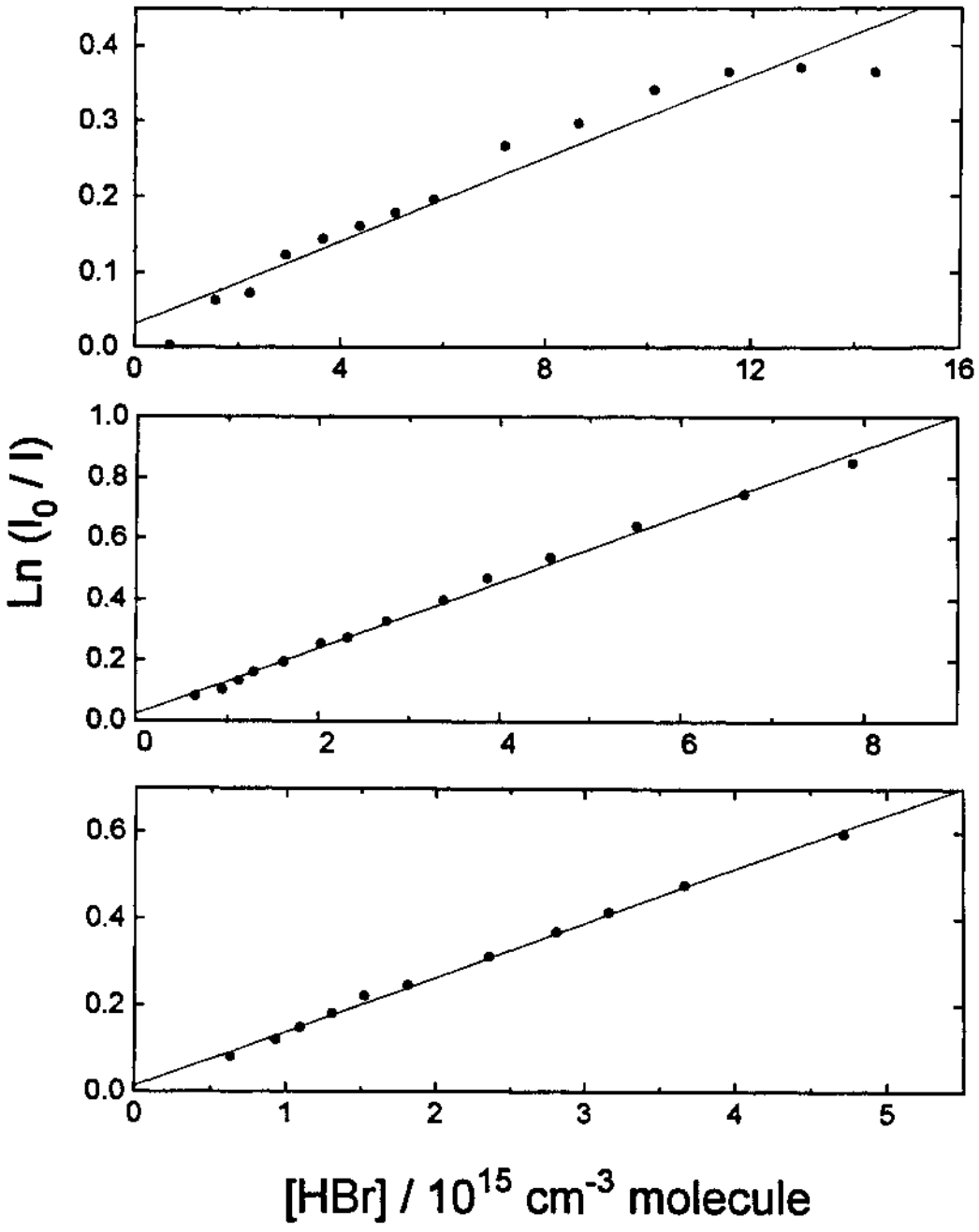

Figure 7. Measurement of the light absorption by HBr at wavelength of 186.5 nm ($\ln(I_0/I)$) vs. [HBr] in the steel reactor. (a) static HBr (b) slow flow of HBr with Ar (30/50 sccm). (c) slow flow of HBr with Ar (50/100 sccm)

B. Kinetic Study Results And Discussion

Study of the alkyl + HBr reactions. Preliminary checks showed that there were no signals from photolysis of either alkyl iodide or HBr alone which could interfere with the observation of Br decay. HBr absorption experiments also showed that there is no HBr loss in either of the reactors employed for kinetic measurements. The rate constants for reaction

$$t\text{-}C_4H_9 + HBr \rightarrow Br + i\text{-}C_4H_{10} \qquad (3.1)$$

at 295 K, obtained under different sets of conditions are listed in Table 2. The weighted mean of the rate constants with 1σ statistical errors are (2.51 ± 0.16) and (2.95 ± 0.18) x 10^{-11} cm^3 $molecule^{-1}$ s^{-1} for the steel and glass reactor, respectively (±1σ precision), and Student's t-test shows no significant dependence on the reactor type at the 95 % confidence level. The results are also independent of the photolysis wavelength, the flash lamp energy F and the precursor concentration, indicating that the primary reaction was successfully isolated from any interference by photolysis or reaction products. The weighted mean $k_{3.1}$ is (2.67 ± 0.13) x 10^{-11} cm^3 $molecule^{-1}$ s^{-1}. Tables 3 and 4 summarize the rate constant measurements for the following two reactions

$$i\text{-}C_3H_7 + HBr \rightarrow Br + C_3H_8 \qquad (3.2)$$

$$C_2H_5 + HBr \rightarrow Br + C_2H_6 \qquad (3.3)$$

at room temperature. The weighted mean values are $k_{3.2}$ = (1.25 ± 0.06) x 10^{-11} cm^3 $molecule^{-1}$ s^{-1} and $k_{3.3}$ = (7.01 ± 0.15) x 10^{-11} cm^3 $molecule^{-1}$ s^{-1}, respectively. Kinetic data for the reaction

$$n\text{-}C_3H_7 + HBr \rightarrow Br + C_3H_8 \qquad (3.4)$$

are summarized in Table 5. There is a similar check for any dependence of $k_{3,4}$ on the experimental parameters, as noted above for $k_{3,1}$, and the independence of $k_{3,4}$ from τ_{res} shows that thermal decomposition of the reagents was negligible at elevated temperatures. The Arrhenius plot for the n-propyl + HBr reaction is shown in Figure 8. Four $k_{3,4}$ measurements were averaged at each temperature, except for the points at 296 and 520 K which included 11 and 8 measurements, respectively. The best fit expression for this reaction is

$$k_{3,4} = (6.19 \pm 1.12) \times 10^{-13} \exp(7.14 \pm 0.58 \text{ kJ mol}^{-1} / RT) \text{ cm}^3 \text{ s}^{-1} \qquad (3.5)$$

where the errors are 1σ precisions and combinations of these errors with the covariance leads to 1σ precisions for $k_{3,4}$ of 3 - 8 %.

Comparison of Alkyl + HBr Rate Constants with Prior Determinations. Table 6 summarizes the other rate constants available[52,53,61,62,63] for alkyl + HBr reactions at room temperature as well as the results in this investigation. For both the C_2H_5 and i-C_3H_7 + HBr reactions, the rate constants measurements obtained here are slightly lower than the data from the other groups, but there no significant difference in the rate constant of t-C_4H_9 radical reaction compared with the others. This means that any systematic errors are not large for these measurements. For the C_2H_5 + HBr reaction, the room temperature rate constant obtained here is about 25% and 20% lower than the values reported by Gutman and co-workers[61] using the laser photolysis/photoionization mass spectroscopy technique and by Wine and co-workers[52] using the laser photolysis/resonance fluorescence technique, respectively. The rate constant, $(1.3 \pm 0.2) \times 10^{-11}$ cm^3 molecule^{-1}

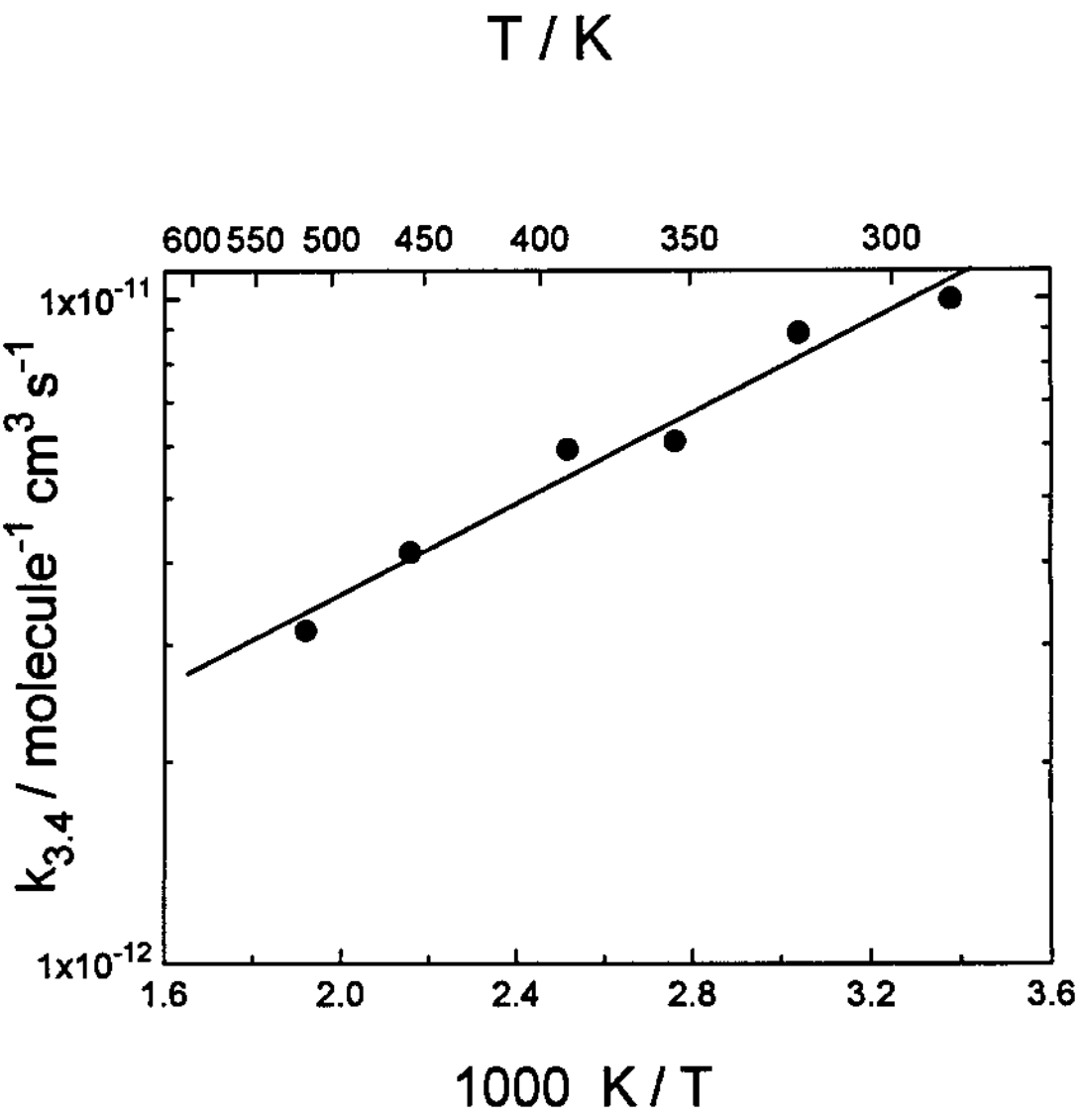

Figure 8. Arrhenius plot of n-propyl + HBr reaction. Solid line is the Arrhenius fit from the linear least-square analysis experimental data.

Table 6 : Comparison of Rate Constants of Alkyl + HBr with Other Measurements

reactions	[a]exp. method	Temp	k, cm^3 $molecule^{-1}$ s^{-1}	ref
C_2H_5 + HBr	LP-PIMS	297	[b](9.4 ± 1.0) x 10^{-12}	[61]
	LP-RF	297	[c](8.7 ± 0.3) x 10^{-12}	[52]
	FP-RF	297	[c](7.0 ± 0.4) x 10^{-12}	this work
i-C_3H_7 +HBr	LP-PIMS	298	[b](1.9 ± 0.6) x 10^{-11}	[61]
	LP-RF	297	[c](1.3 ± 0.2) x 10^{-11}	this work
t-C_4H_9 +HBr	LP-PIMS	298	[b](2.8 ± 0.6) x 10^{-11}	[61]
	LP-RF	297	[b](2.6 ± 0.1) x 10^{-11}	[52]
	LP-RF	298	(3.2 ± 1.0) x 10^{-11}	[53]
	VLPϕ corr.	298	(2.1 ± 0.6) x 10^{-13}	[62]
	LP-DLA	298	[b](1.0 ± 0.2) x 10^{-11}	[63]
	FP-RF	295	[c](2.7 ± 0.1) x 10^{-11}	this work

[a]FP, flash photolysis; RF, resonance fluorescence; LP, laser photolysis; PIMS, photoionization mass spectroscopy; VLPϕ corr., very low photolysis corrected by t-C_4H_9 + DBr; DLA, diode laser absorption
[b]Errors are 2σ and refer to statistical uncertainty only.
[c]Weighted mean values with 2σ precisions.

s^{-1}, at 297 K for i-C_3H_7 + HBr reaction in this study is lower than the only one comparable data which has the value of $(1.9 \pm 0.6) \times 10^{-11}$ cm^3 $molecule^{-1}$ s^{-1}.[61] By far, the most studied alkyl +HBr reactions are those involving the t-C_4H_9 radicals. The two measurements from Seakins et al.[61] and Nicovich et al.,[52] as well as the value in this study, are in pretty good agreement. Richards et al.[63] generated t-C_4H_9 radicals by 193 nm laser flash photolysis of 4,4-dimethyl-1-pentene and monitored the appearance of the products, isobutane, using IR diode laser spectroscopy to obtain the rate constant of the t-C_4H_9 + HBr reaction. The room temperature rate constant, $(1.0 \pm 0.2) \times 10^{-11}$ cm^3 $molecule^{-1}$ s^{-1}, reported by Richards et al., is about the same as one published by Gutman's group in 1988,[64] but much lower than the other following reported data. Gutman's group claimed that the HBr used in their initial investigation was in fact contaminated with large amounts of H_2, an HBr decomposition product, and revised their results in a later publication. Müller-Markgraf et al.[62] studied the reaction DBr + t-C_4H_9 = Br + t-C_4H_9D in a very low pressure photolysis (VLPϕ) apparatus. After correction for the primary isotope effect, they calculated a rate constant of $(2.1 \pm 0.6) \times 10^{-13}$ cm^3 $molecule^{-1}$ s^{-1} at 295 K that is much lower than the three values mentioned above. There is no prior source of n-propyl + HBr data to be compared with. The negative activation energy, -7.4 kJ mol^{-1}, derived from measurements is similar to literature values of -6.4 kJ mol^{-1} for i-C_3H_7 + HBr and -7.8 kJ mol^{-1} for t-C_4H_9 + HBr reactions, and seems to be reasonable.

Study of the Trimethylsilyl + HBr Reaction. In most experiments, trimethylsilyl radicals were generated by flash photolysis of hexamethyldisilane; trimethylsilyl iodide was also

used as the photolysis precursor for some room temperature measurements. Preliminary experiments with resonance fluorescence detection confirmed that I atoms were formed. Halogen exchange between HBr and $(CH_3)_3SiI$ was negligible.[65] Although the photolysis photons were energetic enough to break C-H or Si-C bonds in $Si_2(CH_3)_6$, the rate constants for H and CH_3 with HBr are an order of magnitude smaller than the rate constant measured here.[66] In a separate experiment, $Si(CH_3)_3I$ photolysis through MgF_2 optics combined with the resonance fluorescence detection of H atom (without a CaF_2 window) gave no signals. This indicates that the photolysis of methyl C-H bond is not significant. In the MgF_2 photolysis, a small concentration of Br was produced initially due to photolysis of a small amount of HBr at the shorter wavelength, and this small contribution of Br did not effect the values of rate constant derived. Kinetic results for the reaction

$$Si(CH_3)_3 + HBr \rightarrow Br + HSi(CH_3)_3 \qquad (3.6)$$

are summarized in Table 7, and Arrhenius plot for this reaction is shown in Figure 9. The best fit expression is

$$k_{3.6} = (8.1 \pm 2.0) \times 10^{-12} \exp (5.12 \pm 0.72) \text{ kJ mol}^{-1} / RT \text{) cm}^3 \text{ s}^{-1} \qquad (3.7)$$

for T = 289 - 515 K, where the statistical errors are 1σ. The statistical uncertainty in the fitted $k_{3.6}$ is about 10 %.

Study of the Br + Si_2H_6 Reaction. For the reaction

$$Si_2H_6 + Br \rightarrow \text{products} \qquad (3.8)$$

twenty-nine measurements of $k_{3.8}$ are summarized in Table 8. No consistent variations

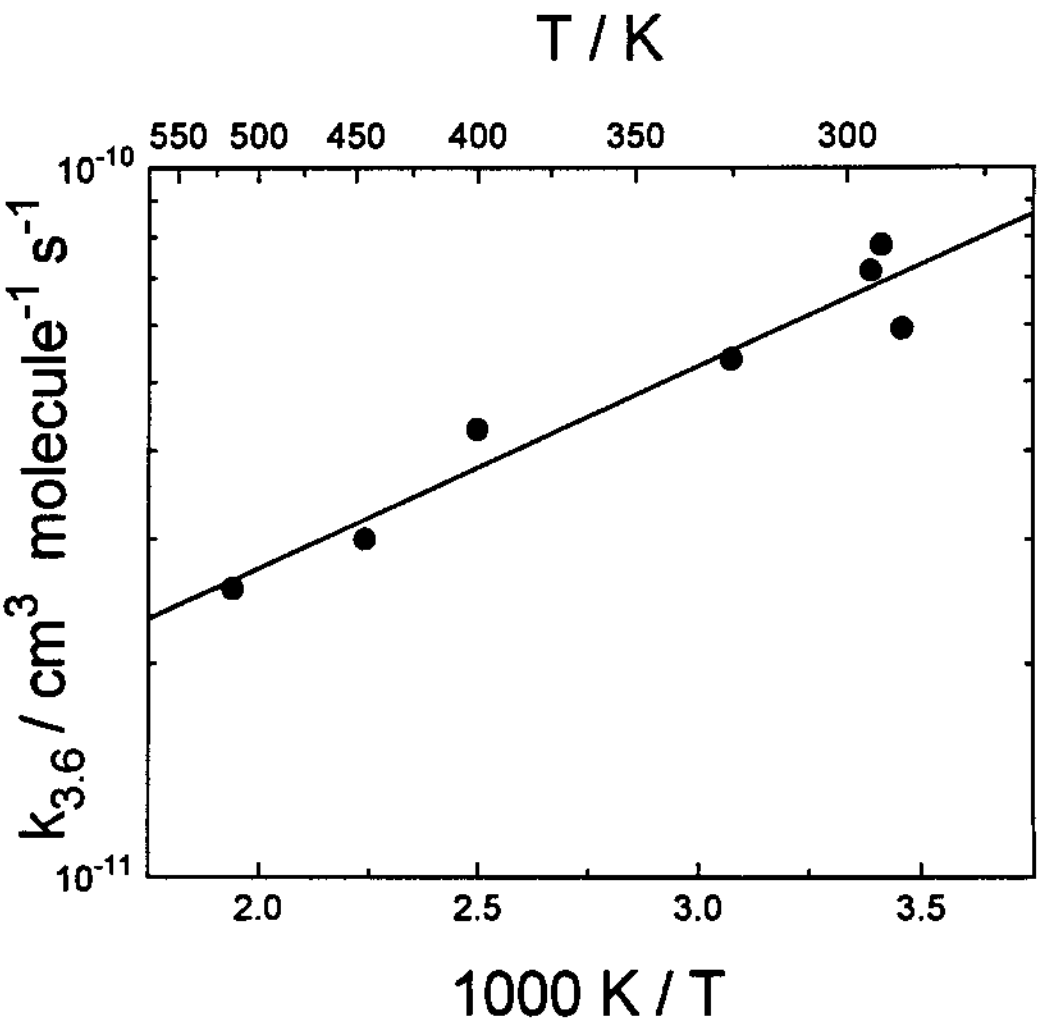

Figure 9. Arrhenius plot of trimethylsilyl + HBr reaction. Solid line is the linear least-square fit to the experimental data.

with the experimental parameters, such as flash energy, pressure, and [CH_2Br_2] were found. This showed that the primary reaction channel was successfully isolated from any secondary reaction which could result from the decomposition of Si_2H_6 with other photolysis products. The results are plotted in Arrhenius form as shown in Figure 10. The fitted line is obtained from linear least-square analysis of the $k_{3.8}$ vs. T^{-1} plot , and the resulting equation is

$$k_{3.8} = (1.35 \pm 0.12) \times 10^{-10} \exp(-3.05 \pm 0.3) \text{ kJ mol}^{-1} / RT) \text{ cm}^3 \text{ s}^{-1} \quad (3.9)$$

for T between 295 and 565 K. Errors in the above expression are 1σ and represent precision only. Consideration of the covariance in A-factor and the activation energy resulted in an uncertainty of $k_{3.8}$ of about 7%. Allowance for unrecognized but possible systematic errors of about 5% leads to estimated accuracy limits of ± 12% of $k_{3.8}$. No previous determination of $k_{3.8}$ has been reported. The only comparison that can be made is with the rate constants of Br + SiH_4 reaction. In this reaction, the pre-exponential factor A measured to be (0.9 ± 0.15)[67] and (1.6 ± 0.6)[50] x 10^{-10} cm^3 s^{-1}, which are similar to the value of $(1.35 \pm 0.12) \times 10^{-10}$ cm^3 s^{-1} in this study of the Si_2H_6 + Br reaction . These close A factors suggest that a similar mechanism, i.e. simple H-atom abstraction, is associated with these two reactions. The smaller activation energy measured here for the Si_2H_6 + Br reaction compared to that of SiH_4 + Br indicated that this reaction is less endothermic than the SiH_4 + Br reaction.

C. Thermochemical Calculations

Theoretical Background. For a general reversible R + HBr reaction,

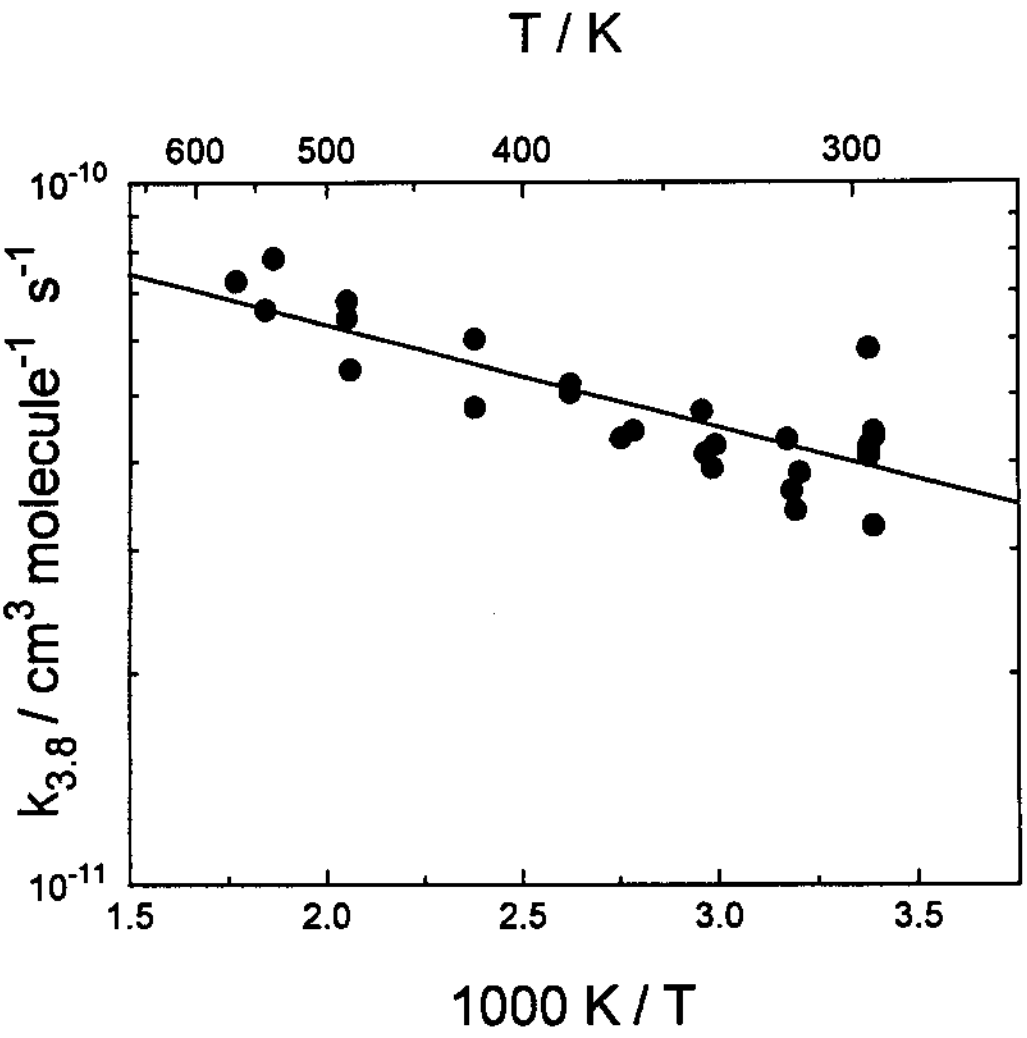

Figure 10. Arrhenius plot of Br + Si_2H_6 reaction. The fitted line is obtained from least-square analysis of $k_{3.8}$ vs. 1000 / T.

$$R + HBr \underset{k_b}{\overset{k_f}{=}} RH + Br \qquad (3.10)$$

if the forward and reverse rate constants (k_f and k_b) can be measured accurately as a function of temperature, the Arrhenius activation energies (E_f and E_b) are established. The difference of the activation energy at a particular temperature, typically the middle temperature of the forward and reverse reactions, is equal to the enthalpy change of the reaction. This enthalpy change can be corrected to 298 K using tabulated or estimated heat capacities, and the bond dissociation energy of R-H was derived via the known BDE_{298} (HBr).

$$\Delta H^0(T)=E_f-E_b \qquad (3.11)$$

$$\Delta H^0_{298}=\Delta H^0(T)+\int_T^{298} dT[C_p^0(RH)+C_p^0(Br)-C_p^0(R)-C_p^0(HBr)] \qquad (3.12)$$

$$BDE_{298}(R-H)=\Delta H^0_{298}+BDE_{298}(HBr) \qquad (3.13)$$

This is the **second law** method for obtaining BDE(R-H). Also, the entropy change can be obtained at the selected temperature in this second law method since the Gibbs energy of the reaction is derived directly from the ratio of the rate constants for the forward and reverse reactions. If k_f and k_b can be determined only at a single temperature, the more limited information must be associated with other thermochemical data, like entropies and heat capacities of the species, to derive BDE (R-H). This is called the **third law** method.

The equations used to derive the result are as follows:

$$\Delta G^0(T) = -RT\ln K_{eq} = -RT\ln\left(\frac{k_f}{k_b}\right) \tag{3.14}$$

$$\Delta S^0(T) = \Delta S^0(T_1) + \int_{T1}^{T} \frac{1}{T}[C_p^0(RH) + C_p^0(Br) - C_p^0(R) - C_p^0(HBr)]dT \tag{3.15}$$

$$\Delta H^0(T) = \Delta G^0(T) + T\Delta S^0(T) \tag{3.16}$$

where T_1 is the temperature at which the entropy information are available. Again, as mentioned above, the enthalpy change can be corrected to 298 K and BDE_{298} (R-H) is obtained [eq.(3.12), (3.13)]. Second and third law methods can be applied to a van't Hoff plot of $\ln K_p$ against 1/T, where the slope is $-\Delta H^0/R$ and the intercept is $\Delta S^0/R$. K_p is the equilibrium constant at several temperatures. A correction to account for the temperature dependence of ΔH^0 and ΔS^0,

$$\text{correction} = \frac{\Delta C_{p,298}^0}{R}\left(\frac{T-298}{T} + \ln\frac{298}{T}\right) \tag{3.17}$$

is applied to $\ln K_p$:

$$\ln K_p + \text{correction} = \frac{\Delta S_{298}^0}{R} - \frac{\Delta H_{298}^0}{RT} \tag{3.18}$$

The modified van't Hoff plot[68,69,70] is a plot of $\ln K_p$ + correction vs. 1/T.

In the second law procedure, the standard entropy and enthalpy of reaction (3.10) were determined as the parameters of the best linear fits to a plot of $\ln K_p$ + correction vs 1/T. The third law procedure uses a separately determined value of the standard entropy of reaction, and, therefore, has only one fitted parameter, ΔH^0_{298}.

Calculations of C-H Bond Energies. The bond dissociation energies of C_2H_5-H, (i-C_3H_7)-H, (t-C_4H_9)-H have been calculated by the third law method. In this method, the equilibrium constants of these reactions ((3.1), (3.2), and (3.3)) was derived as the ratio of the rate constants for the forward reaction at room temperature in this investigation and the rate constants at the same temperature for the backward reactions from Seakins et al.[61] The derived equilibrium constant at room temperature was combined with the thermochemical data, such as entropies and heat capacities, to derive ΔH^0_{298}. The rate constants[61] and thermochemical information (heat capacities, entropies)[71,72,73,74] used in both second and third law calculations for alkyl + HBr reactions are given in Table 9. For the n-propyl + HBr reaction, since the temperature-dependent rate constants were obtained for both forward and backward reactions, the entropy and enthalpy change from the second law method and enthalpy from the third law method were derived from the fit parameters of a modified van't Hoff plot. The correction term in this reaction was calculated using the heat capacities of Br, HBr, n-C_3H_7, and C_3H_8 (see Table 9). The standard enthalpy and entropy of this reaction obtained by the second law method are

$\Delta H^0_{298} = -59.8 \pm 2.7$ kJ mol^{-1} (second law)

$\Delta S^0_{298} = -47.1 \pm 4.1$ J mol^{-1} K^{-1} (second Law)

Table 9: Rate Constants, Entropies, and Heat Capacities Used in the Thermochemical Calculations

	$k_{3,3}$[a] = 7.01 x 10^{12} cm^3 s^{-1}			
	C_2H_5 + HBr ⇌ C_2H_6 + Br			
	$k_{3,-3}$[b] = 9.92 x 10^{-20} cm^3 s^{-1}			
S^0_{300} (J mol^{-1} K^{-1})	248.29[d]	198.70[c]	229.38[d]	175.02[c]
$C_p^0{}_{300}$ (J mol^{-1} K^{-1})	50.74[d]	29.14[c]	52.71[d]	20.79[c]
	$k_{3,2}$[a] = 1.25 x 10^{-11} cm^3 s^{-1}			
	i-C_3H_7 + HBr ⇌ C_3H_8 + Br			
	$k_{3,-2}$[b] = 4.83 x 10^{-17} cm^3 s^{-1}			
S^0_{300} (J mol^{-1} K^{-1})	289.80[e]	198.70[c]	270.37[e]	175.02[c]
$C_p^0{}_{300}$ (J mol^{-1} K^{-1})	66.61[e]	29.14[c]	73.89[e]	20.79[c]
	$k_{3,4}$[a] = (6.19 ±1.12) 10^{-12} exp (7.14 ± 0.58 kJ/RT) cm^3 s^{-1}			
	n-C_3H_7 + HBr ⇌ C_3H_8 + Br			
	$k_{3,-4}$[b] = (2.4 ±1.1) x 10^{-10} exp (-53.4 ± 2.1 kJ/RT) cm^3 s^{-1}			
S^0_{300} (J mol^{-1} K^{-1})	289.41[e]	198.70[c]	270.37[e]	175.02[c]
$C_{p_0}{}^0{}_{300}$ (J mol^{-1} K^{-1})	71.53[e]	29.14[c]	73.89[e]	20.79[c]
$C_p{}_{500}$ (J mol^{-1} K^{-1})	106.16[e]	29.45[c]	113.14[e]	20.80[c]
	$k_{3,1}$[a] = 2.67 x 10^{-11} cm^3 s^{-1}			
	t-C_4H_9 + HBr ⇌ C_4H_{10} + Br			
	$k_{3,-1}$[b] = 1.28 x 10^{-15} cm^3 s^{-1}			
S^0_{300} (J mol^{-1} K^{-1})	320.10[f]	198.70[c]	295.3[f]	175.02[c]
$C_p^0{}_{300}$ (J mol^{-1} K^{-1})	78.61[f]	29.14[c]	97.28[f]	20.79[c]

[a] in this study
[b] ref 61
[c] ref 71
[d] ref 72
[e] ref 73
[f] ref 74

The third law correction method used the separately calculated ΔS^0_{298}, -42.6 J mol-1 K^{-1}, to fit the intercept of the modified van't Hoff plot and yielded

$$\Delta H^0_{298} = -58.2 \pm 1.7 \text{ kJ mol}^{-1} \text{ (third law)}$$

Figure 11 illustrates the modified van't Hoff plot of second and third law methods in determining the thermochemical properties of the n-propyl +HBr reaction. The bond dissociation enthalpies from both methods combined with BDE_{298}[71] (HBr) = 366.3 kJ mol^{-1} yield BDE_{298}(C-H) for different alkanes. In the third law method, the error limits of ΔH are the combined estimated errors in the rate constant measured for both forward and reverse directions, temperature uncertainty, and uncertainties of the calculated reaction entropies. Allowance of a poor accuracy of 15% errors due to systematic or other unrecognized errors in the rate constants measured for both the forward and backward directions will result in about ±0.5 kJ mol^{-1} changes in the Gibbs energy. This value will combine with the contribution from the uncertainties in the entropy change of the reaction and temperature errors. The estimated errors in the calculated entropy change of the reaction are largely determined by the uncertainties of the radical entropies since the entropies of the other species in the reaction are already well known. The assessments of the uncertainty for each radical were discussed in Gutman's publication.[61] He suggested the different error limits, ±3, ±4, and ±6 J mol^{-1} K^{-1} for C_2H_5, i-C_3H_7, and t-C_4H_9, respectively. The uncertainty of radical entropy changes increases with radical complexity due largely to the uncertainty in the magnitude of the barrier to internal rotations which can lower the radical entropies, particularly for t-C_4H_9. Here, a constant of ±4 J mol^{-1} K^{-1} uncertainty in ΔS^0 is assigned for each reaction for simplicity. This introduces an

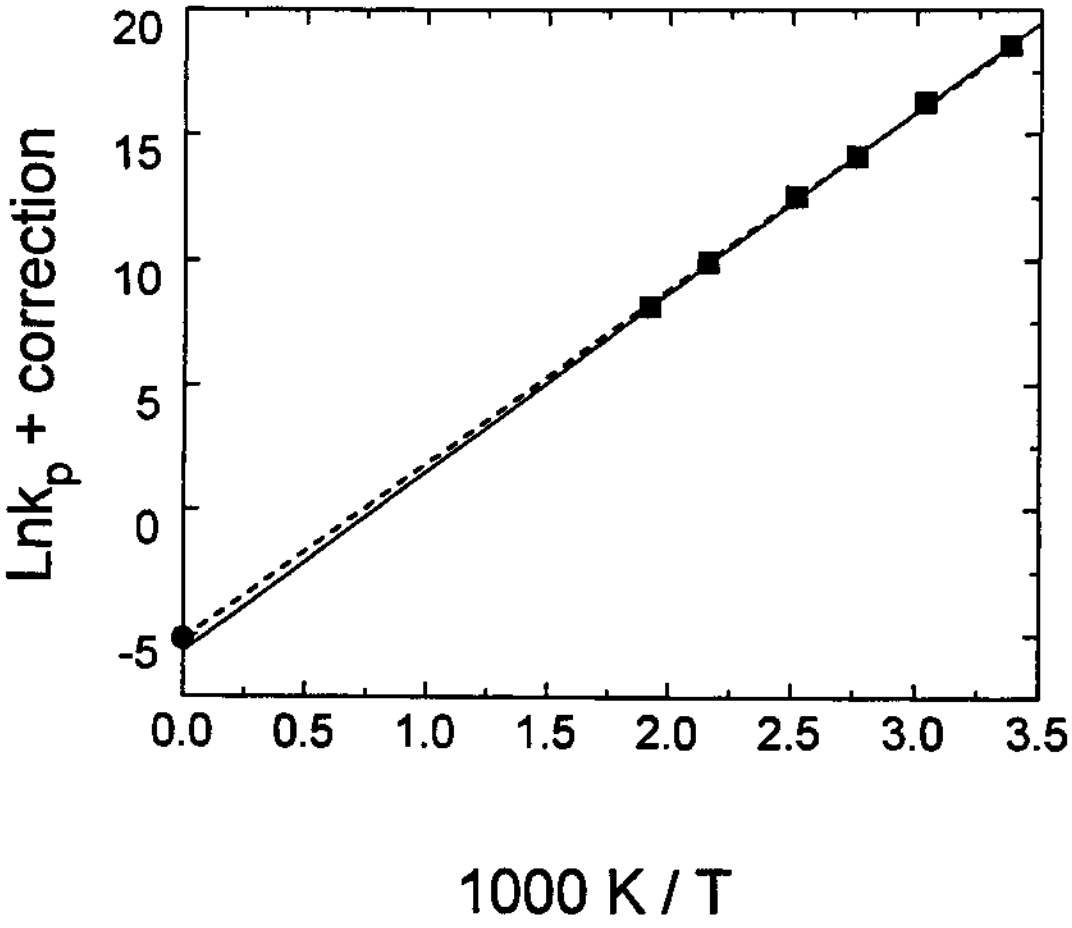

Figure 11. Modified van't Hoff plot of the equilibrium constant of the reaction n-C_3H_7 + HBr ⇌ C_3H_8 + Br. Shown are the second (solid line) and third (dash line) law fits of data (■). The point at 1/T = 0 (●) used in the third law procedure was calculated from the standard entropies of the reagent and product molecules (see text).

uncertainty of 1.2 kJ mol^{-1} into ΔH^0_{298}. Since the uncertainty from the temperature is negligible in ΔH^0_{298} compared to other two sources, a suggested error limit of ±2 kJ mol^{-1} is assigned in the third law calculation of ΔH^0_{298} by the combination of two error sources. In the second law calculation of ΔH^0_{298} for n-propyl + HBr, the measured ΔH^0_{298} is derived from the van't Hoff plot of $\ln K_p$ vs. 1/T over a suitable temperature range. The precision of ΔH^0_{298}, the slope in the plot, needs a good measure of K_p, mainly accurate activation energies for forward and backward reactions. By combinations of the absolute uncertainties in activation energies for both forward and backward reactions, a resulting higher error limit of ± 3 kJ mol^{-1} is suggested for the second law determination of ΔH^0_{298}.

Comparison of C-H Bond Strength of Alkanes with Values Obtained in Previous Studies. The calculated C-H bond strength of alkanes at 298 K were compared with data obtained previously and summarized in Table 10.[25,26,61,52,62] Virtually all the recent determinations of the BDE_{298}(C-H) in C_2H_6 as well as the value in the study are around the range of 422 - 424 kJ mol^{-1}. The only exception is the assessment by McMillen and Golden[26] who used the older thermochemical data for reaction (3.3), where an assumed positive activation energy for the forward reaction was used in the calculation. The same disparities were discovered in the i-(C_3H_7)-H, and t-(C_4H_9)-H molecules which showed lower C-H bond energies than the other data compared here.

The secondary C-H bond strength of propane was calculated by Tsang[25] from the results of several combined kinetic studies that were used to obtain the equilibrium constants for two dissociation processes: (i-$C_3H_7)_2$ (dimethyl-butane) = 2 i-C_3H_7 or i-C_3H_7

$\rightleftharpoons$ i-C_3H_6 + H yielded 415.3 kJ mol^{-1}. Since Tsang's calculations are all third-law determinations of the heats of formation of alkyl radicals, they seem to be more accurate determinations of C-H bond strength than the other second law determinations which used the estimated activation energy in the calculation like one reported by McMillen and Golden.[26] A value of 409.9 ± 2 kJ mol^{-1} i-C_3H_7-H bond energy was suggested in that study which is about 3 and 5.4 kJ mol^{-1} lower than that recommended by Seakins[61] and Tsang's,[25] respectively. The primary C-H bond energies in C_3H_8 (ΔH^0_{298}, C_3H_8 → n-C_3H_7 + H) calculated by second and third law methods in this study showed good agreement. The average of these two values is BDE_{298} (n-C_3H_7-H) = 425.3 ± 3 kJ mol^{-1}. There are no previous direct kinetic data available concerning the equilibrium of HBr + n-C_3H_7 $\rightleftharpoons$ Br + C_3H_8 to access the primary C-H bond strength of C_3H_8, and the only reference data is the C-H bond energy of 422.5 kJ mol^{-1} derived by Tsang's calculation using the association/dissociation equilibria.

For i-C_4H_{10}, the third-law determination of the tertiary C-H bond energy relied on the rate constants at room temperature for the equilibrium reaction of t-C_4H_9 + HBr in the current investigation. The result reported here and those previous investigations from Seakins et al.,[61] and Tsang,[25] based on a zero barrier to methyl group rotation, provided what are believed to be good agreements for tertiary C-H bond strength in i-butane. However, a recent ab initio calculation[75] predicts that the barrier to methyl rotation is about 6.3 kJ mol^{-1} which will reduce the bond strength by about 3 kJ mol^{-1}. In addition to the disparities with the McMillen and Golden study which were discussed above, one study, that of Müller-Markgraf et al.,[62] also casts doubt on the agreement for

BDE(t-C_4H_9-H). They used a rate constant derived for reaction (3.1) by the VLPϕ technique combined with the rate constants for the reverse reaction, based on Russell et al.[76] and Kondo et al.,[77] to obtain ΔH^0_{298}= -5.96 and -6.65 kcal mol^{-1}, respectively. The mean of these two values combined with the 366.3 kJ mol^{-1} bond energy of HBr resulted in an average of 392.7 kJ mol^{-1} for the bond strength of (t-C_4H_9)-H. The reason for this lower bond dissociation energy is due to the rate constant measurements for reaction (3.1) are too low compared to the others.

Table 10: Comparison of R-H Bond Strength of Alkanes (kJ mol^{-1}) with Other Data Available at 298 K

	types of C-H			
	C_2H_5	i-C_3H_7	n-C_3H_7	t-C_4H_9
second law			426.1 ± 3	
third law	423.6 ± 2	409.9 ± 2	424.5 ± 2	405.1 ± 2
ref[61]	422.8 ± 2	412.7 ± 2		403.5 ± 2
ref[52]	423.4 ± 3			403.0 ± 3
ref[62]				392.7
ref[26]	411 ± 4	398 ± 4		390 ± 8
ref[25]		415.3	422.5	404.6[a]

[a]Zero barrier for the methyl rotation

Validation of the Additivity/Similarity Principles Employed in Deriving the Competitive Rate Constants of RH + Br Reactions. One of the main purposes to determine the bond energy of n-C_3H_7-H in this study is to verify the accuracy of the rate constant of C_3H_8 + Br, the reverse reaction of i-C_3H_7 + HBr, that was estimated by Gutman et al.[61]This assessment depends on the reliability of the thermochemistry and the rate constant for the forward reaction. Although there is no previous determination to compare with, the accuracy of $k_{3,4}$ is confirmed by the rate constants of similar reactions determined in the same system as compared with literature values. As mentioned before, all the rate constants of the reverse reaction of R + HBr used in the second and third-law calculations are those reported by Seakins et al.[61] For the propane and i-butane with Br reactions, the most interesting processes are the abstractions of secondary and tertiary H atoms, while the existence of the parallel reactions of primary H atom abstractions by bromine is possible in each case. Seakins and co-workers[61] applied the additivity/similarity principle to characterize the competitive abstraction processes in a single molecule. In this principle, two assumptions were made: (1) The Arrhenius A factor is determined by the collision frequency as well as the steric factor which means the degeneracy of the same type (primary, secondary, or tertiary) of hydrogen abstraction. (2) The activation energy associated with the same type of hydrogen abstraction is expected to be the same. Based on the above concepts, the overall rate constants can the expressed as the sum of the rates of the different hydrogen abstraction mechanisms. In the case of propane which contains six primary hydrogens for abstraction, the rate constant for secondary abstraction should be calculated by subtracting the rate constant of ethane hydrogen abstraction ($k_{3,-3}$) from

the observed rate constant. However, a value of $1.5k_{3,-3}$ will be subtracted to derive the rate coefficient of tertiary hydrogen abstraction for i-butane. These rules were employed to derive $k_{3,-1}$, $k_{3,-2}$, $k_{3,-3}$, and $k_{3,-4}$. Assuming that the concept of rate constant additivity is valid, the rate coefficient of primary hydrogen abstraction of propane, the rate constant of the reverse reaction of n-propyl with HBr, is the same as the observed rate constant of ethane with HBr. The derived Arrhenius parameters of $k_{3,-4}$ from this postulation were combined with the measured $k_{3,4}$ in this study to calculate the primary C-H bond strength of n-propane with the known BDE(HBr). The primary n-C_3H_7-H bond strength calculated from both second and third-law method are in good agreement. Also, the average value of 425.3 kJ mol^{-1} is close to the recommended bond strength of 422.5 kJ mol^{-1} by Tsang[25] using association/dissociation equilibria. This proves the validation of the concept of rate constant additivity in this case.

Si-H Bond Dissociation Energy in $(CH_3)_3SiH$. Both second and third law methods were used to obtain the standard enthalpy for the reaction $(CH_3)_3Si$ + HBr. To calculate the equilibrium constant of this reaction the rate constants measured as a function of temperature in this study were combined with the rate constants for the reverse reaction measured by Ding and Marshall,[37] which had Arrhenius parameters of $(7.6 \pm 3.3) \times 10^{-10}$ cm^3 $molecule^{-1}$ s^{-1} for the pre-exponential factor and (28.4 ± 1.3) kJ mol^{-1} for the activation energy. Thermodynamic properties, like entropies and heat capacities, of $Si(CH_3)_3$ and $HSi(CH_3)_3$ were calculated using the equations from Lewis[78] and the ab initio structural parameters, e.g. moments of inertia and vibrational frequencies, reported by Allendorf and

Melius.[79,80] The parameters and results of thermodynamic calculations used in reaction (3.6) are presented in Table 11.

Table 11: Entropies, and Heat Capacities Used in Trimethylsiliyl + HBr Reaction

Species	S^0_{298} (J mol^{-1} K^{-1})	$C_p{}^0_{298}$ (J mol^{-1} K^{-1})
$Si(CH_3)_3$	343.00[a]	114.95[a]
$HSi(CH_3)_3$	337.94[a]	120.49[a]
Br	175.02[b]	20.79[b]
HBr	198.70[b]	29.14[b]

[a] ref 79,80

[b] ref 71

The calculated entropy change of reaction 3.6 is ΔS^0_{298} = -28.6 J mol^{-1} K^{-1} and the resulting enthalpy from the slope of the modified van't Hoff plot is

ΔH^0_{298} = -30.2 ± 1.2 kJ mol^{-1} (third law)

Here, the 1σ uncertainties represented the combined errors in the accuracy of equilibrium constant which included uncertainties in the fit pre-exponential factor and activation energy, and temperature uncertainty (± 3 K) as well as ±1 J mol^{-1} K^{-1} error in the calculated ΔS^0_{298}. The entropy and enthalpy were derived by the second law method

following the same process as before, and yield

$\Delta H^0_{298} = -32.7 \pm 2.0$ kJ mol^{-1} (second law)

$\Delta S^0_{298} = -35.7 \pm 4.2$ J mol^{-1} K^{-1} (second law)

The 1σ uncertainties indicated in the enthalpy calculation are the combined errors of the activation energies for both forward and backward reactions. Without the correction term, the outlined procedure is equal to calculating the difference of activation energies for both directions to get ΔH^0_{298}. However, the 1σ uncertainties for the entropy reflect the combined errors in the pre-exponential factors since the entropy change of the reaction is proportional to the ratios of the A-factors, in the absence of the correction term. Generally speaking, the entropies and enthalpies derived by the two methods are consistent, except that the second law value of ΔS^0_{298} is more negative than that used in the third law method. As mentioned before, the third law method is more precise because errors in the Arrhenius parameters tend to cancel in the fitted rate constants. The modified van't Hoff plot of the equilibrium constant for the reaction HBr + $(CH_3)_3$-Si ⇌ H-$(CH_3)_3$-Si + Br with the fits of both methods is illustrated in Figure 12.

Combination of the estimates of ΔH^0_{298} above leads to a recommended value of −31.5 kJ mol^{-1}, based on the average of both analyses. So with the well-characterized BDE_{298} (HBr) = 366.3 kJ mol^{-1} and 2 kJ mol^{-1} allowed for the accuracy limits, the resulting BDE ($Si(CH_3)_3$-H) is 397.8 ± 2 kJ mol^{-1}. The value is higher than the previous measurements using iodination[81], electron impact[82], and very low pressure reactor[83] techniques, but in good agreement with two ab initio studies by Ding and Marshall[37,50] and Allendorf and Melius,[79] and laser photolyis/photoionization mass spectrometry by

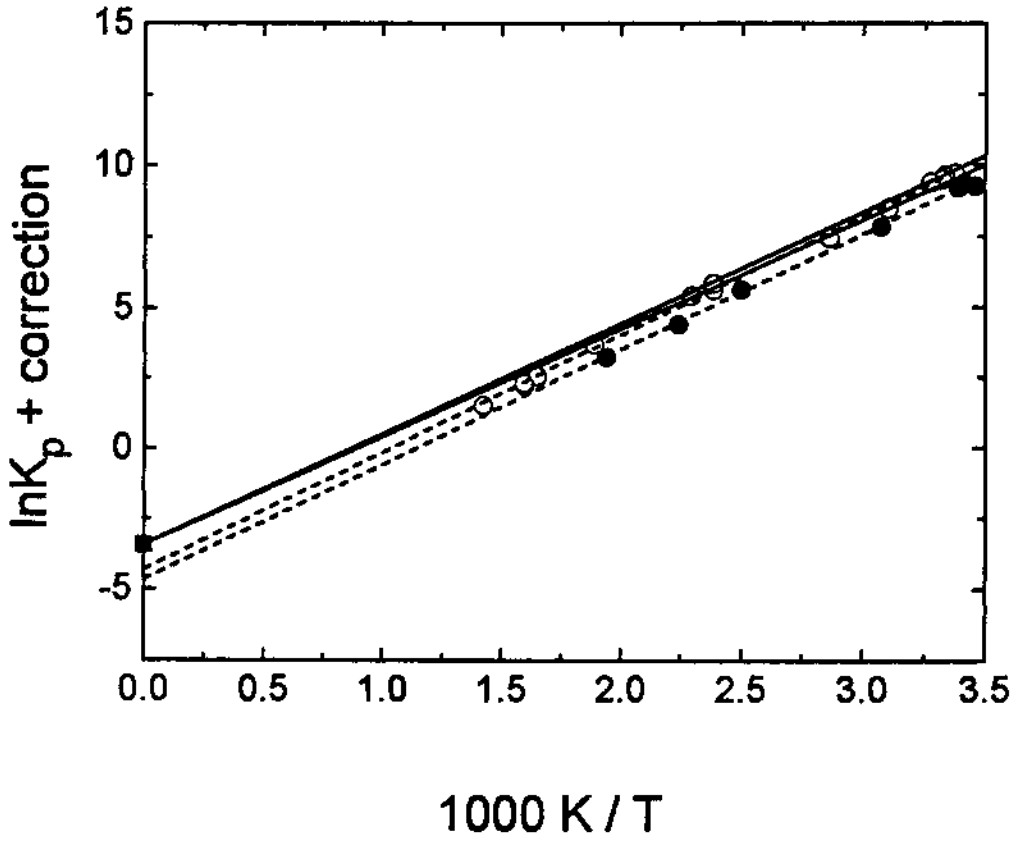

Figure 12. Modified van't Hoff plot of the equilibrium constant of the reaction $Si(CH_3)_3 + HBr \rightleftharpoons Si(CH_3)_3H + Br$. Shown are the second (dashed lines) and third (solid lines) law fits of the FP-RF (○) in this study as well as the data obtained from FP-PIMS (●) technique by kalinovski et al.,1994. The point at 1/T = 0 (■) used in the third law procedure was calculated from the standard entropies of the reagent and product molecules (see text).

Kalinovski et al.[84] (thermochemical parameters are shown in Figure 12). Comparison of the Si-H bond strength of trimethylsilane with that measured for SiH_4, 384.1 ± 2.0 kJ mol $^{-1}$,[50] confirms the methyl-strengthening effect in trimethylsilane. This effect is contrary to hydrocarbons, where the methyl substitution decreases the C-H bond energy is observed in this study.

Si-H Bond Strength in Si_2H_6. The activation energy derived for the reaction of Si_2H_6 + Br can be used to derive BDE_{298} (Si_2H_5-H) by combination with the activation energy for the reverse of the reaction (3.8). There is no direct kinetic information for this backward reaction and the magnitude of $E_{-3.8}$ is *approximated* by averaging the measured activation energies for the reaction SiH_3 + HBr[67] and C_2H_5 + HBr[61] of -0.7 ± 1.2 and -4.2 ± 1.2 kJ mol^{-1}. This leads to $E_{-3.8} \approx$ -2.5 kJ mol^{-1}, with an uncertainty of ± 5 kJ mol^{-1} allowed for in this estimation, so the approximated ΔH^0_{298} for reaction (3.8) is 5.6 ± 5 kJ mol^{-1}. This value combined with BDE_{298} (HBr) = 366.3 kJ mol^{-1} gives BDE_{298} (Si_2H_5-H) = 371.9 ± 5 kJ mol^{-1}, which is larger than the original estimate by Walsh[85] based on the I + Si_2H_6 reaction of 361 ± 8 kJ mol^{-1}, but is close to the "most probable" value of 373.7 kJ mol^{-1} obtained from later PIMS experiments. This result is about 12 kJ mol^{-1} smaller than the Si-H bond strength in SiH_4, and confirms the silyl-weakening effect in silanes. The thermochemistry of the disilyl radical is also obtained. $\Delta H^0_{f\,298}$ (Si_2H_5) = 233.8 ± 5 kJ mol^{-1} is derived from the bond strength calculated here, together with $\Delta H^0_{f\,298}$ (Si_2H_6)[86] = 79.9 kJ mol^{-1}.

Implications of the C-H and Si-H Bond Strengths. The C-H bond enthalpies of C_2H_5-H, i-C_3H_7-H, n-C_3H_7-H, and t-C_4H_9-H as well as Si-H bond enthalpies of Si_2H_6 and $(CH_3)_3$Si-H have been determined in this study. C-H bond weakening by methyl substituents in the simple alkanes is observed here. This is commonly interpreted as the "inductive effect" in which the radical center carbon atom is stabilized by CH_3, an electron donating group. The opposite effect on the Si-H bond as comparing Si-H bond strength of trimethylsilane with silane can be explained in view of the differing electronegativity of Si and C. The higher electronegativity of C than Si makes methyl group less of a donor or better as a withdrawing group, so the trimethylsilyl radical is destabilized by the methyl groups. Also, the Si-H bond strength in disilane is weaker than that in silane. Thus, a silyl substituent, unlike methyl, does induce an Si-H bond weaking. The reason can also be explained by an inductive effect mechanism.

Negative activation energies are observed in both the trimethylsilyl and n-propyl plus HBr reactions. As proposed in a paper by Russell et al.,[76] the mechanism of this type of reaction (R + HBr) is consistent with a complex mechanism involving the reversible formation of a bound intermediate, before H atom abstraction. To investigate this reaction model, the potential energy surface of the reactions can be explored in theoretical studies, such as by ab initio calculations

D. Summary

The rate constants of the reactions C_2H_5 , i-C_3H_7, and t-C_4H_9 with HBr have been measured at room temperature. The rate constants are $(7.0 \pm 0.2) \times 10^{-12}$, $(1.3 \pm 0.1) \times$

10^{-11}, and $(2.7 \pm 0.1) \times 10^{-11}$ cm^3 s^{-1}, respectively. Combination of the rate constant values with other information resulted in C-H bond strengths of 423.6 ± 2, 409.9 ± 2, and 405.1 ± 2 kJ mol^{-1} for C_2H_5, i-C_3H_7, and t-C_4H_9, respectively. The rate constants measured and the C-H bond enthalpies are in excellent agreement with the previous results by Seakins et al.,[61] and the discrepancies in C-H bond strength determined by different equilibria are cleared. Arrhenius parameters of n-C_3H_7, $(CH_3)_3Si$ with HBr have been investigated. From these results, the primary C-H bond strength of propane and the tertiary Si-H bond strength of trimethylsilane have been calculated to be 425.3 ± 3 and 397.8 ± 2 kJ mol^{-1}. The good agreement of the primary C-H bond strength in propane derived in this study with Tsang's value[25] which is determined by the association/dissociation equilibria justifies the additivity/similarity principle in determining the rate constants of different steric types of hydrogen abstraction in alkanes. The negative activation energies observed in the reactions of HBr with n-propyl and trimethylsilyl radicals are consistent with the reaction mechanism proceeding through a weakly bound intermediate complex. The bond strength determination for alkanes and trimethylsilane confirms that methyl substitution decreases the C-H bond energy in alkanes while it increases the Si-H bond energy in trimethylsilane. These phenomena could be explained in terms of the inductive effect. The silyl-weakening effect in silane is justified by the determination of the rate constant of reaction Si_2H_6 with Br. The BDE in disilane is 12 kJ mol^{-1} less than in silane.

CHAPTER 4

REACTION OF Cl + HI

The temperature-dependent rate constant of reaction (4.1),

$$Cl + HI \rightarrow HCl + I \qquad (4.1)$$

was measured by the laser-photolysis / resonance fluorescence technique. The rate constants obtained were compared with previous data derived by different methods. One aim in studying this reaction is applying the double exponential algorithm, which was employed in the study of R + HBr reactions, to analyze the growth of I atom and check with the decay rate of Cl. The Cl decay was analyzed by a simple exponential function. The aim was to check whether the same kinetics were obtained by monitoring I or Cl in this reaction.

A. Results and Discussion

Table 12 summarizes the kinetic measurements for Cl + HI under different experimental conditions between temperature 297 - 390 K. It took at least 20 min. for a flow of HI to saturate the surface of the steel reactor. Alternatively, a few mbar of HI was incubated in the reactor for an hour before starting the measurements. Under these two conditions, the measured rate constants were close to the values from the Pyrex reactor. There was no significant change in the rate constant with the photolysis energy or $[Cl]_0$,

which indicates the secondary reactions from photolyzed radicals with products or other photolysis fragments are negligible.

Comparison of Rate Constant Measured with Previous Data. The Arrhenius plot of the Cl + HI reaction obtained in this study and previous measurements by other techniques are shown in Figure13. Each point in the graph from this study is the weighted mean for that temperature. The best fit of the Arrhenius plot by this laser-photolysis/resonance fluorescence method is

$$k_{4.1} = (1.18 \pm 0.31) \times 10^{-10} \exp(-0.45 \pm 0.77 \text{ kJ mol}^{-1} / RT) \text{ cm}^3 \text{ s}^{-1} \qquad (4.2)$$

and the errors are 1σ. Consideration of the covariance and the 1σ errors gives the estimated statistical uncertainty of 3 - 6 % in $k_{4.1}$. Since the activation energy is not significantly different from zero, an alternative summary of the data over 297 - 390 K is the weighted mean of the measurements, $k_{4.1} = (1.02 \pm 0.02) \times 10^{-10}$ $cm^3 s^{-1}$. The rate constant obtained from either monitoring Cl or I is close (see Figure 5), indicating that the kinetics of this reaction are the same by these two different monitoring methods.

In the early 1970s, Wodarczyk et al.[42] determined the absolute rate constant of this reaction at 295 K by photolyzing Cl_2 with laser pulses and monitoring the reaction via the time-resolved IR chemiluminescence of the vibrationally excited product, HCl. The average value of the rate constant obtained for Cl + HI was $(9.6 \pm 2.4) \times 10^{-11}$ $cm^3 s^{-1}$, and it shows very good agreement with average measurement in this study. Also, the average reaction cross section of Cl + HI (σ), 19 ± 5 $Å^2$, was determined by the relationship of $\sigma = k_{4.1} / \bar{v}$ ($\bar{v}$ is the mean relative velocity) and this value which is about one out of two

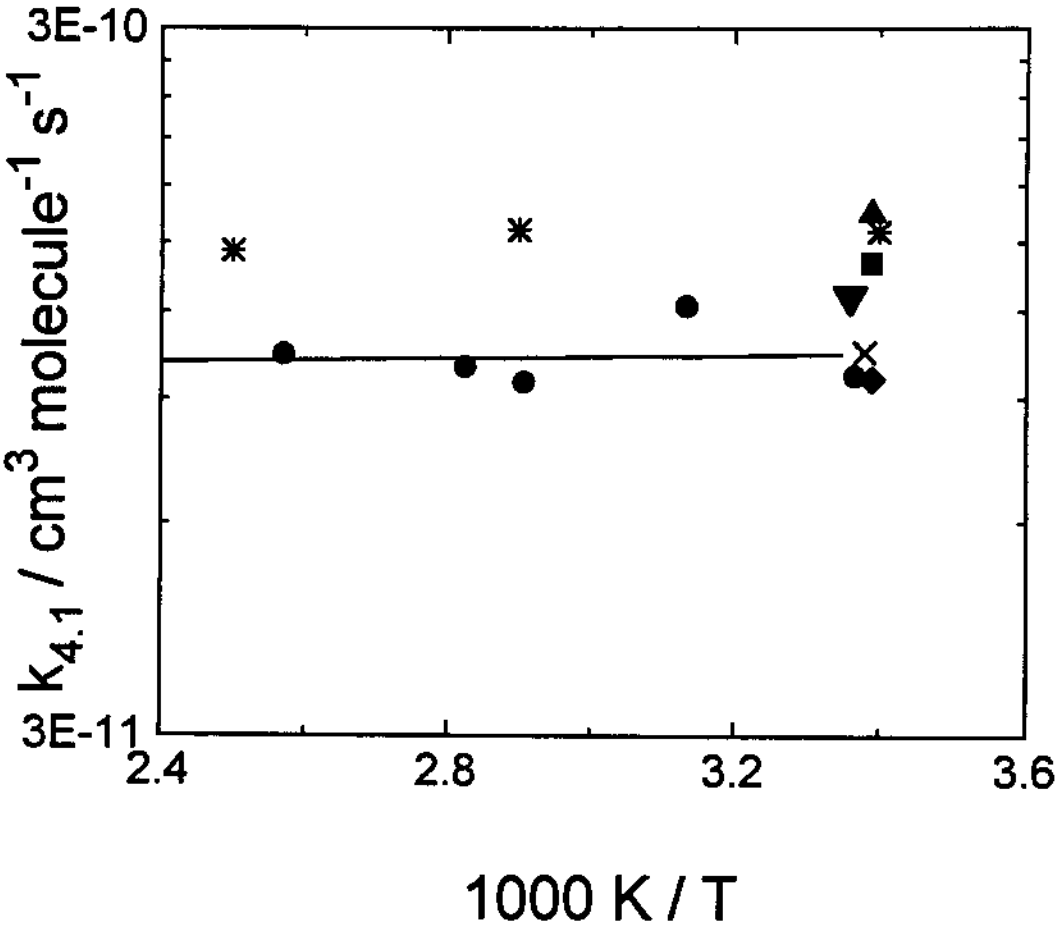

Figure 13. Arrhenius Plot of Cl + HI reaction in this study and other measurements. Symbols represented are:

✳ - Mei et al., 1979
▲- Mei et al., 1977
■ - Dolson et al., 1982
▼- Subramonia et al., 1985
× - Ashutosh
◆ - Wodarczyk et al., 1974
● - this work

kinetic collisions compared to that of determined using hard-sphere model by HI (4.1 Å) and Cl (3.4 Å) from standard values of molecular diameters[87] indicating that there is no or a low barrier for this reaction, which is coincident with the investigation in this study. A year later, a new rate constant, 1.64×10^{-10} cm^3 s^{-1},[43] for Cl + HI reaction was reported by the same group with more accurate [HI] determination and less wall-catalyzed interference. The only one published temperature-dependent reaction rate of this reaction among other data available was proposed by Mei and Moore[44] using the same technique as the above two measurements. The observed reaction rates showed almost no temperature dependence around a temperature range comparable to the present study, although significant variation of $k_{4.1}$ was seen at lower temperatures. A reaction model assuming that the halogen end of the hydrogen-halide was initially attacked by the halogen atom, and the reaction completed by free rotation of the hydrogen atom was proposed based on these results. Dolson and Leone[88] studied the kinetics of the slow chain reactions of X (Br, Cl) + HI → HX($v \leq v_{max}$) + I and I + X_2 → IX + X system by sensitive real-time detection of IR chemiluminescence from the vibrationally excited HX products. Cascading fluorescence was observed from individual vibrational levels, and the results were analyzed by a mathematical function for the multiple state system and their subsequent lower vibrational states. A rate constant of $(1.4 \pm 0.3) \times 10^{-10}$ cm^3 s^{-1} was obtained, and it is about 40 % higher than the value in the present study.

A different approach to obtain the rate constant for reaction (4.1) is illustrated by the study of Subramonia et al.[89] They measured the relative rate constant for removal of Cl by addition of HI as a second substrate using a competitive radiochemical technique. The

absolute rate constant, $(1.26 \pm 0.14) \times 10^{-10}$ cm^3 s^{-1}, is derived through the well-established rate constant of Cl + C_2H_6 reaction. The same technique was applied to the rate constant determinations for several different molecules with Cl, such as C_2H_4, PH_3, and C_2H_2.

One recent study at UNT of the Cl + HI reaction was performed by the discharge-flow / resonance fluorescence technique.[90] Cl radicals were produced by a microwave-discharge of Cl_2 or CCl_4 in Ar, and Cl concentrations after reaction were monitored by atomic resonance fluorescence. The rate constant, $(1.08 \pm 0.18) \times 10^{-10}$ cm^3 $molecule^{-1}$ s^{-1}, was obtained at 295 K and agrees well with the measurement in this study.

As mentioned earlier, the large cross section determined from IR chemiluminescence experiments may be evidence for a surface having an attractive path with no barrier between the reactants HI and Cl. The formation of products having small energy in fluorine and chlorine-induced reactions with HCl, HBr, and HI demonstrates the effective absence of an exit barrier in these cases.[91,92] Intermediate complexes might also exist near the bound halogen. The cross beam experiments performed by Lee and coworkers[93,94] provided evidence for formation of divalent iodide compounds between atoms (or radicals) with diatomic molecules containing iodine. Extensive theoretical work is required to explore the quantitative features of the surface.

CHAPTER 5

REACTION OF H + SiH_4

The reaction

$$H + SiH_4 = SiH_3 + H_2 \qquad (5.1)$$

was reexamined by two approaches in this study. First, important quantities such as the Arrhenius A factor and the activation energy were investigated by kinetic measurements over a wider temperature range and compared with the results published previously. Second, kinetic modeling using transition state theory (TST) and corrections for quantum-mechanics effects combined with the ab initio data was employed to test whether there is good agreement between the theoretical and the measured reaction kinetics.

A. Methodology

Experimental. The FP-RF technique, as described in the second chapter, was also used in the study of this reaction. Here, only the difference between the setups is mentioned. Atomic hydrogen was generated by photolysis of ammonia and the course of the reaction was monitored by time-resolved resonance fluorescence at λ= 121.6 nm (Lyman-α), H(2 ^{2}P) - H(1 ^{2}S). The vacuum UV resonance fluorescence was excited by a microwave-powered discharge lamp through which a mixture of 1% of H_2 diluted in Ar was passed. The pressure of the resonance lamp was kept between 700 - 800 mtorr. Owing to a narrow transmittance band of O_2 at the Lyman-α wavelength,[95] a 2.4 cm dry air filter was

put in front of the PMT to absorb other interfering vacuum UV radiations which were around the neighborhood of the H-atom wavelength. The H atoms reacted with an excess of silane under pseudo-first-order conditions,

$$\frac{d[H]}{dt} = -k_{ps1}[H] = -(k_{5,1}[SiH_4] + k_{diff})[H], \tag{5.2}$$

where k_{diff} represents the loss of H atoms from the reaction zone by diffusion and reaction with ammonia. Figure 14 shows a plot of pseudo-first-order decay coefficient for loss of H vs. $[SiH_4]$ and $k_{5,1}$ was obtained from the slope of this plot.

TST Kinetic Modeling.

General Introduction and Evaluation of Partition Functions. The basic assumption in the transition state theory, TST, is that an equilibrium is reached between the reactants, SiH_4 and H and the activated complex, SiH_5^*.

$$H + SiH_4 \rightleftharpoons (SiH_5)^* \rightarrow H_2 + SiH_3. \tag{5.3}$$

The equilibrium constant in terms of concentration of species and partition functions is

$$K^* = \frac{[(SiH_5)^*]}{[SiH_4][H]} = \frac{Q_{SiH_5^*}}{Q_{SiH_4}Q_H}\exp(-E_0^*/RT) \tag{5.4}$$

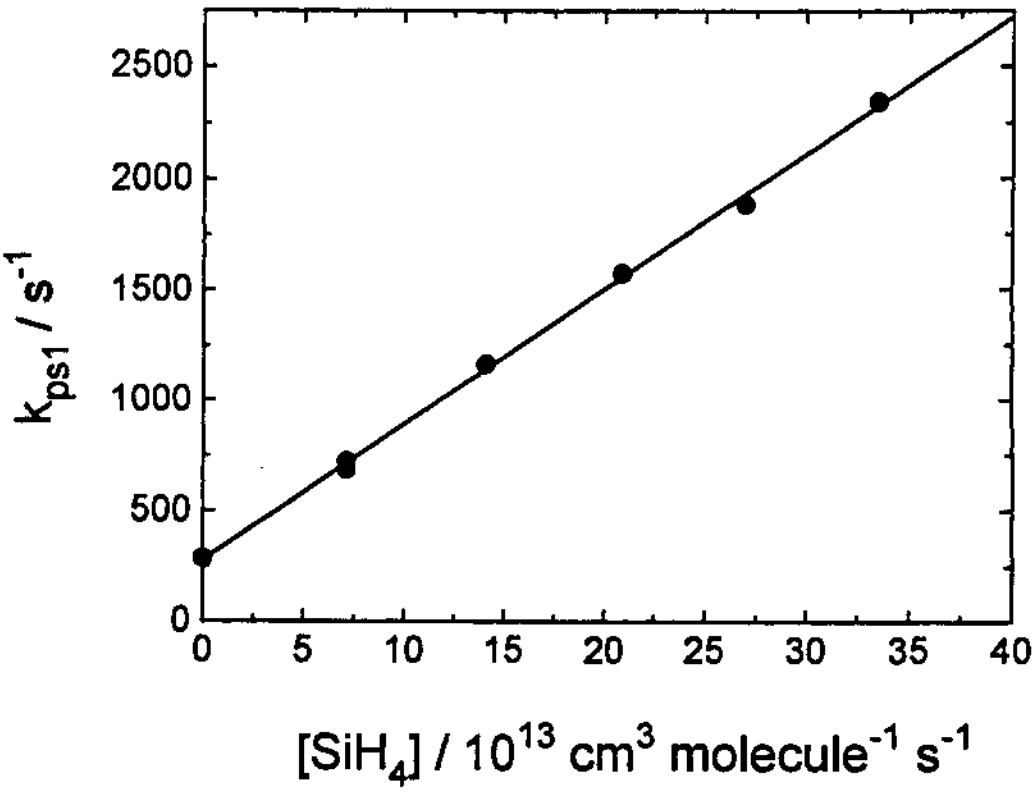

Figure 14. Plot of pseudo-first-order rate constants for loss of H vs. [SiH_4] at 570 K and 46.7 mbar.

where E_0' is the energy of the lowest level of activated complex relative to that of the reactants, and Q_{SiH5}^{*}, Q_{SiH4}, and Q_H are the total partition functions of the activated complex and reactants, respectively. The rate of the reaction is given by

$$\frac{d[SiH_5^*]}{dt} = k_{TST}[SiH_4][H] = \frac{k_B T}{h}[SiH_5^*] \qquad (5.5)$$

Substitution of (5.4) in to (5.5) gives the calculated rate constant, k_{TST}, from TST as follows:

$$k_{TST} = \frac{k_B T}{h}\frac{Q_{SiH_5}'}{Q_{SiH_4}Q_H}\exp(\frac{-E_0^*}{RT}) \qquad (5.6)$$

The total partition functions associated with the internal motion of each molecule are given by the product of the partition functions associated with independent translational, rotational, vibrational , and electronic contributions:

$$Q = Q_{rot}Q_{vib}Q_{elec}Q_{trans} \qquad (5.7)$$

Their symbols and meanings are as follows.

Translational partition function,

$$Q_{trans} = \frac{(2\pi m k_B T)^{2/3}}{h^3} \qquad \text{(per unit volume)}, \qquad (5.8)$$

where m (kg molecule^{-1}) is the mass of the molecule, and k_B and h are the Boltzmann and Planck constants, respectively.

Vibrational partition function,

$$Q_{vib}=\prod_{i=1}^{s}\frac{1}{1-\exp(\frac{hc\nu_i}{RT})} \quad , \tag{5.9}$$

where S = 3N-6 vibrational modes with frequencies ν_i in cm^{-1} for nonlinear molecules of SiH_4 and S = 3N-7 for SiH_5^* (only real frequencies), and N is the number of atoms.

Electronic partition function,

$$Q_{elec}=\sum_i g_i e^{-E_i/k_BT} \quad , \tag{5.10}$$

where g_i is the degeneracy and E_i is the energy above the ground electronic state. In most of the system, only the ground state which involves different degeneracies is considered.

Rotational partition function,

$$Q_{rot}=\frac{8\pi^2(8\pi^3 I_A I_B I_C)^{1/2}(k_BT)^{3/2}}{\sigma h^3} \quad , \tag{5.11}$$

where I_A, I_B, and I_C are the moments of inertia about their principal axes, and σ is the symmetry number.

Three TST Models Used to Fit the Experimental Data. In quantum mechanics a particle with an energy less than the barrier height has a small but non-zero chance of reaching the other side of the barrier with the same energy. This nonclassical barrier penetration phenomena is named the "tunneling effect".[96] It happens most for light particles, such as the H atom. Based on this idea, the rate constant expressed by conventional TST shown in eq. (5.6) is modified as follows:

$$k_{TST}=\Gamma\frac{k_B T}{h}\frac{Q_{SiH_5}^{\ddagger}}{Q_{SiH_4}Q_H}\exp\left(\frac{-E_0^{\ddagger}}{RT}\right) \qquad (5.12)$$

Γ represents a correction factor for quantum-mechanical tunneling and is ≥ 1. Three models were considered: (I) no tunneling ($\Gamma = 1$); (II) Wigner tunneling[97] based on the ab initio complex frequency, $\upsilon^{\ddagger}$, which leads to the decomposition of the activated complex to the products and was reported by Goumri et al.,[98]

$$\Gamma = 1 - \frac{1}{24}\left(\frac{h\nu^{\ddagger}}{k_B T}\right)^2 \quad , \qquad (5.13)$$

and (III) Wigner tunneling based on a value of $\upsilon^{\ddagger}$ derived from fitting to the reaction coordinate (RC) at a higher theory level. The information used in this frequency

calculation was obtained from the ab initio data. Table 13 lists the frequencies,[98] moments of inertia,[98] and other parameters[71] used to calculate the required partition functions for the reactants and the corresponding activated complex which were applied to fit the experimental rate constants in the TST modeling.

Table 13: Frequencies, Moment of Inertia, and Other Parameters Used to Calculate the Partition Functions in the TST Fitting

Parameters	SiH_4	SiH_5^*	H
frequencies[a]	909(3), 955(2), 2207, 2220 (3)	1880i, 333(2), 846, 926(2), 1048(2), 1057, 2192, 2216(2)	
moments of inertia (I)[b]	$I_A = I_B = I_C = 9.71 \times 10^{-47}$ kg m^2	$I_A = 9.80 \times 10^{-47}$ kg m^2 $I_B = I_C = 2.28 \times 10^{-46}$ kg m^2	
symmetry number (σ)[c]	12	3	
Q_{elec}[c]	1	2	2

[a] Vibrational frequencies in cm^{-1}, see ref 98. Degeneracies are shown in parentheses.
[b] ref 98.
[c] ref 71 .

B. Results and Discussion

Experimental Results and Discussion. The conditions employed in the kinetic experiment and the summary of the results are presented in Table 14. The measured rate constants are independent of the concentration of the precursor and flash energy which were varied by

a factor of three and two, respectively. The data indicate that the secondary reactions, such as the recombination between the hydrogen and the silyl radical are insignificant. Also, the absence of variation in the rate constants with the residence time, which was changed by a factor of four, shows that the thermal decomposition of either ammonia or silane was negligible under the conditions applied in the study. The Arrhenius plot of $k_{5.1}$ is shown in Figure 15, and the best fit is

$$k_{5.1} = (1.78 \pm 0.11) \times 10^{-10} \exp(-16.0 \pm 0.2 \text{ kJ mol}^{-1} / RT) \text{ cm}^3 \text{ s}^{-1} \qquad (5.14)$$

for T= 290 to 660 K where the quoted errors are 1σ and represent the precision only. Consideration of the 1σ statistical error, which is about 5% in the fitted $k_{5.1}$ itself, and the allowance of another 5% for potential unrecognized systematic errors leads to a uncertainty of about 10% in $k_{5.1}$.

Table 15 summarizes the rate constants measured at 298 K involving the use of discharge-flow,[99,100] pulse radiolysis,[101] electron spin resonance (ESR),[102] IR diode laser,[103] mass spectroscopy,[104] and flash-photolysis resonance absorption[48] techniques as well as FP-RF in this work. As seen in the table, apart from the first two studies where the rate constants are obviously too high, there is general agreement between the other measurements. The reasons for those two higher rate constants are unknown but possibly can be attributed to be wall effects and/or secondary reactions. The only recent temperature-dependent kinetic measurements were investigated by Arthur et al.[48] They produced H radicals by Hg-sensitized photolysis of H_2, and monitored the reaction by Lyman-α absorption. The temperature-dependent rate constants obtained for 294 - 487 K are

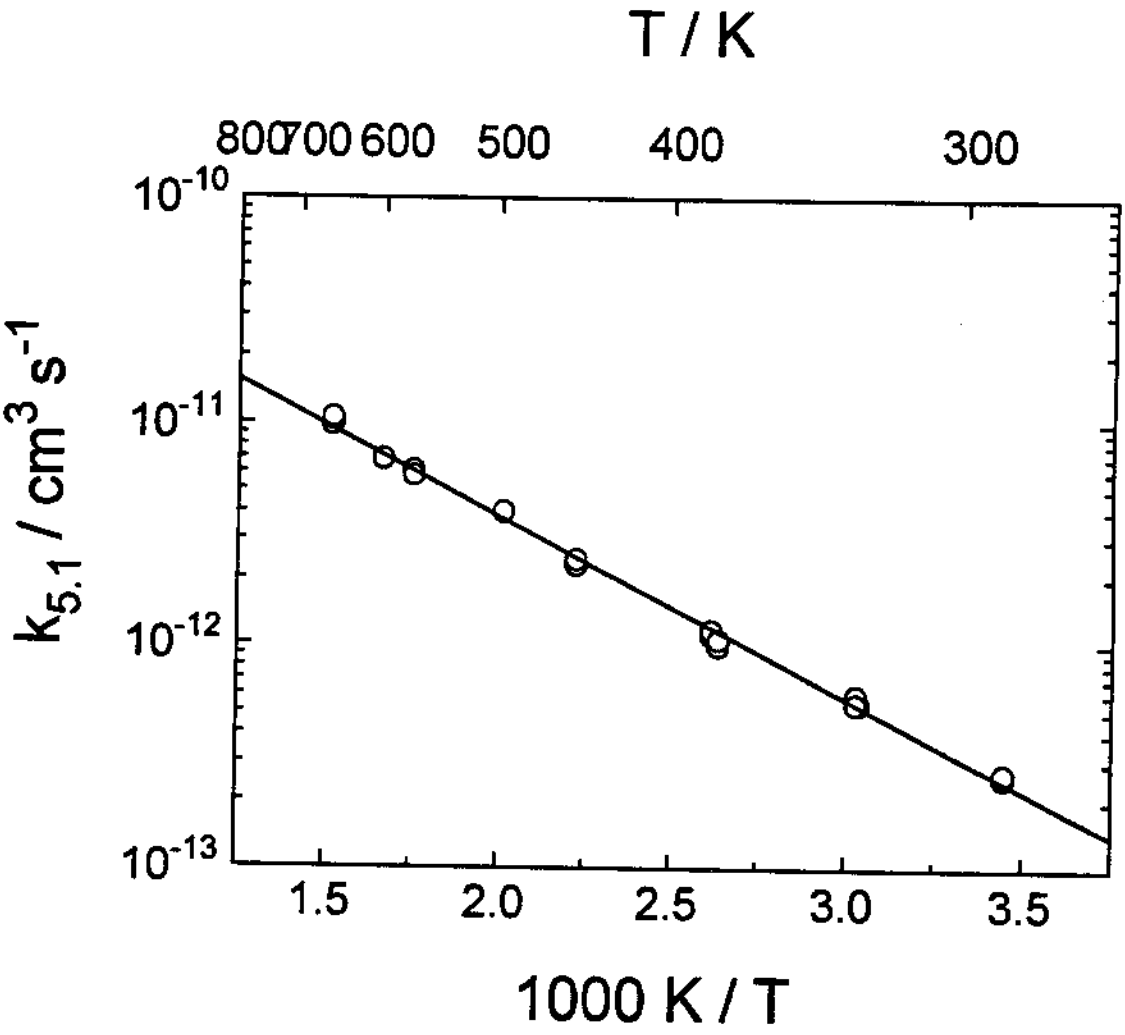

Figure 15. Arrhenius plot of 23 measurements on the H + SiH_4 reaction.

$$k_{5.15} = (2.3 \pm 0.3) \times 10^{-11} \exp(-11.6 \pm 0.3 \text{ kJ mol}^{-1} / RT) \text{ cm}^3 \text{ s}^{-1}, \quad (5.15)$$

and both the Arrhenius parameters are lower than those found in this work. At 298 K, the rate constant derived from eq.(5.15) is in accord with the value from this study within about 25%, while at 487 K, a significant deviation was observed.

Table 15: Summary of Rate Constants Measured for H + SiH_4 at 298 K

$k_{5.1}$ / 10^{-13} cm^3 s^{-1}	techniques	ref.
26 ± 3	discharge-flow / mass spect.	99
85 ± 7	discharge-flow / Lyman α	100
4.6 ± 0.3	pulse radiolyses / Lyman α	101
4.0	flow reactor / ESR	102
2.5 ± 0.5	photolysis / IR diode laser spect.	103
4.3 ± 0.9	photolysis / mass spect.	104
2.0 ± 0.1	photolysis /resonance absorp.	48
2.8 ± 0.3	FP / RF	this work

Kinetic Modeling Analysis. Three kinetic models using TST have been applied to analyze the experimental measurements. The theoretical results calculated from eq. 5.12 were employed to fit the experimental data of eq. 5.14 over a temperature range of 290 - 660 K with only one adjustable parameter, E_0'. Table 16 gives the values of the calculated partition functions for the reactants and the activated complex at several temperatures. In model (I), the tunneling effect is not included. The closest E_0' was approached by the trial

Table 16: The Values of the Calculated Partition Functions of SiH_4, H, and SiH_5^* at Several Temperatures

Partition Functions	T(K) 298	340	400	500	700	1000	1300	2000
$Q_{trans}(H)$	9.79×10^{29}	1.19×10^{30}	1.52×10^{30}	2.13×10^{30}	3.52×10^{30}	6.02×10^{30}	8.92×10^{30}	1.70×10^{31}
$Q_{trans}(SiH_4)$	1.77×10^{32}	2.15×10^{32}	2.75×10^{32}	3.84×10^{32}	6.36×10^{32}	1.09×10^{33}	1.61×10^{33}	3.07×10^{33}
$Q_{trans}(SiH_5^*)$	1.85×10^{32}	2.25×10^{32}	2.88×10^{32}	4.02×10^{32}	6.66×10^{32}	1.14×10^{33}	1.68×10^{33}	3.22×10^{33}
$Q_{vib}(SiH_4)$	1.06	1.11	1.20	1.44	2.34	5.47	13.20	90.89
$Q_{vib}(SiH_5^*)$	1.66	1.94	2.49	3.89	10.18	43.46	170.49	2723.19
$Q_{rot}(SiH_4)$	89.91	109.57	139.82	195.40	323.68	552.67	819.18	1563.18
$Q_{rot}(SiH_5^*)$	848.15	1033.63	1318.98	1843.33	3053.48	5213.72	7727.92	14746.62
$Q_{elec}(H)$	2	2	2	2	2	2	2	2
$Q_{elec}(SiH_4)$	1	1	1	1	1	1	1	1
$Q_{elec}(SiH_5^*)$	2	2	2	2	2	2	2	2
Q_{tot}	1.58×10^{-29}	1.46×10^{-29}	1.34×10^{-29}	1.25×10^{-29}	1.22×10^{-29}	1.31×10^{-29}	1.43×10^{-29}	1.74×10^{-29}

and error method and a value of 14.6 kJ mol^{-1} with a root-mean-square deviation of about 15% was obtained. Model (II) applies the Wigner tunneling correction based on the $\nu^{\ddagger}$ = 1880i cm^{-1} of $SiH_5^{\ddagger}$ derived from ab initio methods. This frequency calculation was done using the Gaussian 90 program at the MP2/6-31G* level (which includes the consideration of electron correlation by perturbation theory).[99] In this model, a close fit to the experimental data was obtained with a standard deviation of 8% using $E_0^{\ddagger}$ = 18.1 kJ mol^{-1}. However, the value of $E_0^{\ddagger}$ from the MP2/6-31G* calculation was in poor agreement (too high) with the one from the experimental fit, which indicates that the energy change along the RC of this reaction was poorly described at this theory level.

A higher theory level (G2) of energy calculation was employed by Goumri et al. to estimate the curvature more accurately, but the frequency calculation was not allowed due to computer limitations at that time. Owing to the availability of the G2 energies and their geometries along the course of the reaction (reactants → TS → products), the vibrational frequency of TS can be calculated on the assumption of a valence force model which was first proposed by Bjerrum[105] in 1914. He assumed that there is a strong restoring force in the line of every valence bond and which opposed the change of angle between two valance bonds if the distances of these two bonds are changed. In this case, the geometry of SiH_3 is almost unchanged along the reaction coordinate, RC, so the C_{3v} symmetry of the transition state can be treated as a linear triatomic molecule SiH_3-H-H. Such a system has two different force constants corresponding to the stretching of the two bonds and one corresponding to bending of the molecule. The two vibrational frequencies of this approximated linear triatomic molecule SiH_3-H-H can be calculated by the formula

outlined by Herzberg,[106]

$$\lambda_1 + \lambda_2 = 4\pi^2(\nu_1^2 + \nu_2^2) = k_1\left(\frac{1}{m_{SiH_3}} + \frac{1}{m_H}\right) + k_2\left(\frac{1}{m_H} + \frac{1}{m_H}\right) \tag{5.16}$$

$$\lambda_1 \times \lambda_2 = 16\pi^4\nu_1^2\nu_2^2 = \frac{m_{SiH_3} + m_H + m_H}{m_{SiH_3} \times m_H \times m_H} \times k_1 \times k_2 \tag{5.17}$$

where m is the mass of the molecule. The force constants k_1 and k_2 were derived from the two coupled equations of Newton's Law,

$$V = \frac{1}{2}k_1x_1^2 + \frac{1}{2}k_2x_2^2 \tag{5.18}$$

where V is the energy level of the selected point relative to the transition state, and x_1 and x_2 are the bond length difference of SiH_3-H and H-H as compared to the equilibriun distance in the transition state, respectively. The energies and bond lengths of these two points on either side of the transition state along the reaction motion as well as the transition state were calculated at the G2 level and are listed in Table 17.

An antisymmetric stretching frequency of $\nu' = 1463i\ cm^{-1}$ was obtained by equations (5.16) and (5.17), and this frequency leads to the fit in the model (III) with a

root-mean-square deviation of 9% and a value of $E_0^{\ddagger} = 17.1$ kJ mol^{-1}. An uncertainty of 3.0 kJ mol^{-1} in $E_0^{\ddagger}$ is estimated to cover the variation of $E_0^{\ddagger}$ with the tunneling model selected, therefore the suggested $E_0^{\ddagger}$ is 17.1 ± 3.0 kJ mol^{-1}.

Table 17: Energies and Bond Lengthes of Two Points As Well As the Transitiion State, $SiH_5^{\ddagger}$, Calculated at the G2 Level

position	[a]V (kJ mol^{-1})	H-H (Å)	SiH_3-H (Å)
TS	0	0.999	1.670
point A	-3.5	1.45	1.475
point B	-29.3	0.762	1.951

[a] The potential energies of point A and B listed here are the relative valuse to transition state (TS)

Table 18 summarizes the parameterization of these three fits to the experimental rate constants for the H + SiH_4 reaction. All the three models fit the experimental data well, but the third model is considered to be most physically realistic and is recommended for the higher temperature extrapolation. Figure 16 shows the measured rate constants from this experiment as well as the fits from both transition state theory and Arthur et al.[48] The good accord of the experimental data with the TST fittings supports the accuracy of the Arrhenius parameters derived here by contrast to those of Arthur et al.[48] The lines of model (I) and (II) are too close for that of (III) to show separately.

Table 18 : Summary of Transition State Theory Fits to Experimental Rate Constants for H + SiH_4 in the Form of $k = A(T/K)^n \exp(-BK / T)$ [c] s^{-1}

TST model (see text)	A	n	B
[a]I	1.07×10^{-15}	1.736	1289
[b]II	4.22×10^{-16}	1.829	1141
[c]III	2.44×10^{-16}	1.903	1102

[a] No tunneling

[b] Includes Wigner tunneling based on the MP2/ 6-31G* value of $\nu^{\ddagger}$.

[c] Includes Wigner tunneling based on a value of $\nu^{\ddagger}$ obtained from fitting to the G2 reaction coordinate.

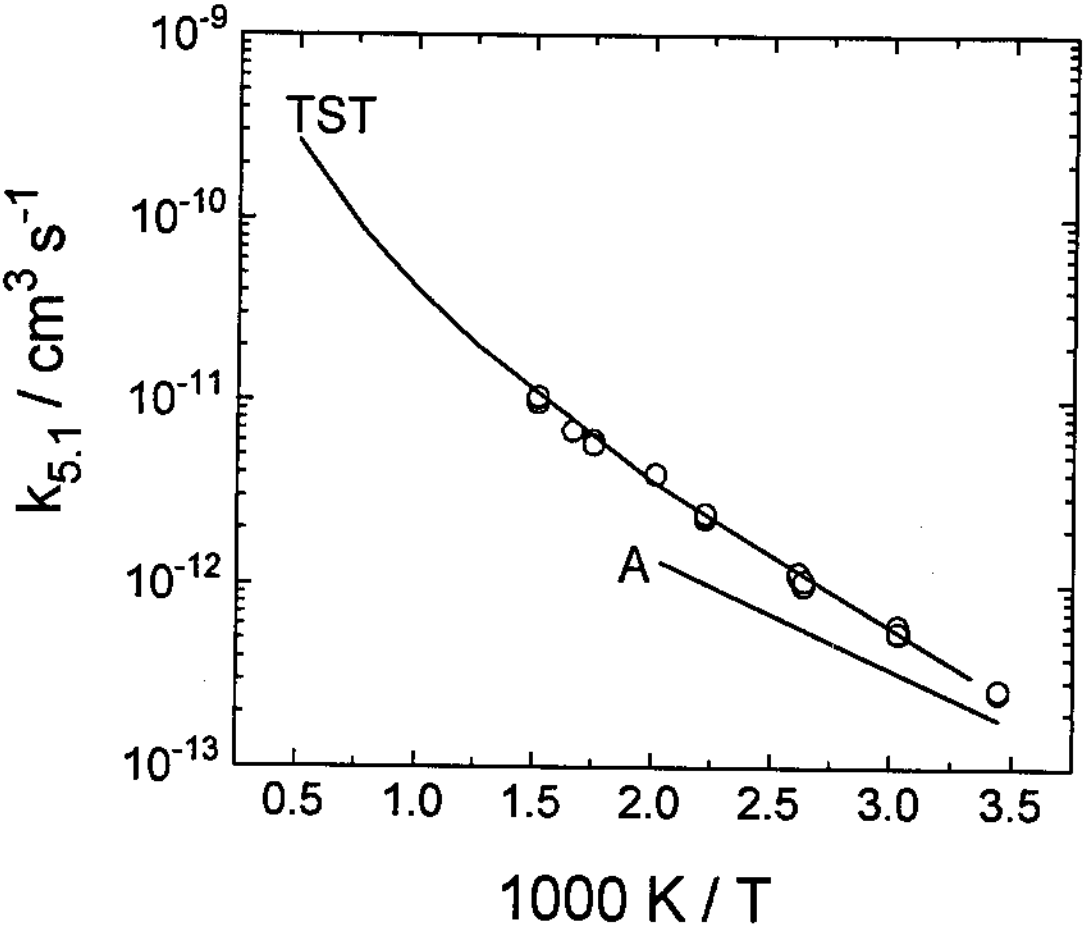

Figure 16: Arrhenius plot showing measured $k_{5.1}$ values (o) ; transition state theory fit (model c) (TST); fit of Arthur et al. see ref. 48 (A).

CHAPTER 6

REACTIONS OF OH WITH SILANE, AND MONO-, DI-, TRI-, AND TETRAMETHYLSILANE AT ROOM TEMPERATURE

The use of volatile silicon compounds may lead to their emission into the atmosphere, where they can be removed by reactions with a variety of reactive species, such as ozone, hydroxyl, and nitrate radicals. For most hydrocarbons, the hydrogen-abstraction reaction by OH radicals is one of the major channels for their removal in the atmosphere, and the rate constants of these reactions have been measured or estimated reliably.[107,108,109] However, the only silane compounds whose reactions with OH have been studied to date are silane,[110,111] tetraethylsilane,[112] and tetramethylsilane.[113] The rate constants for the gas-phase reactions of hydroxyl with silane, and mono-, di-, tri-, and tetramethylsilanes have been determined at room temperature in this study to investigate the effect of methyl-substitution on the reactivity of Si-H bonds toward OH.

A. Experimental Method

The utilization of the FP-RF technique in studies of Br and H radicals was described in the previous chapters. The major difficulty using the original setup for detecting the OH signals was a large decrease in the signal to background (from scattered resonance radiation) ratio. Much time was spent with the focusing optics, cell design, and collimator arrangements. Several modifications, especially in the optics system, have been

made in the apparatus for maintaining good OH detection sensitivity. Some of modifications are listed: (a) A Pyrex reactor consisted of six arms was modified from the one used for the previous studies. The new reactor design has a broader center body and shorter arms than the old one in order to better arrange the focusing of optics. (b) The microwave-discharge flow lamp, source of the resonance radiation, was placed around 30 cm away from one arm of the reactor. A 2% H_2O/Ar mixture was flowed into the lamp and the pressure of the mixture inside the lamp was kept at around 700 mtorr to generate a steady resonance fluorescence. (c)An additional quartz lens (f = 5 cm) was placed in one of the arms, orthogonal to both the discharge and the flash lamps, to collect the resonance fluorescence from the center of the reactor and focus it onto the PMT(Thorn EMI Electron Tubes, 9813 QB). A band pass filter (FWHM = 15 nm) transmitting a λ= 307 nm band of OH ($A^2\Sigma^+$, $\upsilon' = 0 \rightarrow X^2\Pi$, $\upsilon'' = 0$) was fitted in the PMT housing. By the above modifications, a 0.8 cm diameter spot of UV probe radiation was observed in the center of the reaction zone by white paper, and the flash light was aligned to go to the center of this spot. The reactor cell was covered by black cloths and all the optics were aligned well to reduce the scattered light radiation. Figure 17 shows the diagram of the apparatus design for detecting the OH signal.

All the reactants were pre-mixed before entering the reactor. In order to avoid the accumulation of the photolysis and reaction products, all experiments were performed under slow flow conditions so that the gas mixture in the reaction zone was replenished between every flash. H_2O liquid was throughly degassed from liquid-nitrogen traps at 77

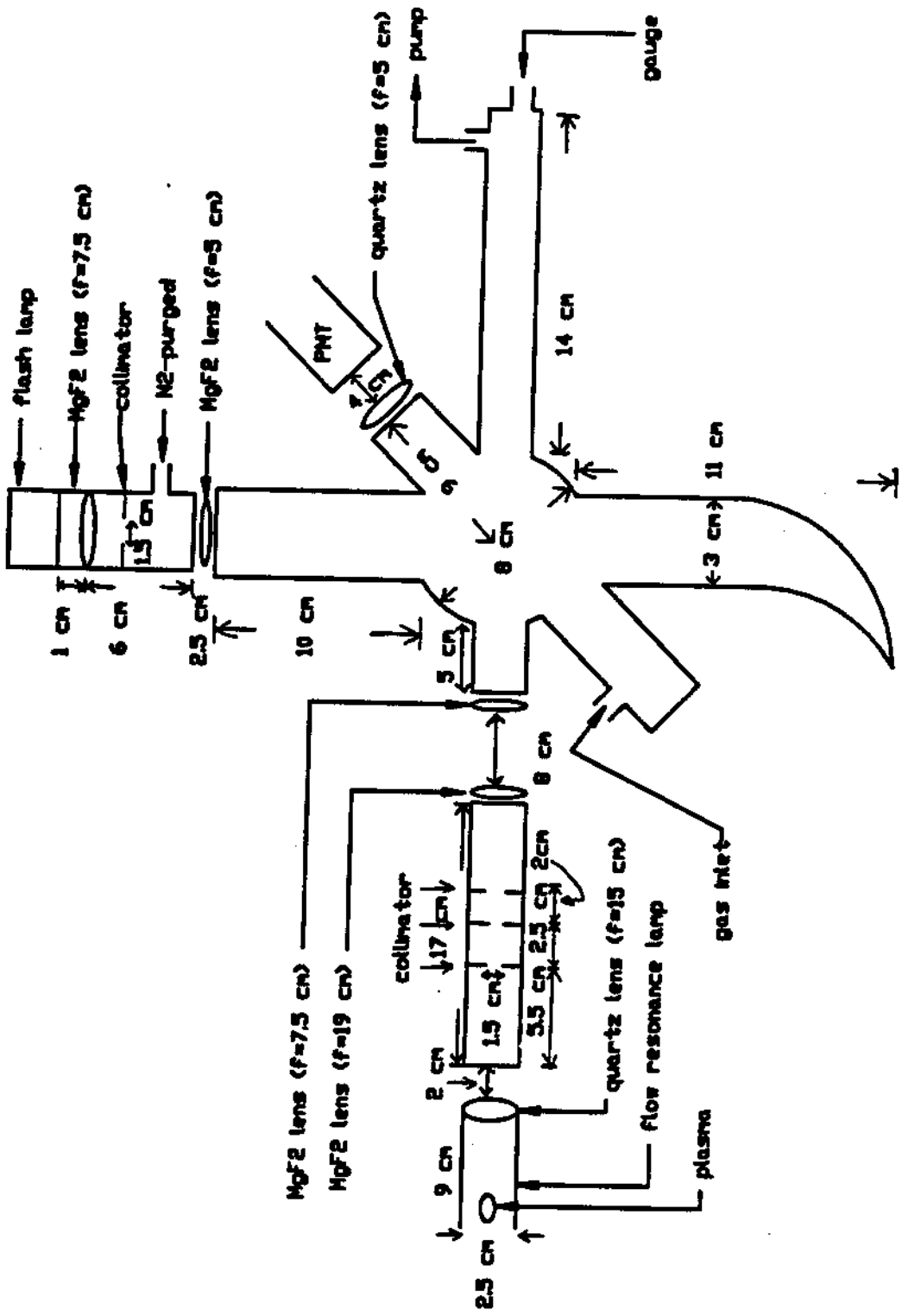

Figure 17. The diagram of the apparatus for detecting the OH signal

K. Ar (Big Three, 99.998 %) and N_2 (Air Products, Industrial Grade) were used as supplied. Silane (Matheson), and mono-, di-, tri-, and tetramethylsilane (Hüls) were degassed by several freeze-pump-thaw cycles and were stored in darkened bulbs before use.

B. Results and Discussion

The main photochemical processes for the photolysis of H_2O in the spectral region of $\lambda > 120$ nm have been described by Okabe[114] as follows:

$$H_2O + h\upsilon\ (\lambda < 242\ nm) \rightarrow H + OH\ (X^2\Pi) \qquad (I)$$

$$H_2O + h\upsilon\ (\lambda < 136\ nm) \rightarrow H + OH\ (A^2\Sigma^+) \qquad (II)$$

$$H_2O + h\upsilon\ (\lambda < 177\ nm) \rightarrow H_2 + O\ (^1D) \qquad (III)$$

Process (I) is the dominant pathway and an estimated ratio of process (I) to (III) is 99: 1 for $\lambda > 145$ nm and 89 :11 for $\lambda = 105 - 145$ nm.[115] Process (II) occurs to an upper limit of 5% at $\lambda < 136$ nm. Even though small amounts of O ($^1D_2$) and OH ($A^2\Sigma^+$) are generated from processes (II) and (III) in the experiments, the rapid H abstraction from H_2O by O ($^1D_2$) to produce OH,[116,117,118] radiative relaxation,[119] and collisional-quenching of OH ($A^2\Sigma^-$) to OH ($X^2\Pi$)[120] are much faster on the experimental time scale than the decay and monitoring of ground state OH. Unlike the previous *atomic* states observed, there is a loss of OH resonance fluorescence by collisional quenching of the emitted OH ($A^2\Sigma^-$), because of the longer radiative lifetime of the excited *molecular* state. As in the analysis by Husain et al.[121,122] in experiments on OH reactions with HBr and DBr, the decay of OH resonance fluorescence in the presence of collisional quenching is expressed

by

$$I_F(t)=I_F^0\frac{\exp(-k't)}{1+k_Q[Q]/k_f} \qquad (6.1)$$

where $I_F(t)$ is the fluorescence intensity at time t in the presence of the reactants and the I^0_F is the intensity at time t without reactants. This term k_Q represents the electronic collisional quenching coefficient, specially for Q = H_2O in this case, since the concentration of H_2O is much higher than the reactant concentration and the quenching by Ar is negligible ($k_Q \leq 4 \times 10^{-14}$ cm^3 molecule^{-1} s^{-1}).[123] The term k_f, the radiation relaxation constant of OH ($A^2\Sigma^+$) → OH ($X^2\Pi$) (0, 0), is the reciprocal of the radiative lifetime of 7 x 10^{-7} s as proposed by Lengel and Crosley.[119] Fairchild et al.[120] evaluated OH quenching by H_2O and found a temperature-independent quenching coefficient of k_Q [OH ($A^2\Sigma^+$) + H_2O] = 4.7 x 10^{-10} cm^3 molecule^{-1} s^{-1}, which is employed here. A plot of resonance fluorescence I_F at λ= 307 nm vs. time is shown in Figure 18. The conditions used in Figure 18 coupled with the constants mentioned above yield $k_Q[Q] / k_f$= 0.5 as an example. This quenching term only affects the sensitivity of the signal, not k', the derived pseudo-first-order rate constant of OH.

Before starting the measurements on the reactions of interest, a test reaction

$$OH + H_2 \rightarrow H_2O + H\,, \qquad (6.2)$$

was performed first to verify that the reaction conditions produced rate constants consistent with those derived from other techniques. Nine measurements of reaction (6.2)

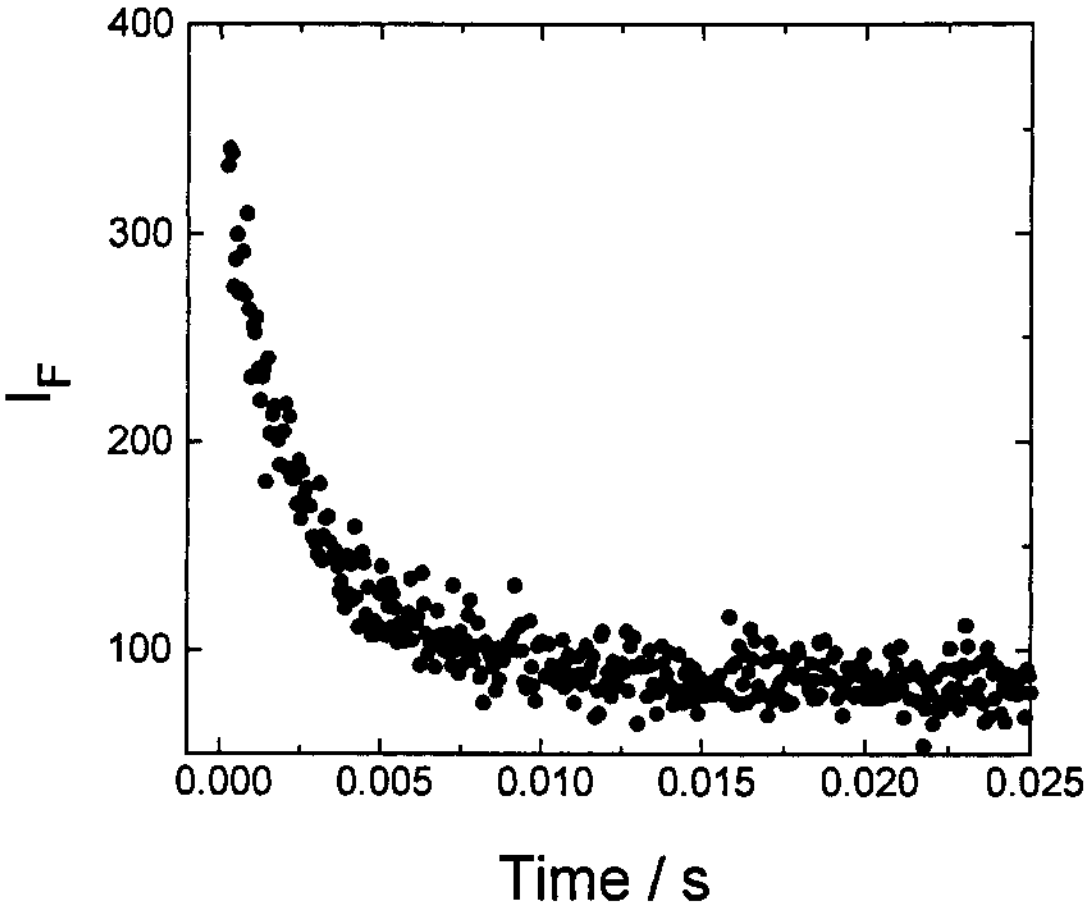

Figure 18. Plot of fluorescence intensity (I_F) of OH vs. Time at 72.7 mbar and T = 295 K where $[H_2O] = 1.45 \times 10^{15}$ molecule cm^{-3} and $[Si(CH_3)_2H_2] = 8.1 \times 10^{12}$ cm^3 $molecule^{-1}$ s^{-1}.

were carried out at an average temperature of 294 K and the weighted mean rate constant of $(5.07 \pm 0.51) \times 10^{-15}$ cm^3 molecule^{-1} s^{-1} was obtained (1σ error limit). Table 19 summarizes the rate constant measurements. This reaction has been studied by a number of workers[124,125,126,127] and $k_{6.2}$ derived in this research is comparable with the recommended reference result of $k_{6.2} = (6.09 \pm 0.61) \times 10^{-15}$ cm^3 molecule^{-1} s^{-1} at 294 K,[128] thus confirming the reliability of the setup and the rate constants measured. Rate constants for the reactions of OH with silane (6.3), and mono-(6.4), di-(6.5), tri-(6.6), and tetramethylsilanes (6.7) were determined at room temperature.

$$OH + SiH_4 \rightarrow \text{products} \qquad (6.3)$$

$$OH + Si(CH_3)H_3 \rightarrow \text{products} \qquad (6.4)$$

$$OH + Si(CH_3)_2H_2 \rightarrow \text{products} \qquad (6.5)$$

$$OH + Si(CH_3)_3H \rightarrow \text{products} \qquad (6.6)$$

$$OH + Si(CH_3)_4 \rightarrow \text{products} \qquad (6.7)$$

Under the experimental conditions used, the pseudo-first-order decay of OH was observed, so that

$$-\frac{d[OH]}{dt} = (k_a[Si(CH_3)_xH_{4-x}] + k_{diff})[OH] = k_{ps1}[OH] \qquad (6.8)$$

where k_{ps1} is the exponential decay constant for the loss of OH, obtained from nonlinear least-square fits to the fluorescence signals. k_{diff} represents the loss of OH radicals from the reaction zone to the walls of the reactor or other slow processes with photolysis fragments, and k_a (a = 6.3 - 6.7) was derived from the slope of a linear plot of k_{ps1} against

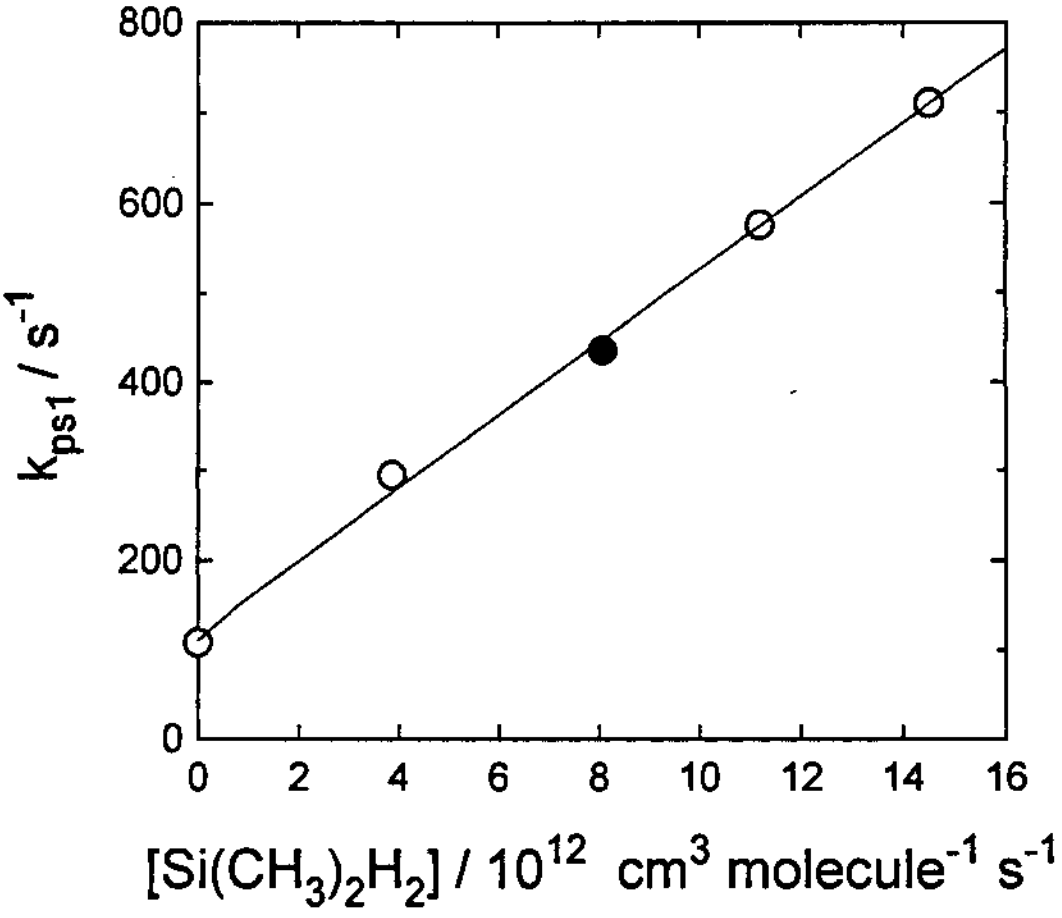

Figure 19. Plot of pseudo-first-order rate constant of OH radical vs. [$Si(CH_3)_2H_2$] at 295 K. The solid circle marked is the one whose OH fluorescence signal plus background is shown in Figure 18.

several reactant concentrations (a minimum of four, on average, five). Figure 19 illustrates one such plot for $k_{6.5}$ at 295 K. The measured values of $k_{6.3}$ to $k_{6.7}$ at room temperature are summarized in Tables 20 through 24, respectively. Variations in the flash energy by a factor of two, the variation of the pressure by a factor of three, and the variation of $[H_2O]$ by a factor of two yielded no dependence of the derived rate constants on these parameters. This indicates that side reactions, if any, have a negligible effect on the measured rate constants under the conditions used.

Only one room temperature measurement of reaction (6.7) has been reported previously. In addition, one study of reaction (6.3) was conducted over several temperatures. Recently, Atkinson[113] investigated the kinetics of a series of organosilicon compounds with OH, NO_3, and O_3 at 297 K by photolysis / gas chromatography with flame ionization detection, and reported a value of $(1.0 \pm 0.3) \times 10^{-12}$ cm^3 molecule^{-1} s^{-1} for the rate constant of OH + $Si(CH_3)_4$, $k_{6.7}$. This rate constant is in good agreement with the value of $(1.09 \pm 0.05) \times 10^{-12}$ cm^3 molecule^{-1} s^{-1} obtained in this study (where the error is 1σ and refers to the precision only). With consideration of the instrumental accuracy, which consists of the propagation errors from the pressure gauge, the flow meters, and the thermocouple, the potential systematic error then added to the precision error gives a total error limit of about 10%. Therefore, the weighted mean $k_{6.7}$ can be rewritten to be $(1.09 \pm 0.11) \times 10^{-12}$ cm^3 molecule^{-1} s^{-1}. The same error limits apply to the other rate constants measured in this study. Reaction (6.3) was studied by Atkinson and Pitts[110] using photolysis / resonance fluorescence over a temperature range of 297 - 438 K. They reported a room temperature rate measurement of the H abstraction rate of $(1.26 \pm 0.2) \times$

10^{-11} cm^3 $molecule^{-1}$ s^{-1} and a zero barrier activation energy for OH + SiH_4. It agrees very well with the value of (1.22 ± 0.12) x 10^{-11} cm^3 $molecule^{-1}$ s^{-1} derived in this study.

In order to assess the influence of these volatile silane compounds if emitted into the atmosphere, the lifetimes of these compounds need to be determined. The atmospheric lifetimes of these silane compounds were estimated by comparing the reactivity of a silane compound with that of methylchloroform (CH_3CCl_3) under the assumption that the reaction with OH is the dominant removal process in the troposphere for both CH_3CCl_3 and the silane compound. Ideally, we should compare the rate constants of these silane compounds with CH_3CCl_3 at 277K to determine the lifetimes of these compounds because this temperature, 277K, is the average temperature for the degradation reactions with OH in the troposphere.[129] However, a rough calculation on the atmospheric lifetimes of these molecules is made here with the only available, room temperature, rate constants. Hence, the tropospheric lifetime, τ(silane), can be approximated[139] by

$$\tau(\text{silane}) / \tau(CH_3CCl_3) = k_{295}(CH_3CCl_3) / k_{295}(\text{silane}) \qquad (6.9)$$

where $\tau(CH_3CCl_3)$ is the tropospheric lifetime of CH_3CCl_3 regarding to reaction with OH, and $k_{295}(CH_3CCl_3)$ and k_{295}(silane) are the rate contants of OH with CH_3CCl_3 and silane, respectively. The rate constants and lifetimes of silanes as well as CH_3CCl_3[129,131] are listed in Table 25.

The rate constants for the reactions of the OH radical with silane and its methyl-substituted compounds studied are in the range of (0.1 - 4.5) x 10^{-11} cm^3 $molecule^{-1}$ s^{-1}. The total rate constant increases with an increase in the number of methyl group from 0 - 2, drops off with the third methyl-substituent and then goes to a lowest value with the

Table 25: Rate Constants of OH plus Silane Compounds at 295 K and their Atmospheric Lifetimes

molecules	k (295K) / cm^3 $molecule^{-1}$ s^{-1}	lifetimes (τ)
CH_3CCl_3	1.2×10^{-14}	5.5 yr.
SiH_4	1.22×10^{-11}	2.2 day
$Si(CH_3)H_3$	3.43×10^{-11}	0.8 day
$Si(CH_3)_2H_2$	4.48×10^{-11}	0.6 day
$Si(CH_3)_3H$	2.67×10^{-11}	1.0 day
$Si(CH_3)_4$	1.09×10^{-12}	24.9 day

addition of the fourth methyl group. The magnitude of these room temperature OH radical reaction rate constants and the observed dependence on the number of methyl-substituted groups indicates that the reaction procedes by H abstraction mainly from the Si-H bond, because of the much lower rate constant of OH plus $Si(CH_3)_4$, which can only proceed via reaction of C-H bonds toward OH. Figure 20 shows the trend of the rate constants of OH radicals with differently methylated silanes. The contribution of H abstraction from a C-H group is around 3% for trimethylsilane and less for the mono- and dimethylsilanes. With this small correction for C-H bond reactivity toward H abstraction, the H abstraction rate constants per Si-H bond were calculated and are also shown in Figure 20. This increasing rate constant per Si-H bond from silane through mono- and di- to trimethylsilane illustrates the increasing Si-H bond reactivity with the increasing number of methyl groups.

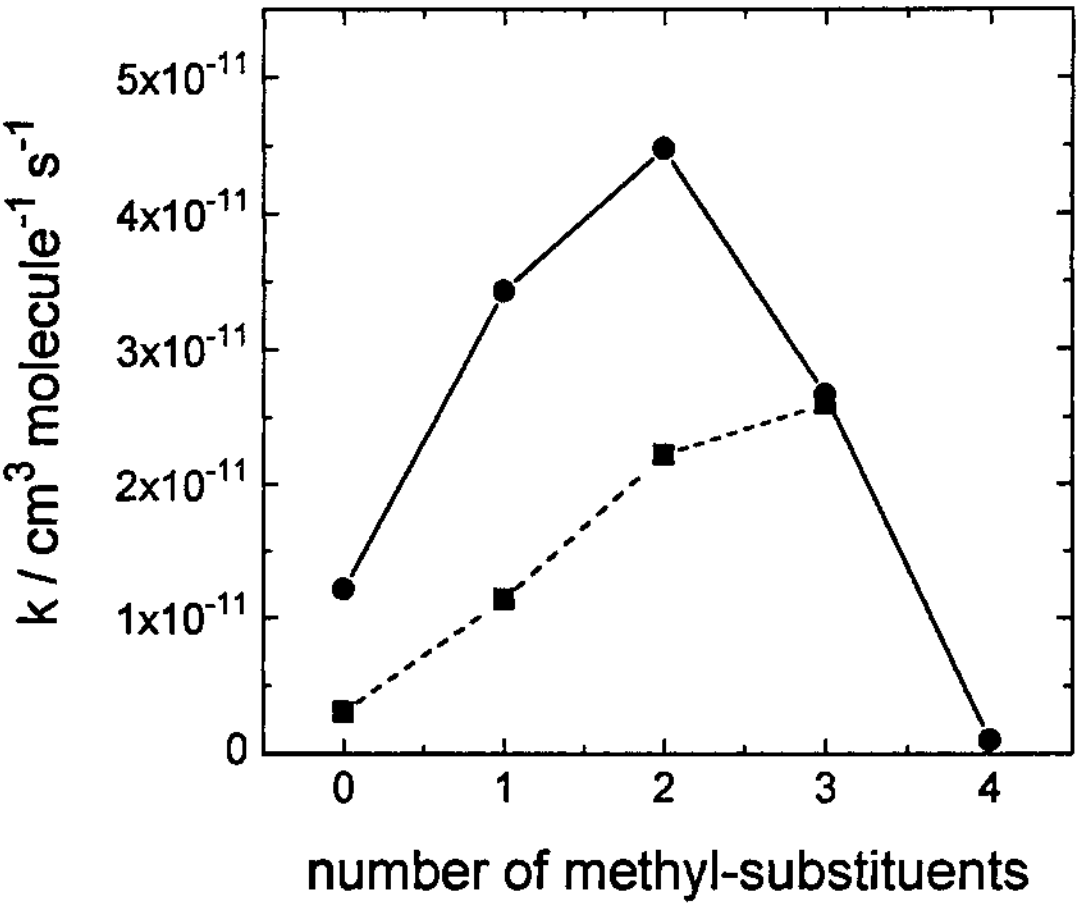

Figure 20: Second-order rate constant of OH radical with different numbers of methyl-substituted silanes. (●) and solid line show the trend of total H abstraction rate constants of silane and its different number of methyl-substituted compounds, and (■) and dashed line indicate the rate constants per Si-H bond.

The study of the trimethylsilyl radical described in chapter 3 suggests that BDE_{298} $((CH_3)_3Si\text{-}H) > BDE_{298}(SiH_3\text{-}H)$ by measuring the rate constants of the reversible reaction of $Si(CH_3)_3$ plus HBr. Thus the stronger Si-H bond is found to be more reactive towards OH. The investigation in the present study is coincident with the implication from the measurements of O (^3P) + $(CH_3)_3SiH$ by Misra et al.[132] which suggest that alkylation increases the reactivity of Si-H bonds towards atomic oxygen and that this effect is independent of the nature of the alkyl group. The reason for this higher reactivity of trimethylsilane than silane toward OH could be explained by the differing electronegativity of CH_3 and H.[133,134] The more electronegative CH_3 group leads to a central Si atom that is more positive in trimethylsilane than in silane. Thus the more polar Si-H bond in trimethylsilane is more labile than that in silane. This fact of the stronger Si-H bond having a higher reactivity towards OH may be due to the lower barrier to the reaction and can be explained in terms of the HOMO and LUMO of silane. For the silane plus OH reaction, the σ bonding MO between Si-H results a greater portion in H due to the higher electronegativity of H. Thus the σ antibonding MO has a greater portion in the Si atom when the higher electronegative OH donates electron density in the breakage of the Si-H bond. The σ antibonding MO, which is partially occupied in the transition state, is stabilized by the electronegative alkyl groups on the Si center in trimethylsilane, therefore the barrier of this reaction of trimethylsilyl plus OH is lower and the reactivity is higher.

CHAPTER 7

CONCLUSION

In conclusion, rate constants of alkyl and silyl radicals plus HBr reactions as well as the reaction of Br plus disilane have been measured. The C-H bond dissociation enthalpies of alkanes and Si-H bond strength of trimethylsilane calculated from the derived rate constants, along with the other thermochemical data, show that alkylation decreases the C-H bond strength of alkanes, whereas it increases the Si-H bond energy in silane. Also, the silyl-weaking effect in silane is observed. All these observations could be explained by the "inductive effect" which is due to the differing electronegativity of Si and C. Future work in terms of the bond strength varied by the electron withdrawing or donating groups can be extended to the study of germanium chemistry.

As a matter of fact, the electronegativity of germanium compared to other elements of group IV of the periodic table has been argued. But most researchers agree that the electronegativity of germanium (2.0 -2.1) lies between Si (1.7 - 2.0) and C (2.4 - 2.5), and is close to that of H. The study of alkyl and germyl substituents on the Ge-H bond strengths of germanium hydrides will be promising to test the inductive effect. In light of the silyl-weaking effect in silane, one of the interesting projects in the future will be reactions involving multiple silyl substituents on silane. It is worth testing whether, as seems likely, cumulative silyl substitution will produce a greater weakening.

To extend the study on alkanes, experimental rate constant measurements on the

reactions involving cycloalkyl radicals, such as the forward and backward reactions of cyclopropyl plus HBr, will be also interesting to see the effect of ring strain on the C-H bond strength.

The temperature-dependent rate constants of the HI + Cl reaction were measured. The rate constant determined from either monitoring Cl or I are close, indicating that the kinetics of this reaction are not dependent on these two different monitoring methods. The kinetics of hydrogen plus silane were investigated by both experimental measurements and TST modeling. The rate constants resolve a discrepancy concerning the pre-exponential factor, and are coincident with TST calculations based on new ab initio theoretical results with a Wigner tunneling correction.

The room-temperature rate constants for the gas-phase reaction of hydroxyl with silane, and mono-, di, tri, and tetramethylsilanes have been determined to investigate the methyl-substitution on the reactivity of Si-H bonds towards OH. It is indicated that the stronger Si-H bonds in silanes have greater reactivity towards OH. This effect can be explained in terms of the LUMO orbital of trimethylsilane, partially occupied in the transition state, in which the Si center is stabilized by the electronegative alkyl-group. This explanation can be tested by further experiments, such as the reaction of OH plus trichlorosilane. The more electronegative Cl substituent in silane is expected to lower the reaction barrier more, and result in a higher reactivity towards OH compared to SiH_4.

New theoretical calculations can provide the evidence to test or improve the experimental results. For example, in the study of alkyl radical reactions, one of the uncertain quantities is the entropy of the radicals. Ab initio calculations involving the

entropy of radicals and enthalpy of the reactions can result in better estimates for the C-H bond strength of alkanes. Theoretical calculations can also characterize the potential energy surface to investigate the hypothesis that the radical plus HBr and HI + Cl reactions proceed via bound intermediates, and show a slight negative or almost zero activation energy for the overall reaction.

APPENDIX

SUMMARY OF RATE CONSTANT MEASUREMENTS

Table 2 : Summary of Rate Constant Measurements on t-C_4H_9 + HBr Reactions Under Different Conditions

Reactor Surface	P, mbar	F, J	τ, s	$[HBr]_{max}$, 10^{13} cm^{-3}	$[(CH_3)_3CI]$, 10^{14} cm^{-3}	Lens[b] Type	$k_{3.1} \pm \sigma_{k3.1}$, 10^{-11} cm^3 s^{-1}
Pyrex	31.3	4.05	1.0	7.8	2.0	quartz	2.57 ± 0.12
Pyrex	31.3	4.05	1.0	7.7	4.1	quartz	3.33 ± 0.22
Pyrex	31.1	4.05	1.9	7.6	4.0	quartz	3.60 ± 0.17
Pyrex	31.0	5.00	0.9	7.6	2.0	quartz	2.39 ± 0.79
Pyrex	31.0	2.45	0.9	7.6	2.0	quartz	2.81 ± 0.68
Pyrex	30.3	4.05	0.9	7.4	1.9	MgF_2	2.59 ± 0.24
Pyrex	30.3	4.05	0.9	7.4	3.9	MgF_2	3.21 ± 0.28
steel	29.0	4.05	1.0	14.4	1.3	quartz	2.39 ± 0.66
steel	28.6	5.00	0.9	9.7	1.3	quartz	2.49 ± 0.67
steel	28.6	2.45	0.9	9.8	1.3	quartz	2.28 ± 0.08
steel	29.5	5.00	0.9	10.0	1.3	MgF_2	2.38 ± 0.18
steel	29.5	2.45	0.9	6.5	1.3	MgF_2	3.01 ± 0.11
							[c]2.67 ± 0.13

[a]All measurements made at about 295 K. [b]Lens used in flash photolysis system. [c]weighted mean value with 1σ precision.

Table 3: Summary of Kinetic Measurements for i-C_3H_7 + HBr Reaction

T, K	P, mbar	τ_{res}, s	F, J	[i-C_3H_7I], 10^{14} cm^{-3}	$[HBr]_{max}$, 10^{13} cm^{-3}	$k_{3.2}\pm\sigma_{3.2}$, 10^{-11} cm^3 s^{-1}
294	32.4	0.7	4.05	2.5	5.0	1.45 ± 0.22
294	32.1	0.7	5.00	1.1	6.0	1.01 ± 0.06
294	32.1	0.7	2.50	1.1	6.0	1.03 ± 0.04
295	31.2	0.5	4.05	1.0	7.4	1.15 ± 0.04
295	30.5	1.0	4.05	1.9	8.4	1.55 ± 0.03
295	31.6	1.0	4.05	1.0	8.8	1.31 ± 0.01
296	32.7	0.5	4.05	1.8	7.8	0.97 ± 0.03
296	33.1	0.5	4.05	1.1	8.1	0.97 ± 0.03
295						[a]1.25 ± 0.06

[a]weighted mean value with 1 σ precision at this average temperature.

Table 4 : Summary of Rate Constant Measurements for C_2H_5 + HBr Reaction

T, K	P, mbar	τ_{res}, s	F, J	$[C_2H_5I]$, 10^{14} cm^{-3}	$[HBr]_{max}$, 10^{13} cm^{-3}	$k_{3,3} \pm \sigma_{k3,3}$ 10^{-12} cm^3 s^{-1}
296	30.0	0.5	4.05	1.1	14.4	7.65 ± 0.34
296	30.1	0.5	4.05	2.1	14.3	7.20 ± 0.05
297	35.1	0.6	4.05	1.4	9.1	6.62 ± 0.15
297	31.1	0.5	5.00	1.1	13.7	6.80 ± 0.11
297	31.1	0.5	2.45	1.1	13.7	6.61 ± 0.11
297	31.3	1.0	4.05	2.1	13.4	7.82 ± 0.23
297	31.9	0.5	4.05	1.2	14.0	6.63 ± 0.10
297	32.1	0.5	4.05	2.3	13.9	6.34 ± 0.16
297	32.1	0.5	4.05	2.3	12.4	6.20 ± 0.26
297	29.7	0.5	4.05	1.2	13.1	8.27 ± 0.48
297	29.2	0.9	4.05	2.1	16.5	8.87 ± 0.21
297						[a]7.01 ± 0.15

[a]weighted mean value with 1σ precision at this average temperature.

Table 5: Summary of Kinetic Measurements for n-C_3H_7 + HBr Reaction

T, K	P, mbar	τ_{res}, s	F, J	[n-C_3H_7I], 10^{14} molecule cm^{-3}	$[HBr]_{max}$, 10^{13} molecule cm^{-3}	$k_{3.4} \pm \sigma_{k3.4}$, 10^{-12} molecule^{-1} cm^3 s^{-1}
295	31.5	0.5	4.05	1.7	6.5	10.86 ± 1.13
295	33.3	0.5	2.50	2.2	11.8	10.68 ± 0.36
295	33.3	0.5	5.00	2.2	11.8	9.12 ± 0.37
295	33.1	1.0	4.05	2.1	11.5	10.47 ± 0.89
295	33.2	0.5	4.05	1.1	12.0	9.45 ± 0.27
295	33.5	0.5	4.05	2.1	12.0	9.08 ± 0.25
296	30.0	0.5	4.05	2.0	11.4	9.04 ± 1.46
296	39.9	0.6	4.05	2.2	15.4	11.15 ± 0.21
296	38.2	1.2	4.05	2.1	14.4	13.02 ± 0.37
296	33.9	0.5	5.00	1.0	16.0	9.28 ± 0.17
296	33.9	0.5	2.50	1.0	15.9	9.65 ± 0.33
296						9.98 ± 0.34[a]
329	29.6	0.4	5.00	0.6	14.1	9.07 ± 0.30
329	29.6	0.4	2.50	0.6	14.1	9.22 ± 0.13

329	30.4	0.4	4.05	0.6	14.6	8.73 ± 0.12
329	29.7	0.8	4.05	0.6	10.9	8.74 ± 0.12
329						8.89 ± 0.13[a]
362	31.3	0.4	5.00	1.3	13.7	6.01 ± 0.08
362	31.3	0.4	2.50	1.3	13.7	6.05 ± 0.07
362	31.2	0.4	4.05	0.7	13.7	6.31 ± 0.11
362	30.4	0.8	4.05	1.3	14.3	6.53 ± 0.19
362						6.11 ± 0.09[a]
397	30.4	0.4	4.05	0.9	10.5	5.82 ± 0.12
397	32.9	0.8	4.05	1.0	17.4	6.50 ± 0.17
397	34.0	0.4	5.00	1.0	11.7	5.88 ± 0.07
397	34.0	0.4	2.50	1.0	11.7	5.95 ± 0.13
397						5.94 ± 0.11[a]
463	30.0	0.6	4.05	1.5	19.2	3.85 ± 0.09
463	30.3	0.6	5.00	2.5	19.0	4.29 ± 0.08
463	30.3	0.6	2.50	2.5	19.0	4.22 ± 0.13
463	33.3	0.3	4.05	1.4	12.5	4.20 ± 0.10
463						4.14 ± 0.11[a]

463						4.14 ± 0.11[a]
520	39.0	0.4	2.50	0.9	13.1	3.27 ± 0.16
520	39.0	0.4	5.00	0.9	13.1	3.03 ± 0.16
520	39.1	0.4	4.05	0.5	13.1	3.27 ± 0.11
520	38.8	0.7	4.05	0.9	15.0	3.10 ± 0.18
520	31.3	0.3	5.00	0.9	19.1	3.14 ± 0.10
520	31.3	0.3	2.50	0.9	19.1	3.00 ± 0.06
520	31.3	0.3	4.05	0.5	19.2	3.23 ± 0.05
520	30.8	0.6	4.05	0.9	21.0	3.31 ± 0.07
520						3.16 ± 0.04[a]

[a] weighted mean value with 1σ precision at this average temperature.

Table 7 : Summary of Kinetic Measurements for $Si(CH_3)_3$ + HBr Reaction

T, K	P, mbar	τ_{res}, s	F, J	$[Si_2(CH_3)_6]$ 10^{14} molecule cm^{-3}	$[HBr]_{max}$ 10^{13} molecule cm^{-3}	$k_{3.6} \pm \sigma_{k3.6}$[a] 10^{-11} cm^3 $molecule^{-1}$ s^{-1}
287	42.7	0.7	4.05	1.45	9.31	6.92 ± 0.50
287	42.7	0.7	4.05	2.38	11.50	5.83 ± 0.30
289	31.5	0.5	5.00	1.36	10.60	6.19 ± 0.67
289	31.5	0.5	2.45	1.36	7.13	6.49 ± 0.12
289	31.6	0.5	4.05	2.45	11.90	6.59 ± 0.52
289	31.5	0.5	5.00	1.30	9.91	6.50 ± 0.47
289	31.5	0.5	2.45	1.30	9.91	6.22 ± 0.44
289	31.3	0.5	4.05	0.87	7.90	6.42 ± 0.17
290	32.0	0.5	4.05	0.90	9.95	4.47 ± 0.15
290	32.0	0.5	4.05	1.61	8.32	5.96 ± 0.40
289						5.94 ± 0.16[b]
295[c]	31.0	1.0	4.05	0.91	4.39	7.22 ± 0.48
295[c]	30.2	1.0	4.05[d]	0.83	4.26	7.33 ± 0.20
296[c]	31.4	1.9	4.05[d]	1.03	7.65	5.92 ± 0.37
296[c]	31.4	1.9	4.05[d]	2.05	7.60	7.43 ± 0.12

294[c]	29.1	1.8	4.05[d]	0.96	5.53	6.93 ± 0.48
294[c]	29.7	0.9	4.05[d]	0.97	4.89	6.64 ± 0.30
294[c]	31.0	1.9	5.00[d]	2.03	10.70	6.11 ± 0.53
294[c]	31.0	1.9	2.45[d]	2.03	10.70	6.16 ± 0.71
295						7.17 ± 0.20[b]
296	45.2	0.7	4.05	3.06[e]	4.03	8.53 ± 0.62
291	47.3	0.8	5.00	3.16[e]	4.81	10.50 ± 0.65
291	47.3	0.8	2.45	3.16[e]	4.81	10.10 ± 0.57
292	46.0	1.0	4.05	4.69[e]	11.00	5.74 ± 0.29
289	46.1	0.6	4.05	3.03[e]	4.03	5.73 ± 0.44
289	45.5	0.5	4.05	1.21[e]	4.28	10.19 ± 0.20
289	32.0	0.5	4.05	2.46[e]	6.12	5.20 ± 0.71
289	31.2	0.5	4.05	2.44[e]	5.84	5.98 ± 0.56
293						7.80 ± 0.80[b]
323	31.3	0.5	4.05	1.05	7.93	5.52 ± 0.24
323	31.3	0.5	4.05	2.58	7.92	4.84 ± 0.29
327	40.0	0.6	4.05	2.44	10.20	5.63 ± 0.27
327	40.0	0.6	4.05	2.44	9.96	5.74 ± 0.69
325						5.38 ± 0.20[b]

396	32.0	0.4	4.05	1.60	7.63	4.17 ± 0.13
396	32.0	0.4	4.05	0.60	7.61	5.39 ± 0.24
404	31.2	0.4	5.00	1.33	7.24	3.73 ± 0.28
404	31.2	0.4	2.45	1.33	7.24	4.13 ± 0.19
400						4.29 ± 0.14[b]
444	40.0	0.4	4.05	1.56	10.00	2.87 ± 0.73
444	40.0	0.4	4.05	3.01	9.95	2.93 ± 0.12
444	40.0	0.4	5.00	1.33	10.20	2.75 ± 0.13
444	40.0	0.4	2.45	1.33	10.20	2.90 ± 0.20
449	32.0	0.4	4.05	1.42	5.68	3.36 ± 0.18
449	32.0	0.4	4.05	0.78	5.69	3.62 ± 0.23
446						3.00 ± 0.10[b]
512	32.0	0.3	4.05	1.13	3.77	3.10 ± 0.44
515	33.1	0.3	4.05	3.33	5.76	2.28 ± 0.20
515	33.1	0.3	4.05	1.27	5.81	2.60 ± 0.19
517	32.0	0.3	4.05	1.62	7.08	2.93 ± 0.39
515						2.55 ± 0.14[b]

[a] 1σ presision of the slope of a plot of $k_{3,6}$ vs [HBr]. [b] weighted mean value with 1σ precistion at this average temperature.
[c] Pyrex reactor employed. All other measurements were made in the steel reactor.
[d] Photolysis through Suprasil quartz optics. MgF_2 used for all other experiments.[e] $Si(CH_3)_3I$ used as the precursor.

Table 8: Summary of Kinetic Measurements for Br + Si_2H_6 Reaction

T, K	P, mbar	τ_{res}, s	F, J	$[CH_2Br_2]$ 10^{14} molecule cm^{-3}	$[Si_2H_6]_{max}$ 10^{12} molecule cm^{-3}	$k_{3.8} \pm \sigma_{k3.8}$ 10^{-11} cm^3 $molecule^{-1}$ s^{-1}
295	69.2	1.5	4.05	6.03	16.6	3.25 ± 0.20
295	134.8	4.4	4.05	23.60	10.4	4.33 ±0.20
295	140.6	4.5	5.00	16.00	9.6	4.42 ± 0.69
295	140.6	4.5	2.45	16.00	9.4	4.33 ± 0.16
296	130.6	2.2	4.05	3.76	12.7	4.21 ± 0.12
296	137.8	2.2	4.05	8.05	13.4	5.81 ± 0.34
296	68.8	1.5	4.05	5.00	16.6	4.12 ± 0.10
296	68.0	1.5	5.00	6.00	14.3	4.22 ± 0.25
296	68.0	1.5	2.45	6.00	14.3	4.08 ± 0.11
312	69.2	1.4	4.05	5.71	15.6	3.86 ± 0.20
313	136.6	4.1	4.05	15.90	8.4	3.42 ± 0.13
314	75.5	1.6	4.05	5.91	13.9	3.64 ± 0.15
315	68.6	1.4	4.05	5.60	15.5	4.31 ± 0.13
334	75.4	1.5	4.05	5.33	13.1	4.23 ± 0.12
335	69.0	1.3	4.05	4.40	14.6	3.92 ± 0.83

337	72.6	1.4	4.05	5.26	12.5	4.11 ± 0.17
338	68.6	1.3	4.05	5.20	14.4	4.73 ± 0.21
359	79.0	1.4	4.05	6.14	12.7	4.43 ± 0.15
363	68.0	1.8	4.05	8.03	15.5	4.33 ± 0.13
381	67.3	1.1	5.00	3.86	11.0	5.17 ± 0.17
381	67.3	1.1	2.50	3.86	11.0	5.03 ± 0.15
420	67.7	1.6	4.05	5.92	13.4	4.79 ± 0.20
420	71.8	1.1	4.05	4.57	10.1	6.00 ± 0.14
485	66.2	1.3	4.05	6.79	10.9	5.43 ± 0.22
487	67.5	1.3	4.05	4.89	10.4	6.42 ± 0.15
487	71.6	0.9	4.05	3.91	8.1	6.79 ± 0.17
536	72.8	0.7	4.05	3.62	7.9	7.82 ± 0.28
542	77.2	1.4	4.05	5.04	12.5	6.61 ± 0.20
565	72.6	0.6	4.05	3.07	8.2	7.25 ± 0.17

Table 12 : Summary of Rate Constant Measurements for HI + Cl

T, K	P, mbar	τ_{res}, s	$[HI]_{max}$, 10^{13} cm^{-3}	$[Cl_2]$, 10^{13} cm^{-3}	Laser E mJ	$[Cl]_0$, 10^{12} cm^{-3}	Monitored atom	$k_{4.1} \pm \sigma_{k4.1}$, 10^{-10} $molecule^{-1}$ cm^3 s^{-1}
296	34.4	0.4	3.3	22.0	43	1.8	Cl	1.07 ± 0.27
296	23.3	0.5	1.8	15.6	43	1.3	Cl	1.01 ± 0.18
297	29.0	0.6	2.8	5.1	58	0.6	Cl	0.93 ± 0.03[b]
297	29.0	0.7	2.2	12.1	58	1.3	Cl	0.96 ± 0.02[b]
297	29.3	0.8	6.9	11.8	47	1.0	I	1.49 ± 0.13[b]
297	29.3	0.8	5.5	8.0	47	0.7	I	1.24 ± 0.17[b]
297	28.6	0.8	5.4	14.8	43	1.2	I	1.27 ± 0.14[b]
297	28.6	0.8	5.4	14.8	43	1.2	I	1.14 ± 0.19[b]
297	33.3	0.7	5.3	12.2	40	0.9	I	1.12 ± 0.13[b]
297	33.4	0.7	5.3	24.0	40	1.8	I	1.10 ± 0.12[b]
297								0.97 ± 0.03[a]
319	29.9	0.8	5.7	16.6	50	1.6	I	1.30 ± 0.05
319	29.8	0.4	4.3	8.1	50	0.8	I	1.05 ± 0.03
319	29.9	0.4	3.6	16.1	50	1.6	I	1.28 ± 0.02

319								1.22 ± 0.07[a]
344	30.0	0.8	3.3	14.2	43	1.1	I	0.90 ± 0.02
344	30.7	0.4	3.1	7.2	43	0.6	I	1.05 ± 0.03
344								0.95 ± 0.07[a]
353	31.0	0.4	3.3	19.6	36	1.3	Cl	1.10 ± 0.22
353	31.0	0.4	3.0	19.6	36	1.3	Cl	1.04 ± 0.17
354	23.7	0.4	4.0	8.8	58	1.0	I	0.98 ± 0.06
354	34.7	0.3	4.0	6.6	58	0.7	I	1.03 ± 0.47
354	34.4	0.3	3.9	6.5	29	0.4	I	1.23 ± 0.37
354								1.00 ± 0.02[a]
386	31.0	0.4	5.1	14.9	54	1.5	I	0.93 ± 0.06
390	30.9	0.3	4.8	14.6	40	1.1	I	1.04 ± 0.01
390	31.0	0.7	4.0	14.6	40	1.1	I	0.97 ± 0.04
390	31.0	0.7	4.0	28.7	40	2.1	I	1.14 ± 0.04
389								1.04 ± 0.02[a]

[a] weighted average for each temperature.

[b] measurements were done in the Pyrex reactor.

Table 14 : Summary of Rate Constant Measurements for H + SiH_4

T, K	P, mbar	τ_{res}, s	F, J	$[NH_3]$, 10^{15} cm^{-3}	$[SiH_4]_{max}$, 10^{14} cm^{-3}	$k_{5.1} \pm \sigma_{k5.1}$, 10^{-12} cm^3 s^{-1}
290	42.7	0.7	4.05	0.84	7.92	0.26 ± 0.06
290	42.7	0.7	4.05	1.39	8.03	0.27 ± 0.04
329	45.3	0.9	4.05	2.57	11.10	0.55 ± 0.06
330	43.1	0.8	5.00	2.10	12.90	0.60 ± 0.01
330	43.1	0.8	2.45	2.10	12.90	0.55 ± 0.01
379	43.7	0.6	2.45	1.57	4.32	0.99 ± 0.03
379	43.7	0.6	5.00	1.57	4.32	1.06 ± 0.03
382	42.5	1.1	2.45	3.06	2.80	1.11 ± 0.09
382	42.5	1.1	5.00	3.06	2.80	1.17 ± 0.17
449	43.9	1.0	2.45	1.48	4.83	2.30 ± 0.06
449	43.9	1.0	5.00	1.48	4.83	2.44 ± 0.05
449	59.7	1.4	4.05	2.02	5.14	2.44 ± 0.06
496	40.9	0.4	5.00	1.12	1.57	3.97 ± 0.13
496	40.9	0.4	2.45	1.12	2.07	3.99 ± 0.16
570	46.7	0.8	4.05	1.95	3.35	6.05 ± 0.12
570	46.7	0.8	4.05	0.98	3.52	5.81 ± 0.12

570	46.7	0.8	5.00	1.95	3.56	6.09 ± 0.12
570	46.7	0.8	2.45	1.95	3.36	5.76 ± 0.12
600	42.7	0.3	4.05	0.97	1.34	6.82 ± 0.14
600	41.6	0.7	4.05	1.05	2.50	6.85 ± 0.33
658	71.1	1.1	4.05	3.28	1.57	9.73 ± 0.43
658	70.3	1.0	4.05	3.25	1.28	10.35 ± 0.21
658	69.9	0.5	4.05	1.66	1.29	10.51 ± 0.21

Table 19: Rate Constant Measurements for OH + H_2

T, K	F, J	τ_{res}, s	P, mbar	$[H_2O]$ 10^{15} molec. cm^{-3}	$[H_2]_{max}$ 10^{16} molec. cm^{-3}	$k_{6.2} \pm \sigma_{k6.2}$ 10^{-15} molec.$^{-1}$ cm^3 s^{-1}
294	4.05	1.8	44.3	2.99	3.56	5.03 ± 0.03
294	5.00	1.0	33.6	1.84	2.46	6.32 ± 0.22
294	2.50	1.0	33.6	1.84	1.95	6.39 ± 0.24
296	4.05	1.0	40.4	1.52	2.15	6.79 ± 0.19
294	4.05	1.7	64.7	2.27	3.45	4.11 ± 0.25
294	5.00	2.4	97.1	3.30	5.27	5.04 ± 0.04
294	2.50	2.4	97.1	3.30	4.10	5.05 ± 0.34
293	4.05	2.4	96.6	3.71	8.93	4.61 ± 0.15
293	4.05	1.5	95.8	2.02	4.64	5.38 ± 0.31
294						5.07 ± 0.51

[a] weighted mean value at that average temperature and 1σ represents 10% for statistical and instrumental errors.

Table 20: Rate Constant Measurements for OH + SiH_4

T, K	F, J	τ_{res}, s	P, mbar	$[H_2O]$ 10^{15} molec. cm^{-3}	$[SiH_4]_{max}$ 10^{13} molec. cm^{-3}	$k_{6.3} \pm \sigma_{k6.3}$ 10^{-11} molec.$^{-1}$ cm^3 s^{-1}
294	4.05	1.3	42.0	3.41	6.14	1.08 ± 0.05
294	5.00	1.2	49.9	2.93	6.14	1.15 ± 0.04
294	2.50	1.2	49.9	2.93	6.14	1.17 ± 0.02
294	4.05	1.6	102.4	2.88	4.45	1.20 ± 0.02
294	4.05	0.9	53.7	1.58	4.29	1.28 ± 0.07
295	5.00	1.0	55.7	1.60	5.79	1.44 ± 0.05
295	2.50	1.0	55.7	1.60	5.79	1.44 ± 0.05
296	4.05	0.9	49.5	1.29	6.23	1.64 ± 0.08
297	4.05	1.6	69.4	2.67	4.87	0.86 ± 0.06
297	4.05	1.2	31.2	2.05	4.23	0.93 ± 0.04
294						[a]1.22 ± 0.12

[a] weighted mean value at that average temperature and 1σ represents 10% for statistical and instrumental errors.

Table 21: Rate Constant Measurements for OH + $Si(CH_3)H_3$

T, K	F, J	τ_{res}, s	P, mbar	$[H_2O]$ 10^{15} molec. cm^{-3}	$[Si(CH_3)H_3]_{max}$ 10^{13} molec. cm^{-3}	$k_{6.4} \pm \sigma_{k6.4}$ 10^{-11} molec.$^{-1}$ cm^3 s^{-1}
294	4.05	0.8	40.3	1.31	2.33	3.20 ± 0.10
295	5.00	1.5	72.9	2.49	2.34	3.57 ± 0.14
295	2.50	1.5	72.9	2.49	2.33	3.73 ± 0.04
295	4.05	0.9	68.9	1.40	1.14	3.29 ± 0.22
292	4.05	1.2	52.7	1.93	1.92	3.29 ± 0.22
292	5.00	0.9	63.2	1.35	0.60	4.18 ± 0.13
292	2.50	0.9	63.2	1.35	0.48	3.47 ± 0.27
293	4.05	1.6	82.5	2.65	1.13	3.17 ± 0.11
293	4.05	0.9	45.6	1.82	1.01	2.98 ± 0.07
296	4.05	1.7	86.5	2.69	0.95	2.96 ± 0.11
296	4.05	1.0	45.0	1.69	0.97	3.22 ± 0.11
295	5.00	1.4	76.9	2.27	0.97	3.25 ± 0.16
295	2.50	1.4	76.9	2.24	0.97	3.10 ± 0.10
294						[a]3.43 ± 0.34

a weighted mean value at that average temperature and 1σ represents 10% for statistical and instrumental errors.

Table 22: Rate Constant Measurements for OH + $Si(CH_3)_2H_2$

T, K	F, J	τ_{res}, s	P, mbar	$[H_2O]$ 10^{15} molec. cm^{-3}	$[Si(CH_3)_2H_2]_{max}$ 10^{13} molec. cm^{-3}	$k_{65} \pm \sigma_{k6.5}$ 10^{-11} molec.$^{-1}$ cm^3 s^{-1}
294	4.05	1.7	72.4	3.29	2.88	4.93 ± 0.08
294	4.05	0.9	43.2	1.74	1.71	4.35 ± 0.19
294	5.00	2.1	89.0	1.68	3.35	4.73 ± 0.11
294	2.50	2.1	89.0	1.68	3.35	4.18 ± 0.19
294	4.05	1.2	53.5	1.41	2.00	4.73 ± 0.07
293	4.05	1.8	77.6	0.97	3.17	4.32 ± 0.17
294	4.05	0.9	64.1	0.62	1.66	4.45 ± 0.10
294	5.00	0.9	61.9	0.69	1.61	4.06 ± 0.08
294	2.50	0.9	61.9	0.69	1.61	3.83 ± 0.17
295	4.05	1.6	72.7	1.45	2.73	4.31 ± 0.20
295	4.05	1.0	73.6	0.89	1.77	4.39 ± 0.11
295	4.05	0.8	34.7	0.78	1.44	4.99 ± 0.15
295	4.05	1.6	59.4	0.96	3.74	4.38 ± 0.05

295	4.05	1.6	80.1	0.78	3.30	4.55 ± 0.17
295						[a]4.48 ± 0.45

[a] weighted mean value at that average temperature and 1σ represents 10% for statistical and instrumental errors.

Table 23: Rate Constant Measurements for OH + $Si(CH_3)_3H$

T, K	F, J	τ_{res}, s	P, mbar	$[H_2O]$ 10^{15} molec. cm^{-3}	$[Si(CH_3)_3H]_{max}$ 10^{13} molec. cm^{-3}	$k_{6.6} \pm \sigma_{k6.6}$ 10^{-11} molec.$^{-1}$ cm^3 s^{-1}
294	4.5	0.9	58.1	1.44	1.11	3.54 ± 0.15
294	4.5	2.2	117.6	2.07	2.47	3.54 ± 0.18
294	5.0	1.1	39.3	0.97	0.95	3.49 ± 0.13
294	2.5	1.1	39.3	0.97	0.95	3.36 ± 0.18
295	5.0	1.5	71.9	2.28	3.45	2.82 ± 0.11
295	2.5	1.5	71.9	2.28	3.45	2.78 ± 0.06
295	4.5	1.1	41.7	1.63	3.23	2.60 ± 0.02
295	4.5	1.3	39.3	1.03	3.28	3.32 ± 0.10
295	4.5	1.8	58.6	2.00	3.58	3.15 ± 0.14
294	4.5	2.1	40.6	2.00	3.45	3.30 ± 0.16
294	4.5	1.7	112.9	2.09	4.78	2.50 ± 0.04
295						[a]2.67 ± 0.27

[a] weighted mean value at that average temperature and 1σ represents 10% for statistical and instrumental errors.

Table 24: Rate Constant Measurements for OH + $Si(CH_3)_4$

T, K	F, J	τ_{res}, s	P, mbar	$[H_2O]$ 10^{15} molec. cm^{-3}	$[Si(CH_3)_3H]_{max}$ 10^{13} molec. cm^{-3}	$k_{6.7} \pm \sigma_{k6.7}$ 10^{-12} molec.$^{-1}$ cm^3 s^{-1}
295	4.5	0.9	57.4	1.37	3.26	1.31 ± 0.03
295	4.5	1.0	44.3	1.65	2.52	1.33 ± 0.09
294	5.0	1.0	46.8	1.58	2.96	0.97 ± 0.02
294	2.5	1.0	46.8	1.58	2.96	0.92 ± 0.02
295	4.5	1.2	83.1	1.99	2.98	1.11 ± 0.05
294	4.5	1.4	63.5	2.21	4.86	1.35 ± 0.06
294	2.5	1.4	63.5	2.21	4.87	1.18 ± 0.03
295	2.5	1.6	69.6	2.48	4.34	0.91 ± 0.06
295	5.0	1.6	69.6	2.48	4.34	1.03 ± 0.09
293	4.5	2.4	60.0	1.89	3.37	1.57 ± 0.07
293	4.5	2.4	108.7	3.56	7.96	1.07 ± 0.09
295						[a]1.09 ± 0.11

[a] weighted mean value at that average temperature and 1σ represents 10% for statistical and instrumental errors.

REFERENCES

1. Corey, J. Y. *The Chemistry of Organic Silicon Compounds*, edited by Patai, S.; Rapporport, Z. **1989**, Chapter 1, John Wiley & Sons
2. Powlenko, S. *Organosilicon Chemistry*, **1986**, Walter de Gruyeer, Berlin
3. Walsh, R. *Acc. Chem. Rev.* **1981**, 14, 246
4. Kanabus-Kaminska, J. M.; Hawari, J. A.; Griller, D.; Chatgilialoglu, C. *J. Am. Chem. Soc.* **1987**, 109, 5267
5. Kerr, J. A. *Chem. Rev.* **1966**, 66, 465
6. Kistiakowsky, G. B.; Van Artsdalen, E. R. *J. Chem. Phys.* **1944**, 12, 469
7. O'Neal, H. E.; Benson, S. W. *In Free Radicals*; Kochi, J. K.; Ed.; Wiley: New York, **1973**, Vol 2, Chapter 17.
8. Golden, D. M.; Benson, S. W. *Chem. Rev.* **1969**, 69, 125
9. Rogers, A. S. *ACS Symp. Ser.* **1978**, 66, 296
10. Baghal-Vayjooee, M. H.; J.; Benson, S. W. *J. Am. Chem. Soc.* **1978**, 101, 3214
11. Baghal-Vayjooee, M. H.; Colussi, A. J.; Benson, S. W. *Int. J. Chem. Kinet.* **1979**, 11, 147
12. Golden, D. M., Spokes, G. N.; Benson, S. W. *Angew. Chem. Int. Ed. Engl.* **1973**, 12, 534
13. Choe, M.; Choo, K. Y. *Chem. Phys. Lett.* **1982**, 89, 115
14. Pacansky, J.; Horne, D. E.; Gardini, G. P.; Bargon, *J. Phys. Chem.* **1977**, 81, 23

15. Pacansky, J.; Coufal, H. *J. Chem. Phys.* **1980**, 12, 3298

16. Pacansky, J.; Chang, J. S. *J. Chem. Phys.* **1981**, 74, 5539

17. Glick, H. S.; Squire, W.; Hertzberg, A. *Fifth Symposium on Combustion (Intl)*, Williams & Wilkins, Baltimore, **1955**, 393

18. Tsang, W. *J. Chem. Phys.* **1964**, 41, 2487

19. Tsang, W. *In Shock Waves in Chemistry*, **1981**, ed. A. Lifshitz, New York: Dekker, 59

20. Hiatt, R.; Benson, S. W. *J. Am. Chem. Soc.* **1972**, 94, 25

21. Hiatt, R.; Benson, S. W. *J. Am. Chem. Soc.* **1972**, 94, 6886

22. Hiatt, R.; Benson, S. W. *Int. J. Chem. Kinet.* **1972**, 4, 151

23. Hiatt, R.; Benson, S. W. *Int. J. Chem. Kinet.* **1972**, 4,, 479

24. Tsang, W. *Int. J. Chem. Kinet.* **1978**, 10, 821

25. Tsang, W. *J. Am. Chem. Soc.* **1985**, 107, 2872

26. McMillen, D. F.; Golden, D. M. *Ann. Rev. Phys. Chem.* **1982**, 33, 493

27. Carlson, T. A. *Ann. Rev. Phys.* **1974**, 26, 211

28. Rosenstock, H.; Draxl, K.; Steiner, G.; Herron, J. *J. Phys. Chem. Ref. Data* **1977**, 6, supplement No. 1

29. Sen Sharma, D. K.; Franklin, J. L. *J. Am. Chem. Soc.* **1973**, 95, 6562

30. Rosenstock, H. M.; Buff, R.; Ferreora, M. A.; Lias, S. G.; Parr, A. C.; Stocabauer, R. L.; Holmes, J. L. *J. Am. Chem. Soc.* **1982**, 104, 2337

31. Ruscic, B.; Berkowitz, J.; Curtiss, L. A.; Pople, J. A. *J. Chem. Phys.* **1989**, 91, 114

32. Berkowita, J.; Ellison, G. B.; Gutman, D. *J. Phys. Chem.* **1994**, 98, 2744

33. Russic, B.; Berkowitz, J. *J. Chem. Phys.* **1991**, 95, 2416

34. Walsh, R. *In the Chemistry of Organic Silicon Compounds*; Patai, S.; Rappoport, Z.; Eds.; Wiley: New York, **1989**, Chapter 5

35. McKean, D. C.; Torto, I.; Morrisson, A. R. *J. Phys. Chem.* **1982**, 86, 307

36. Bernheim, R. A.; Lampe, F. W.; O'Keefe, J. F.; Qualey, J. R. *J. Phys. Chem.* **1985**, 89, 1087

37. Ding, L.; Marshall, P. *J. Am. Chem. Soc.* **1992**, 114, 5756

38. Bernstein, R. B.; Levine, R. D. *J. Chem. Phys.* **1972**, 57, 434

39. Levine, R. D.; Bernstein, R. B. *Acc. Chem. Res.* **1974**, 7, 393

40. McDonald, J. D. Ph. D. thesis, **1971**, Harvard University, Cambridge, Massachusetts

41. Maylotte, D. H.; Polanyi, J. C.; Woodall, K. B. *J. Chem. Phys.* **1972**, 57, 1547

42. Wodarczyk, F. J.; Moore, C. B. *Chem. Phys. Lett.* **1974**, 26, 484

43. Mei, C. C.; Moore, C. B. *J. Chem. Phys.* **1977**, 67, 3936

44. Mei. C. C.; Moore, C. B. *J. Chem. Phys.* **1979**, 70, 175

45. Kushner, M. J. *J. Appl. Phys.* **1987**, 62, 2803

46. Kushner, M. J. *J. Appl. Phys.* **1988**, 63, 2532

47. Jasinski, J. M.; Gates, S. M. *Acc. Chem. Rev.* **1991**, 24, 9

48. Arthur, N. L.; Potzinger, P.; Reimann, B; Steenbergen, H. P. *J. Chem. Soc., Faraday Trans 2* **1989**, 85, 1447

49. Shi. Y.; Marshall, P. *J. Phys. Chem.* **1991**, 95, 1654

50. Ding, L.; Marshall, P. *J. Phys. Chem.* **1992**, 96, 2197

51. Okabe, H., *Photochemistry of Small Molecules*, **1978**, Wiley, New York

52. Nicovich, J. M.; van Dijk, C. A.; Kreutter, K. D.; Wine, P. H. *J. Phys. Chem.* **1991**, 95, 9898

53. Seakins, P. W.; Pilling, M. J. *J. Phys. Chem.* **1991**, 95, 9874

54. Husain, D.; Krause, L.; Slater, N. K. H. *J. Am. Chem. Soc., Faraday Trans 2*, **1977**, 73, 1678

55. DeMore, W. B.; Sander, S. P.; Golden, D. M.; Hampson, R.F.; Howard, C. J.; Ravishankara, A. R.; Kolb, C. E.; Molina, M. J.; Kurylo, M. *J. Chemical Kinetic and Photochemical Data for Use in Stratospheric Modeling*, **1992**, 10

56. Vogel, A. I. *Textbook of Macro and Semimicro Qualitative Inorganic Analysis*, **1953,** 4th edition, Longmans, Green and Co. Ltd. 358

57. *Mellor's Modern Inorganic Chemistry*, revised and edited by Parkers, G. D. 1967, Wiley 531

58. Romand, J. *Ann. Phys.* (Paris) **1948**, 4, 527

59. Goodeve, C. F.; Taylor, W. C. *Proc. Roy. Soc.* **1935**, A152, 221

60. Nee, J. B.; Suto, M.; Lee, L. C. *J. Chem. Phys.* **1986**, 85, 4919

61. Seakins, P. W.; Pilling, M. J.; Niiranen, J. T.; Gutman, D.; Krasnoperov, L. N. *J. Phys. Chem.* **1992**, 9847

62. Muller-Margraf, W.; Roses, M. J.; Golden, D. M. *J. Am. Chem. Soc.* **1989**, 111, 956

63. Richards, P. D.; Ryther, R. J.; Weitz, E. *J. Phys. Chem.* **1990**, 94, 3663

64. Jorma, A. S.; John, J. Russell, J. J. Gutman, D. *J. Am. Chem. Soc.* **1990**, 112, 1347

65. Doncaster, A. M.; Walsh, R. *J. Phys. Chem.* **1979**, 83, 3037

66. Talukdar, R. K.; Warren, R. F.; Vaghijiani, G. L.; Ravishankara, A. R. *Int. J. Chem. Kinet.* **1992**, 24, 973

67. Seetula, J. A.; Feng, Y.; Gutman, D.; Seakins, P. W.; Pilling, M. J. *J. Phys.Chem.* **1991**, 95, 1658

68. Benson, S. W. *Thermochemical Kinetics*. 2nd ed.; Wiley: New York, **1976**

69. Morgan, C. A.; Pilling, M. J.; Tulloch, J. M.; Ruiz, R. P.; Bayes, K. D. *J. Chem. Soc., Faraday. Trans. 2* **1982**, 78, 1323

70. Slagle, I. R.; Ratajczak, E.; Heaven, M. C.; Gutman, D.; Wagner, A. F. *J. Am. Chem. Soc.* **1985**, 107, 1838

71. Chase, M. W.; Davis, Jr. C. A.; Downey, Jr.; Fruip, Jr. D. J.; McDonald, R. A.; Syverud, A. N. JANAF Thermochemical Tables, 3rd ed.; *J. Phys. Chem. Ref. Data* **1985**, 14, suppl. no.1

72. Tsang, W.; *J. Phys. Chem. Ref. Data*, **1987**, 16

73. Tsang, W.; *J. Phys. Chem. Ref. Data* **1988**, 17

74. Tsang, W. *J. Phys. Chem. Ref. Data* **1990**, 19

75. Pacansky, J.; Yoshimine, M., *J. Phys. Chem.*, **1986**, 90, 1980

76. Russell, J. J.; Seetula, J. A.; Timonen, R. S.; Gutman, D.; Nava, D. J.; *J. Am. Chem. Soc.* **1988**, 110, 3084

77. Benson, S. W.; Kondo, O.; Marshall, R. M. Int. *J. Chem. Kinet.* **1987**, 19, 829

78. Lewis, G. N.; Randall, M. *Thermodynamics* **1961**, revised by Pitzer, K. S.; Brewer, L.; 2nd edition, McGraw-Hill, Chapter 27

79. Allendorf, M. D. Melius, C. F. *J. Phys. Chem.* **1992**, 96, 428

80. Allendorf, M. D.; Melius, C. F. *Sandia Report* **1991**, SAND91-8550, UC-411

81. Doncaster, A. M.; Walsh, R. *J. Chem. Soc., Faraday Trans. 1* **1979**, 75, 1126

82. Potzinger, P.; Ritter, A.; Krause, J. *Z. Naturforsch.* **1975**, 30a, 347

83. (a) Choe, M.; Choo, K. Y. *Chem. Phys. Lett.* **1982**, 89, 115. (b) Choo, K. Y.; Choe, M. H. *Bull. Korean Chem. Soc.* **1985**, 6, 196.

84. Kalinovski, I. J.; Gutman, D.; Krasnoperov, L. N.; Goumri, A.; Yuan, W. -J.; Marshall, P. *J. Phys. Chem.* **1994**, 98, 9551

85. Doncaster, A. M.; Walsh, R. unpublished result

86. Pedley, J. B.; Iseard, B. S. *CATCH Tables for Silicon Compounds*, **1972**, University of Sussex

87. Hirschfelder, J. O.; Curtis, C. F.; Bird, R. B. *Molecular Theory Gases and Liquids*, **1954**, Wiley, New York, 1111

88. Dolson, D. A.; Leone, S. R. *J. Chem. Phys.* **1982**, 77, 4009

89. Subramonia, R.; Rowland, F. S. Roger, R .*J. Phys. Chem.* **1983**, 87, 3799

90. Ashutosh, M. unpublished result

91. Jonathan, N.; Melliar-Simith C. M.; Okuda, S.; Slater, D. H.; Timlin, D. *Mol. Phys.* **1971**, 22, 561

92. Anlauf, K. G.; Charters, P. E.; Horne, D. S.; Macdonald, R.. G.; Maylotte, D. H. Polanyi, J. C.; Skrlac, W. J.; Tardy, D. C.; Woodall, K. B. *J. Chem. Phys.* **1970**, 53, 4091

93. Farrar, J. M.; Lee, Y. T. *J. Chem. Phys.* **1975**, 63, 3639

94. Hoffmann, S. M. A.; Smith, D. J.; Bradshaw, N.; Grice, R. *Mol. Phys.* **1986**, 57, 1219

95. Samson, A. R. *Techniques of Vaccum Ultraviolet Spectroscopy*, **1967**, John Wiley

& Sons, 205

96. Johnston, H. S. *Gas Phase Reaction Rate Theory*, **1966**, Ronald, New York, Chapter 2

97. Mulcahy, M. F. R. *Gas Kinetics*, **1973**, Nelson, London

98. Goumri, A.; Yuan, W.-J.; Ding, L.; Shi, Y.; Marshall, P. *Chem. Phys.* **1993**, 233

99. Cowfer, J. A.; Lynch, K. P.; Michael, J. V. *J. Phys. Chem.* **1975**, 79, 1139

100. Choo, K. Y.; Gasper, P. P.; Wolf, A. P. *J. Phys. Chem.* **1975**, 79, 1752

101. Mihelcic, D.; Schubert, V.; Schindler, R. N. *J. Phys. Chem.* **1977**, 81, 1543

102. Johnson, N. M.; Walker, J.; Stevens, K. S. *J. Appl. Phys.* **1991**, 69, 2631

103. Loh, S. K.; Jasinski, J. M. *J. Chem. Phys.* **1991**, 95, 4914

104. Austin, E. R.; Lampe, F. W. *J. Phys. Chem.* **1977**, 81, 1134

105. Bjerrum, N.; Verh, d. d. *Phys. Ges.* **1914**, 16, 737

106. Herzberg, G. *Molecular Spectra and Molecular Structure, Vol 2. Infrared and Raman Spectra of Polyatomic Molecules*, **1945**, Van Nostrnd, New York, Chapter 4.

107. Finlayson-Pitts, B. J.; Pitts, J. N., Jr. *Atmospheric Chemistry: Fundamentals and Experimental Techniques*, **1986**, Wiley, New York

108. Atkinson, R.; Carter, W. P. L. *Chem. Rev.* **1984**, 84, 437

109. Atkinson, R. *Chem. Rev.* **1986**, 86, 69

110. Atkinson, R.; Pitts, J. N., Jr. *Int. J. Chem. Kinet.* **1978**, 10, 1151

111. Kharutunyan, S. A.; Mkryan, T. G.; Sarkisyan, E. N. *Oxidation Communications*, **1984**, 7, 49

112. Baldwin, R. R.; Everett, C. J.; Walker, R. W. *Trans. Faraday, Soc.* **1968**, 64, 2708

113. Atkinson, R. *Environ. Sci. Technol.* **1991**, 25, 863

114. Okabe, H. *Photochemistry of Small Molecules*, **1978**, Wiley, New York, Chapter 6

115. Stief, L. J.; Payne, W. A.; Klemm, R. B. *J. Chem. Phys.* **1975**, 62, 4000

116. Heidner III, R. F.; Husain, D.; Wiesenfeld, J. R. *J. Chem. Soc., Frarday, Trans. 2* **1973**, 69, 927

117. Heidner III, R. F.; Husain, D. *Int. J. Chem. Kinet.* **1973**, 5, 819

118. Davidson, J. A.; Sadowski, C. M.; Schiff, H. I.; Streit, G. E.; Howard, C. J.; Jennings, D. A.; Schmeltekopf, A. L. *J. Chem. Phys.* **1974**, 61, 2213

119. Lengal, P. K.; Crosley, D. R. *Chem. Phys. Lett.* **1975**, 32, 261

120. Fairchild, P. W.; Smith, G. P.; Crosley, D. R. *J. Chem. Phys.* **1983**, 79, 1795

121. Husain, D.; Plane, J. M. C.; Slater, N. K. H. *J. Chem. Soc., Faraday Trans. 2*, **1981**, 77, 1949

122. Husain, D.; Plane, J. M. C.; Xiang, C. C. *J. Chem. Soc., Faraday Trans. 2*, **1984**, 80, 713

123. Schofield, K. *J. Phys. Chem. Ref. Data*, **1979**, 8, 764

124. Cohen, N.; Wesbberg, K. *J. Phys. Chem.* **1979**, 83, 46

125. Tully, F. P.; Ravishankara, A. R. *J. Phys. Chem.* **1980**, 84, 3126

126. Ravishankara, A. R.; Nicovich, J. M.; Thompson, R. L.; Tully, F. P. *J. Phys. Chem.* **1981**, 85, 2498

127. Furue, H.; Pacey, P. D. *J. Phys. Chem.* **1990**, 94, 1419

128. Atkinson, R.; Baulch, D. L.; Cox, R, A.; Hampson, R. F.; Kerr, Jr.; J. A.;

Troe, J. *Journal of Physical and Chemical Reference Data*, **1992**, 21, 1164

129. Talukdar, R. K.; Mellouki, A.; Schmoltner, A.-M.; Watson, T.; Montzka, S.; Ravishankara, A. R. *Science*, **1992**, 257, 227

130. Zhang, Z.; Padmaja, S.; Saini, R. D.; Huie, R. E.; Kurylo, M. J. *J. Phys. Chem.* **1994**, 98, 4312

131. Prather, M.; Spivakovsky, C. M. *J. Geophys. Res.* **1990**, 95, 18723

132. Ashutosh, M.; Ding, L.; Marshall, P.; Buchta, C.; Stucken, D.-V.; Vollmer, J. T.; Wagner, H. G. *J. Phys. Chem.* **1994**, 98, 4020

133. Mullay, J. *J. Am. Chem. Soc.* **1984**, 106, 5842

134. Boyd, R. J.; Boyd, S. L. *J. Am. Chem. Soc.* **1992**, 114, 1652